Calibration and Image Formation in the ABACUS Sonar System

Ferdinand Ng

A dissertation submitted to the Department of Electrical Engineering, University of Cape Town, in fulfilment of the requirements for the degree of Master of Science in Engineering.

Cape Town, September 2005

Declaration

I declare that this dissertation is my own, unaided work. It is being submitted for the degree of Master of Science in Engineering in the University of Cape Town. It has not been submitted before for any degree or examination in any other university.

Signature of Author.....

Cape Town
11 September 2005

Abstract

The ABACUS (Advanced Beam-former for Acoustic Counting of Underwater Scatters) project aims to develop a high-resolution narrowband sonar system for determining volume density in dense fish or squid aggregations. In 1995, engineers at Marine & Coastal Management proposed an interferometric beamformer for accurate counting of targets in high-density situations. The hardware was developed in the mid to late 90's. It consisted of two 16-element arrays, operating at 420 kHz, with a 32-channel data acquisition system and the signal processing software consisting of a simple DOS based data logging software, which was never completed.

The objectives of this thesis are to revive the project and to develop signal processing software for image formation.

For the purpose of capturing data in various sea trial events, an improved server-client data capturing front-end for interfacing with ABACUS hardware was implemented to replace the old software.

A modified interpolated delay and sum beamformer for separating targets in the azimuth direction and the interferometric concept were for determining position of the target in elevation direction were studied and implemented in Matlab.

A calibration procedure was developed to derive compensation factors for gain and phase variations in the receiving channels. This made use of measurements from calibration targets made in a measurement tank at the Institute of Maritime technology (IMT) in Simons Town.

Finally, the resulting images in various sea trials are shown and discussed, and the results are compared to those obtained from an existing EK500 sonar system.

Acknowledgements

The author would like to thank the following for their assistance in completion of this dissertation:

- A sincere thanks to Dr. A. J. Wilkinson for his valuable advice and time throughout the duration of this dissertation. Without his assistance, this dissertation could not be completed.
- Sincere thanks to Mike Soule and Ian Hampton from Fisheries Resource Surveys for giving us the opportunities on working in the interesting ABACUS project, and all staff at MCM for their assistance in various sea trial experiments and financial funding. Special thanks to Mike Soule for spending his valuable time on reviewing my thesis and providing valuable recommendations.
- South African Squid Management Industrial Association (SASMIA) for their financial support during the research period.
- All the members in the Algoa and the Africana research ships for their assistance in various sea trial events and for taking care of me when I was sea-sick.
- Thanks to UCT for the support in hardware equipment.
- Sally Burt in PCU department for valuable advice on my grammar and structure.
- All the friends that I made in the UCT signal processing group.
- My girlfriend, Angel Yung who took care of my living during the research period.
- My family in Hong Kong and Taiwan for their continuous support.

List of Symbols

λ: *The wavelength*

Ψ: *Angle of arrival in y-z plane*

c: *The speed of sound in water, the default value is 1500 m/s (The actual value depends on temperature and salinity)*

B: *Bandwidth*

f_0: *Carrier frequency of the signal*

α: *Angle of arrival in y-z plane*

dB: *Deci-Bel, a unit standard used in log scale measurement.*

DT: *Detection Threshold*

SL: *Source Level*

DI: *Directivity Index*

TL: *Transmission Loss*

TS: *Target Strength*

NL: *Noise Level*

P: *Transmitted Power*

r: *Measured distance between the source and target*

p(t): *intensity of pressure*

l_s, *Ls*: *Spreading loss*

l_a: *Attenuation loss*

P_r: *Reflected power by the target*

P_i: *Received power by the transducer*

TS: *Target strength*

NSL: *Noise level from the noise source*

E: *Signal energy*

M: *Total number of sensor elements*

dx: *distance between the centre of two sensors.*

V_{rx}: *Receiving signal*

V_m:	*Matched signal*
V_{bb}:	*Basebanded signal*
S:	*division between far field and near field*
D:	*Length of array*
p_{pt}:	*Position of point target*
p_{rx}:	*position of receiving elements*

Nomenclature

ABACUS: Project code name of "Advance Beam-former for Acoustic Counting of Under Water Scatterers".

TVG: Time-Varying Gain for hardware spread loss compensation.

SONAR: Sound Navigation and Ranging.

Matlab: A mathematical software development environment and toolbox.

Delphi: A industrial standard of software development environment developed by Borland.. It is the inheritance of Pascal.

IMT: Institution of Maritime Technology, a government based institution for experiments, research and development of sonar system. It has a tank facility for sonar calibration and experiment.

MCM: Marine and Costal Management, a government funded organization which is responsible for monitoring South African Coastal and Marine Resources.

Pascal: Pascal is an old software development environment developed by Borland. The old data capturing software was implemented using it.

Azimith: Angle in horizontal plane.

Elevation: Angle in vertical plane.

Algoa: A 58 m converted French stery trawler used as a general purpose research vessel by Marine and Coastal Management. The November sea trials are taken place on it.

Africana: A 78m purpose designed research vessel used during the August sea trials.

Peralex: A digital signal processing company based in Cape Town. The two DSP cards and the old data capturing software are the product of them.

OpenGL: An industrial standard programmatic library for implementing graphic using hardware acceleration. The polar display of the Delphi data capturing software is implemented using that.

Pilchard: This is a type of fish and the research target in Africana April 2004 Sea Trial.

Anchovies: This is a type of fish and the research target in Africana April 2004 Sea Trial.

EK500: A scientific multi-frequency echo-sounder manufactured by SIMRAD. It operates at 38 kHz, 120 kHz and 200 kHz. This echo sounder is used on the Algoa ship for hydro-acoustic surveying.

SIMRAD: The Norwegian company named Norwegian Simonsen Radio AS (SIMRAD) plays the leading role of development in all type of fishery sonar.

List of Figure

List of Table

Table of Contents

Chapter 1

Introduction

There has been an increase in the demand for underwater food resources around the world due to the increase in the world population since WWII. Due to this huge demand, most of the commercially interested underwater species have been heavily fished and many countries' fish stocks have collapsed. Fisheries research is responsible for studying the biological processes of underwater species. Hydro-acoustic surveys are carried out to estimate the biomass or abundance of the various fish stocks considered to be economically important. The results obtained are used by biologists and mathematically modellers to provide managers with the information necessary for setting Total Allowable Catch (TAC) limits for the commercial fishing industry. The estimates are critically reliant on target strength measurements. There are many conventional methods of estimating target strength in situ, but they generally require the targets to be dispersed. In the practical world, this is not always the case [27], especially during day time (at night, the fishes tend to be more dispersed). If this method is used on dense aggregations, it can introduce significant errors in biomass estimation, due to the false acceptance of multiple or overlapping echoes as valid single targets.

The South African underwater resource is monitored and controlled by Marine and Coastal Management (MCM), a branch of the Department of Environmental Affairs and Tourism. They provide funding and conduct most of the research relating to marine and underwater technologies. ABACUS (Advanced Beam-former for Acoustic Counting of Underwater Scatter) [27] is one of the projects proposed by MCM engineers in the early 1990's. The intention of ABACUS is to provide a higher resolution sonar system than existing sonar systems to improve estimates of target strength and hence the precision of biomass estimates in general. The existing sonar

system is a 38 kHz and 120 kHz EK500 sonar system from SIMRAD. It provides a circular beam width of 7 degrees. With the ABACUS system, the focused beam width is approximately one degree over an observation angle of about 12 degrees (comprised of 12 1° segments). Therefore ABACUS will enable a great improvement in resolution capability.

1.1 History of Fishery Sonar

Sonar stands for Sound Navigation and Ranging. In some instances, sonar can also be called ASDICS, which stands for Anti-Submarine Detection Investigation Committee [2]. In 1906, an English meteorologist, Lewis Nixon, invented the first sonar system which was intended for detecting icebergs. Interest from the Americans, the British and then French in SONAR rose during WWI, due to its capacity for detecting submarines and icebergs. Unfortunately at that time, sonar systems were simple and ineffective. Since then, significant research on the sonar technologies such as sound propagation in the sea and the absorption phenomena over the entire frequency range has been undertaken in the field of sonar technology. During WWII, sonar provided a great advantage, allowing for the early alert of submarines and underwater enemies in the vicinity.

After WWII, interest in using sonar grew in commercial industry such as marine survey, oil prospecting, scientific investigation and fishery. The research and development then grew rapidly in the area of acoustic transducers, signal processing and signal generators. The interest in signal processing for improving efficiency and capability of sonar systems is growing together. The first application in underwater acoustics was the digital multi-beam steering system (DIMUS) which used a digital shift registry to provide delays for the beamformer [25]. The development of fast transforms and the improved technology of digital components gave rise to the design of all digital signal-processing systems after 1970.

The first fishery sonar application in history is the recording of cod made by Oscar Sund in 1935 in the Norwegian Fisheries Research Ship. Since the existing sonar

system at the time was derived from military sonar, they were all vertically scanning sonars (not appropriate for shallow water fishery), and often too bulky to install in the ordinary fishery boats. The development of horizontal scanning sonar was then begun in 1950.

Today, searching fish shoals by sonar has become the essential tool of mid-water fisherman. ABACUS is vertical imaging sonar (i.e. the beam points vertically downwards towards the bottom), designed not for fish finding as the horizontal system, but for in-situ fish density estimation over aggregated fish and squid.

1.2 Overview of the ABACUS System

1.2.1 ABACUS System Hardware

The ABACUS system as developed by MCM and delivered to UCT in 2003, is composed of four units as shown in Figure 1 below. The connections between them are shown in Figure 2.

a)

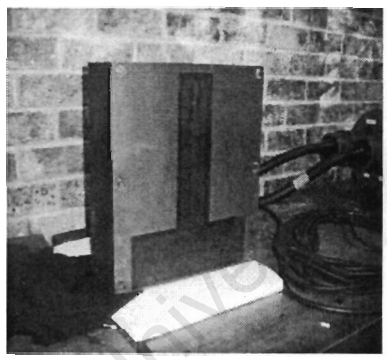

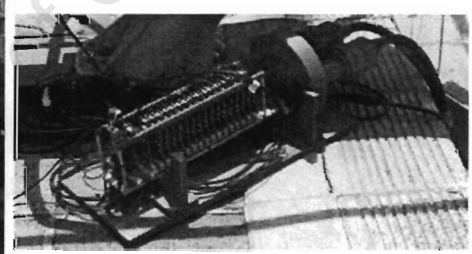

b)

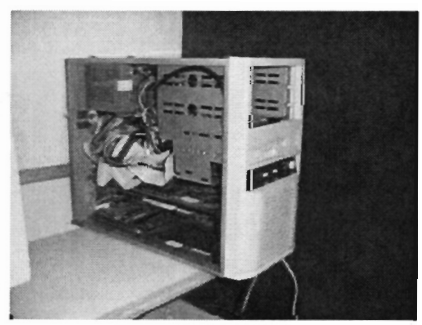

c) d)

Figure 1: ABACUS system components:

a) The ABACUS transducer head. b) The digital triggering and data capturing unit pod. c) The transmitter power amplifier unit. d) The DSP cards and controlling PC unit.

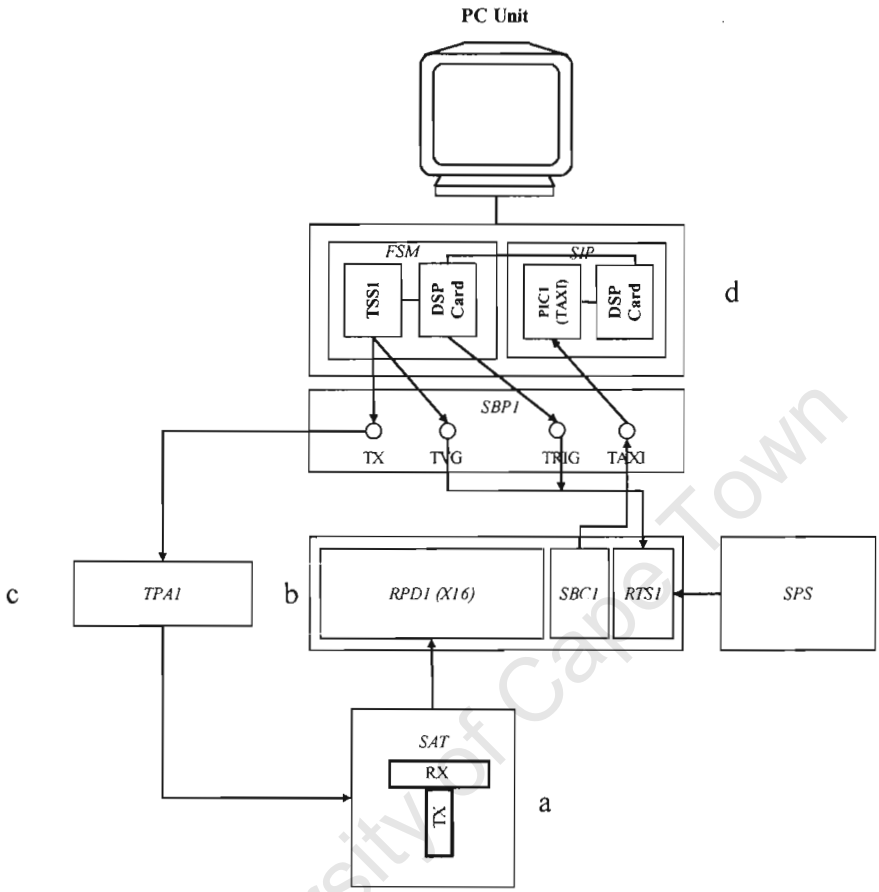

Figure 2: The ABACUS system connection layout

The four units are as follows:

a) The transducer head unit

Figure 1a shows the transducer head unit. The transducer elements are laid out in a T-shape. It consists of 1 row of 16 transmitter transducer elements and two rows of 16 rectangular receiving transducer elements. The illustration of the transducer element layout with dimension in meters is shown in Figure 3.

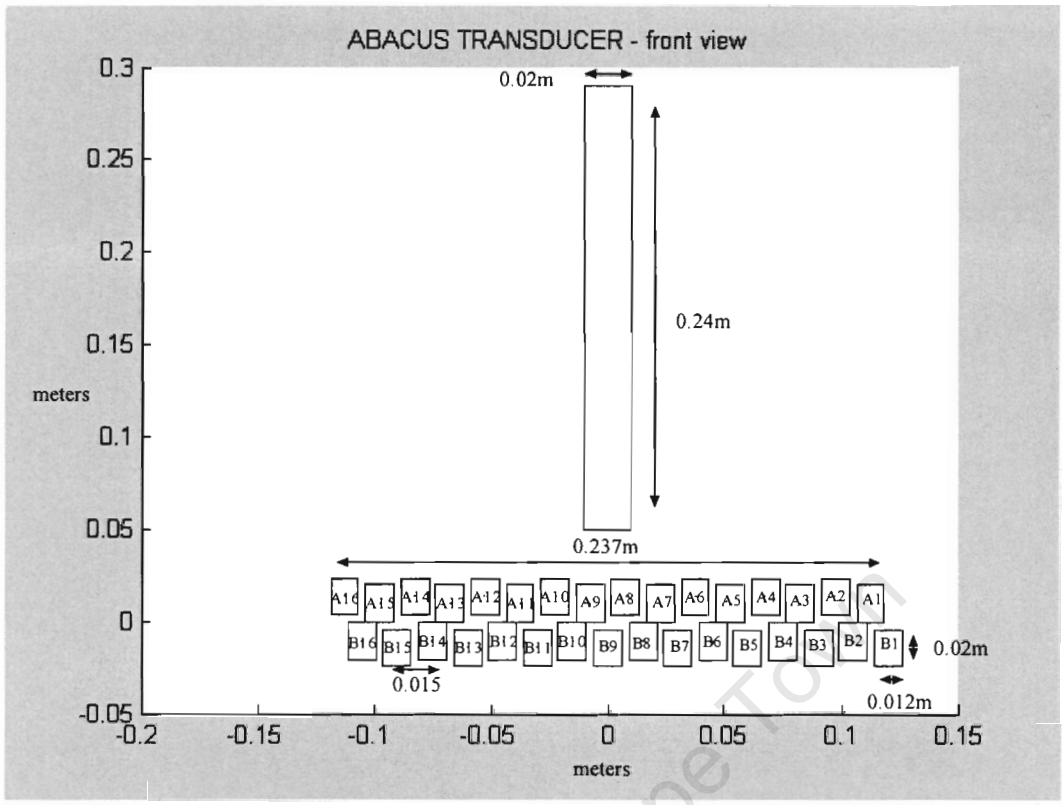

Figure 3: The ABACUS transducer elements layout (element number also shown in the Figure) with dimension shown in meters

b) The digital triggering and data capturing pod unit

Figure 1b shows the digital triggering and data capturing rack. It consists of 16 receiver channel pre-amp digitizer cards (RPD1), a receiver controller and a telemetry transmitter card (SBC1) and a digital triggering synthesizer card (RTS1).

The RPD1 cards are responsible for receiving an analogue signal from each channel. They then pre-amplify with time variable gain (TVG signal). The pre-amplified signal then passes through an A/D converter and it is sent to the SBC1 card via the system bus. Each RPD1 card can handle two channels at a time. At the current state, only half of the RDP1 board is populated with components. If the other half of board is used the system will be able to handle 32 channels.

The SBC1 card is responsible for collecting digital data from each channel through the system bus. It then serializes the data and sends it to the DSP card (SIP) located in the controlling PC using a dedicated serial communications chip known as a "TAXI" chip.

The RTS1 card is responsible for generating a voltage ramping signal, defined by the Falcon DSP card (TSS1) located in the PC side, for the time varying gain (TVG) in each RPD1 card. The triggering signal also feeds into this card from the Falcon DSP card (TSS1) located in the PC side and pass to the transmitter head (SAT) through the Transmitter Power Amplifier (TPA1).

The photos of RDP1, SBC1 and RTS1 cards are shown in Appendix A.

*c) **The Transmitter amplifier unit***

Figure 1c shows the transmitter amplifier unit which amplifies the transmitted signal generated by the PC DSP card (Falcon) to the ABACUS transducer head.

*4) **The Controlling PC with DSP cards unit***

Figure 1d shows the PC unit. This is the computer used to control the ABACUS system. It is a 300MHz AMD K6, 128mb ram PC with a Windows 98 Operating System. There are two Digital Signal Processing cards plugged in (SIP and Falcon) and they were designed by a local company Peralex.

SIP is responsible for receiving the 16 channel serialized digital data from the SBC1 through the TAXI chip and providing buffering for this data.

Falcon is responsible for generating the transmitted pulse, ramping signals and control signals to the ABACUS hardware respectively.

The photographs of these two DSP cards are shown in Appendix A.

1.3.2 The specification of the ABACUS System

The specifications of the ABACUS system are listed below:

Centre frequency:	420 kHz
Wavelength:	3.62 mm
Bandwidth:	10 kHz or 20 kHz
Range resolution:	7.6 cm or 3.8 cm
Sampling frequency:	45.455 kHz
Number of range samples:	4096 samples

1.3.3 Conceptual overview of the ABACUS System

To explain the concept of the ABACUS system, an illustration of the ABACUS system is provided in Figure 4. As soon as the Falcon card creates the chirp pulse, the signal passes through the power amplifier to the ABACUS transducer head. The chirp signal then propagates into the water forming a fan beam (1° x 10°) [26] vertically down to the ocean floor. The fan beam will create an elongated footprint on the sea floor as shown in Figure 4.

Part of the echo returns to the receiving array. As mentioned earlier, the transducer head consist of two arrays and each array consists of 16 elements. The elements are arranged in an up-down fashion (staggered).

With an appropriate beam forming signal-processing technique, which will be discussed in Chapter 2 and Chapter 3, a focused receiving beam can steer left and right as shown in Figure 4. The cross-over zone of the transmitting beam defines the receiving beam is the resolution cell of the ABACUS system. Since the ABACUS system is operated at 420 kHz, it is high enough to allow a fine 1° angular resolution with an array length of 23.7 centimetres. In practical experiments, the resolution cell was measured to be 1.0° by 1.6° [26].

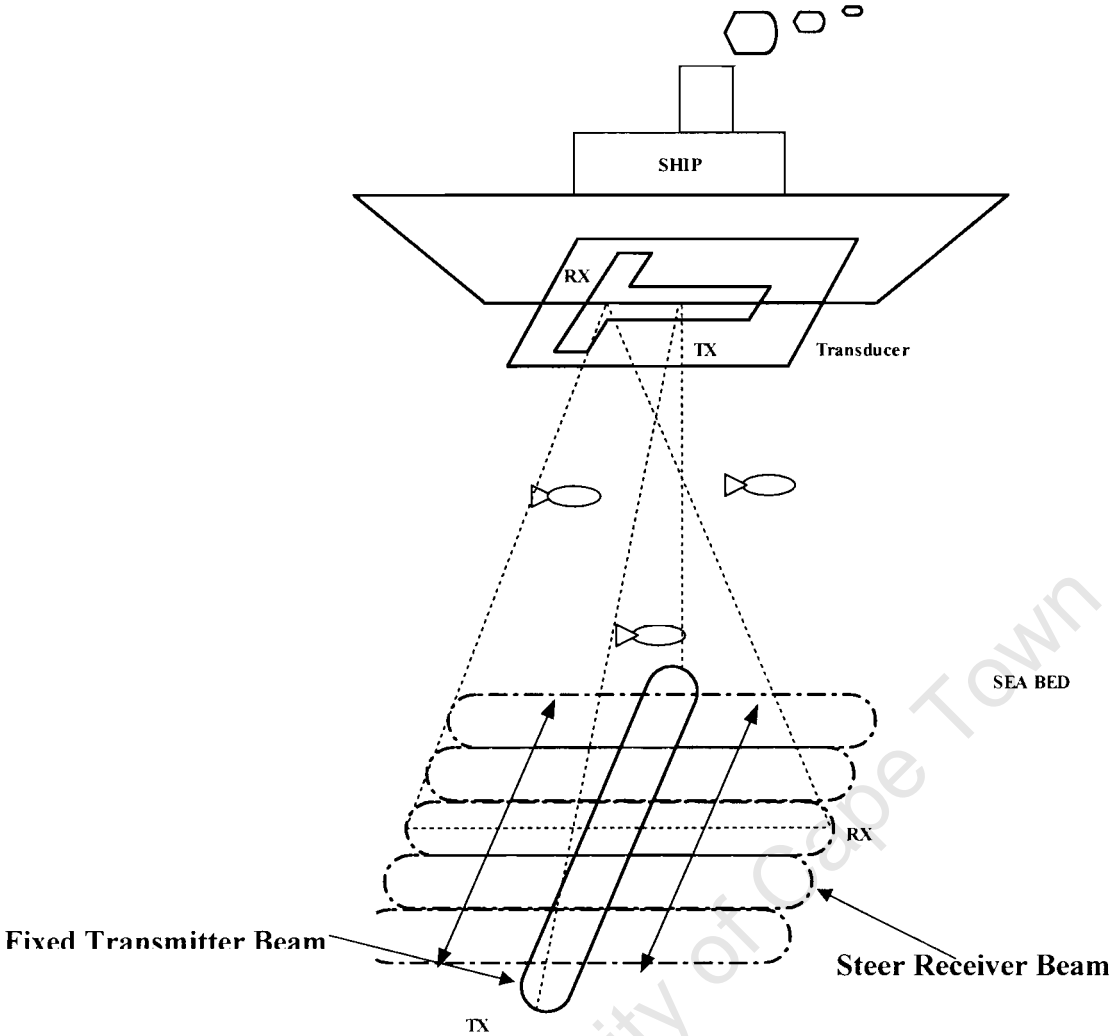

Figure 4: The illustration of the concept of ABACUS system

Using a chirp bandwidth of 10 kHz, the range resolution is 7.6cm, which is fine enough to identify separate individual fish in a range dimension. The cross range resolution is dependent on the depth. For example, if a target is located in a depth of 20m, the cross range resolution is approximately 30cm.

The angle of the receiving beam can be steered although it is limited to 14° due to spatial aliasing phenomena. This aliasing phenomenon will be discussed in more detail in Chapter 3. It is noted however that the transmit "fan" beam illuminates a 10

dB beamwidth of 17 degrees and the individual elements have a 3 dB beamwidth of approximately 10 degrees [26].

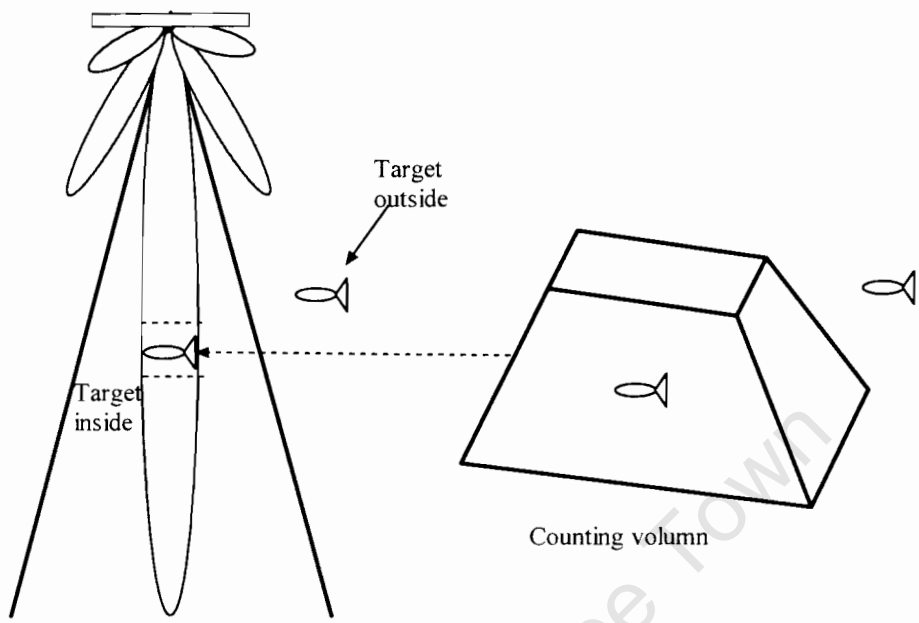

Figure 5: The illustration of the ghost targets created by the spatial aliasing phenomena

The spatial aliasing phenomenon creates ghost targets within the receiving beam. This phenomenon is illustrated in Figure 5. If the target is located outside the resolution cell, due to the spatial aliasing phenomenon, it will also have a duplicated image exist inside the resolution cell. Therefore interferometry (which utilises the two receiving arrays) is used to distinguish targets located outside the counting volume. The spatial aliasing phenomenon is discussed in Section 2.4.1 and the interferometry is discussed in Section 2.5 and Section 3.3.

1.4 Objectives of the dissertation

The objectives of the work described in this dissertation are as following:

- Develop suitable array based signal and image processing algorithms for the ABACUS hardware.
- Develop a front-end interface to the hardware for data capturing.
- Acquire real data sets in different environments:

- In a controlled tank environment using calibration targets.
- At sea using squid, pilchard and anchovies.

- Apply the image formation algorithm and characterize the resolution achieved.
- Devise a suitable calibration method to improve the focussed point target response, particularly the reduction of side-lobe levels, and quantify the result achieved with regard to
  - dB side-lobe improvement
  - Angular beam resolution

1.5 Scope and Limitations

The ABACUS system consists of a total of 32 transducer elements as mentioned above in paragraph 1.3.1 and depicted in Figure 2. Each A/D signal capturing board is capable of handling two channels. Unfortunately, during the research period of this dissertation, only half of the each RPD board was populated. This means that each card can only handle one channel instead of two. The experiment and results obtained in this thesis are therefore limited to 16 channels and only half of the potential of ABACUS system is shown.

1.6 Plan of Development

The reminder of this dissertation is organized as follows:

Chapter 2 is concerned with the basics of vertical imaging sonar. There include:

- the signal processing of the received signal, such as the pulse compression technique for achieving fine range resolution.
- the beamformer which resolves the location of the target in an angular position.
- interferometry which is used to determine the precise location of a target in the direction "orthogonal to the fan beam".

All these methods are examined in detail.

Chapter 3 describes the signal and image formation algorithms developed for processing the ABACUS data.

Chapter 4 discusses

- various issues that arose during the development of the Delphi data capturing front end
- the structure of the software and
- the capability of the software.

Chapter 5 discusses the calibration experiments that took place at the Institute of Maritime Technology (IMT) in Simons Town. The methods of deriving the gain and phase compensation factors are explained and their improvement on the image formation will be shown.

Chapter 6 explains in detail of the images from a swimming pool experiment and from various sea trial experiments using the algorithm discussed in Chapter 3. The resultant images are also compared to the images created by EK500, to contrast and verify the performance of the ABACUS system.

Chapter 7 draws conclusions based on the finding of this dissertation

Chapter 8 recommends possible future work of ABACUS.

Chapter 2

Sonar Theory relevant to the ABACUS System

The objective of this chapter is to outline the theory behind the signal processing used in the ABACUS system. This section will initially describe the basic equation of the sonar system in Section 2.1. This equation outlines all the factors that have to be considered with processing signals from underwater. It will then lead to the description of the transmitted pulse used in the ABACUS system and the pulse compression method for maximizing the S/N ratio. Next a classical time domain beamformer will be described as well as the theory of interferometry, which is adopted in the layout of the ABACUS transducer elements in order to locate the position of a target in 3-D space.

2.1 Basic Sonar Equation

The sonar equation in Equation 1 presents an active, noise background and directional sonar equation guideline which is reviewed by Urick [8]. The equation aims to determine the level of detectability of received signal, in order words, the detection threshold (DT), expressed in decibels.

$$DT = SL + 2DI - 2TL + TS - NL \qquad \text{[dB]} \qquad (1)$$

Each term within the equation is described in the following subsections.

2.1.1 Source Level (SL)

The source level is the power flux that is delivered into the water media by the transducer sources. Assuming the acoustics pressure is omni-directional in spread, the source level is given as:

$$\text{SL} = 10 \log\left(\frac{\text{intensity of source}}{\text{reference intensity}}\right) \text{ [dB]} \qquad (2)$$

Coates [13] reviewed that the intensity of source is calculated by $I_s = \frac{P}{4\pi r^2}$ where I_s is the intensity of source, P is the transmitted power and r is the measured distance between the source and the target. The reference intensity is given by $I_r = \frac{p(t)}{\rho c}$, where ρc is the acoustic impedance of the water media and *p(t)* is the intensity of sound pressure. The reference target location is 1 m from the source transducer.

2.1.2 Directivity Index (DI)

For the ABACUS system, the phased array is directional instead of omni-directional in spread. Therefore the directivity index factor must be added in the Sonar Equation. The directivity index is the ratio

$$DI = \frac{I_0}{I_m} \qquad (3)$$

to achieve a given power density a fixed distance from the hydrophone. I_0 is the radiated intensity at the beam axis and I_m is the mean intensity for all directions.

2.1.3 Transmission Loss (TL)

As the acoustic energy propagates outwards from the source, the power density decreases with distance. This reduction in intensity is caused by the energy spreading

and the transformation to heat during propagation. These two losses are the spreading loss (l_s) and the attenuation loss (l_a). The sum of these two losses is the transmission loss

$$TL = l_s + l_a \tag{4}$$

The fundamental spreading loss can be described as spherical spreading, which can be approximated by inverse square law

$$L_s = k \log R \tag{5}$$

where k is the factor dependent on the kind of energy spreading. For spherical spreading it is +20 and for cylindrical spreading it is +10.

The ABACUS system operates at 420 kHz, and the attenuation loss is mainly caused by viscous friction. The attenuation loss is described as

$$L_a = \alpha R \tag{6}$$

α is the attenuation factor, which is plotted in Figure 6 [13] as a function of frequency. It illustrates the attenuation in seawater and distilled water. In the case of the ABACUS system at 420 kHz, the attenuation factor is approximately 0.1 dB/m.

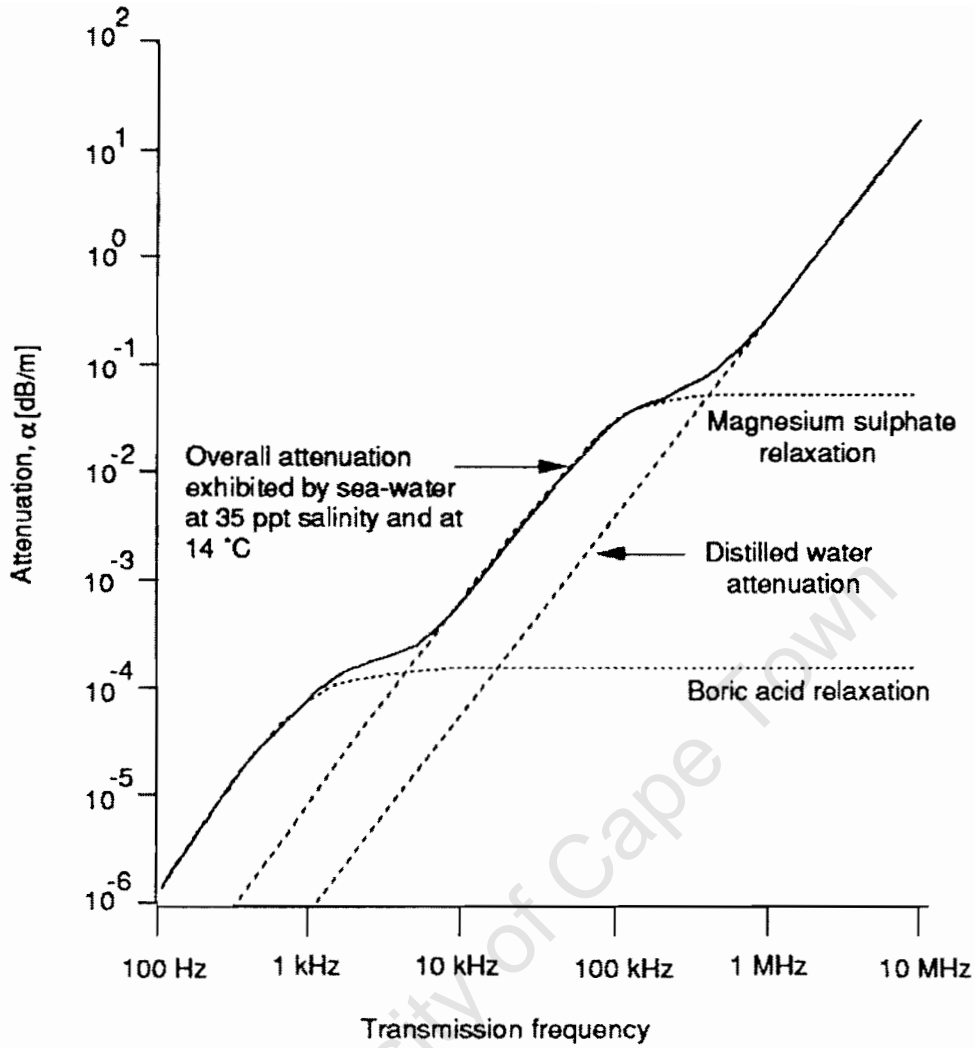

Figure 6: Attenuation in distilled water and in sea water [13]

2.1.4 Target strength (TS)

The ratio of the received acoustic power density (P_r) to transmitted power density from an object as at 1 meter from the transmitted (P_t) is the target strength. The target strength defined to be:

$$TS = 10 \log \frac{P_r}{P_t} \tag{7}$$

A more in detail introduction on the target strength can be found in [8]. The method of obtaining the target strength can be divided into in-situ and ex-situ. The ex-situ target strength measurement is taken in a controlled environment where targets are of known size and weight. This disadvantage of this method is that it affects the natural behaviour of the underwater animal and the TS data are often not reliable [20]. The in-situ method is more reliable because the animals are behaving naturally. The In-situ method can be further divided into the indirect method and direct method. A detail explanation on various in-situ TS estimation method (e.g. inverse techniques such as Expectation, Maximization and Smoothing (EMS), Singular Value Decomposition (SVD) and Wavelet Decomposition) can be found in [20][21].

2.1.5 Noise Level (NL)

The sea is a very noisy environment. Noise can come from marine animals, ship engines, rainfall, thermal energy or even the boundary of the sea floor and the surface. In a sonar system, the noise can be separated into two categories, ambient noise and reverberation.

The ambient noise is normally considered as isotropic. Figure 7 [13] illustrates the gross spectral behaviour of acoustic noise observed in the open sea. ABACUS is operated at 420 kHz, and according to the graph, the ambient noise is dominated by thermal noise.

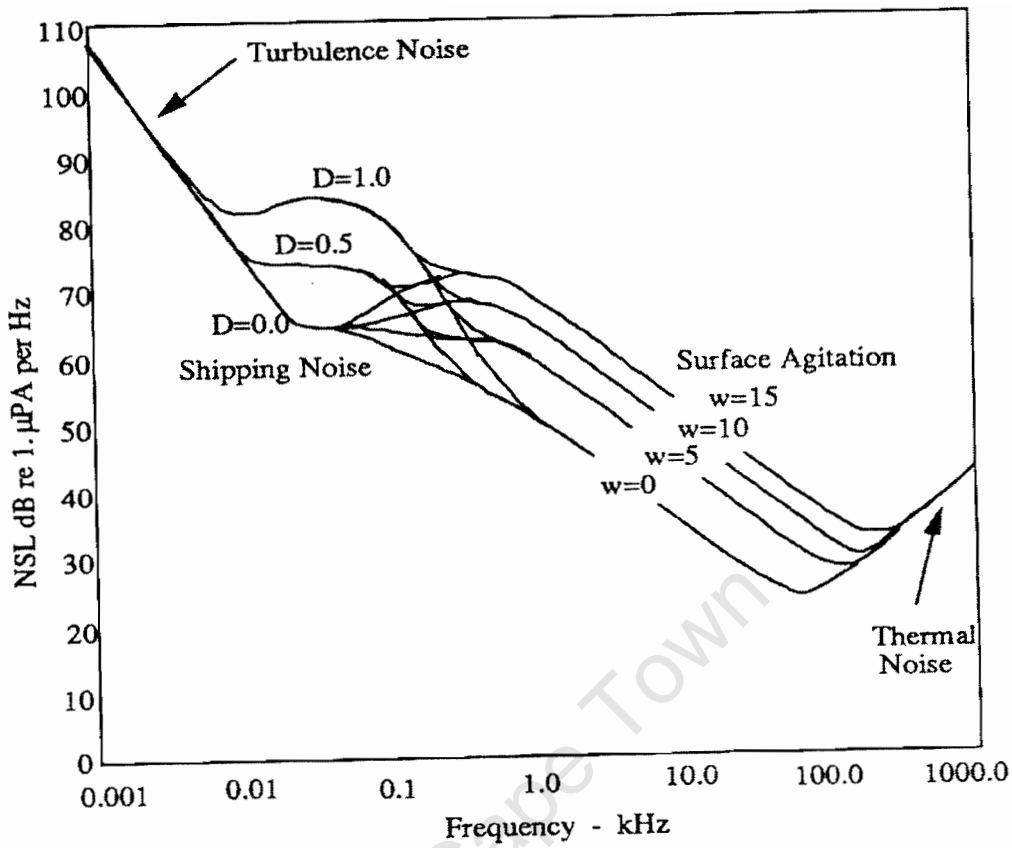

Figure 7: Deep-water ambient noise spectrum level [13]

The thermal noise level can be calculated by

$$NL = NSL + 10\log B \tag{8}$$

where B is the transmission bandwidth and NSL is the sum of the noise level from the noise sources. The NSL can be obtained empirically by dropping a hydrophone into the sea.

Reverberation is created by many factors, including multi-path, the reflection from the bubbles and organic animals in the surrounding water (Volume Reverberation). It can also be created by the reflection from the sea surface or the sea bed (Surface Reverberation). Transmitting more power can minimize the effect of other noise

sources such as ambient noise, however since reverberation is proportional to the transmitted power, the increase in transmitted power will increase the reverberation level. A more detailed study on reverberation can be found in [13].

2.2 Linear FM Chirp Pulse

The ABACUS sonar makes use of a transmitted waveform known as "Linear FM Chirp pulse". It is a swept frequency waveform. This means that the signal frequency changes with respect to time. Its time waveform [3] is

$$v(t) = rect\left(\frac{t}{T}\right)\cos\left(2\pi\left[f_0 t + \frac{1}{2}Kt^2\right]\right) \tag{9}$$

Where t is the time variable and K, f_0 and T are constants, which control the characteristic of the chirp. K defines the rate of change in the frequency of the chirp (Hz/s). T defines the length of the pulse. More detailed information on chirp pulses can be found in Chapter 4 in [3].

2.3 Matched Filtering for improving Signal to Noise Ratio (SNR)

Matched filtering is used in the ABACUS sonar to detect signals of known shape which are buried in noise. The matched filter is a linear filter which maximizes the signal to noise ratio (S/N) The peak S/N at the output of a matched filter can be shown to be

$$\text{Peak } S/N = \frac{E}{\left(\frac{\eta}{2}\right)} \tag{10}$$

where E is the signal energy in the received pulse and $\frac{\eta}{2}$ is the white noise power spectral density. The signal to noise ratio is proportional to the transmitted energy and independent of the pulse duration or bandwidth.

The matched filter model is shown in Figure 8. The input $x(t)$ is the received signal and the $n_i(t)$ is white noise. $P(\omega)$ is the transmitted pulse and H_{bb} is the receiver model. The received signal $x(t)$ of a point target, $\xi(t)e^{-jw_o t}$, is modelled by [3]

$$x(t) = \xi(t)e^{-jw_o t} \otimes p(t) = \xi_o p(t-\tau) \tag{11}$$

where p(t) is the transmitted pulse, ξ_o is the magnitude of the response of the point target and τ is the time delay of the received signal.

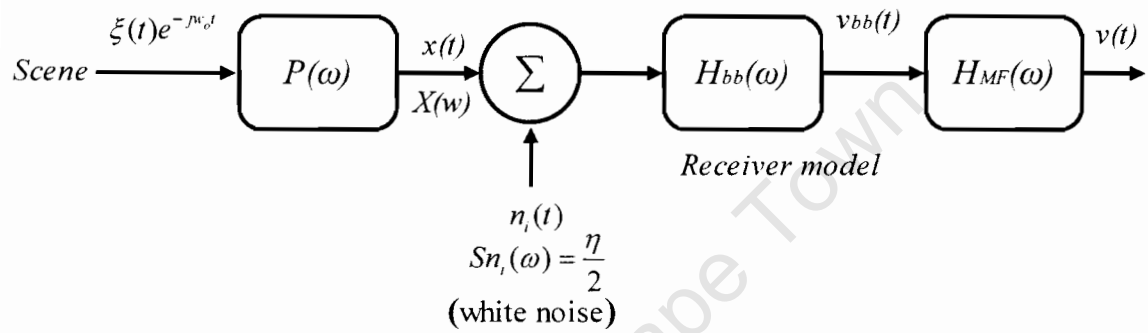

Figure 8: Matched Filter Model [3]

To maximize the SNR, and remove distortion introduced by the receiver, the $HMF(\omega)$ is therefore

$$HMF(\omega) = \frac{P^*(\omega)}{H_{bb}(\omega)} \tag{12}$$

where $P^*(\omega)$ is the conjugate of the transmitted pulse. By multiplying with the matched filter response, $HMF(\omega)$, the signal to noise ratio is maximized.

2.4 Time domain beamformer

Beamforming is spatial filtering. It enhances signals from a particular angular direction while suppressing the signal from other directions. By doing so, a beam can

be steered to the desired direction without physically moving the transducer head. Before explaining the beamforming algorithm, the idea of spatial filtering should be discussed first.

2.4.1 Spatial Filtering

Imagine a pressure wavefront arriving at twelve-element transducer array; this is illustrated in Figure 9a. If the wavefront is arriving at boresight, there is no different in the phase in the transducer elements because there is no difference in the time of arrival.

Now, if the acoustic source emits a pressure wavefront at 30° as illustrated in Figure 9b, each transducer element experiences a phase difference due to different time of arrival. This result is plotted in Figure 10b.

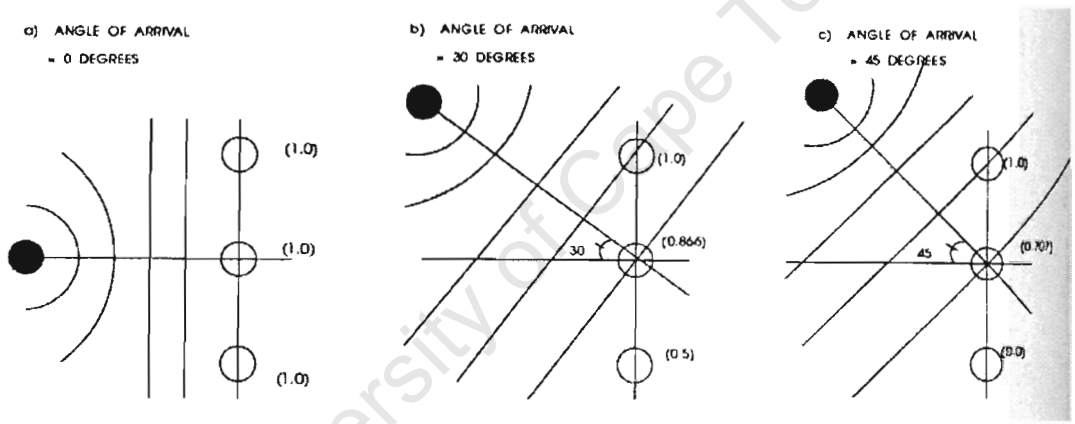

Figure 9: The illustration of the pressure wavefront on the transducer element. [6]

If the acoustic source is moved to 45° as illustrated in Figure 9c, the transducer elements will experience even greater phase variation on them and it is shown in Figure 10c.

From this result, one can see that the phase variation for each element depends on the angle of arrival of the pressure wavefront. This variation in phase is called spatial frequency.

Based on the concept of spatial frequency, one can create a filter which retains signals from desired angles while suppressing signals from other angles. This kind of filtering is called spatial filtering.

References [6] and [23] have a more in depth section on the topic of spatial filtering.

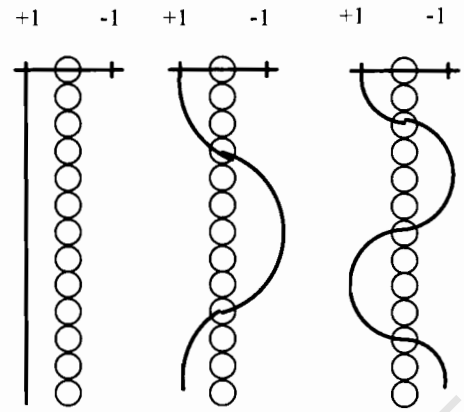

Figure 10: The concept of spatial filtering [6].
a) boresight wavefront, b) 30 degree wavefront, c) 45 degree wavefront

2.4.2 Delay and sum beam-former (far field approximation)

The linear change in the phase across the array is illustrated in Figure 10, by the frequency of the sinusoidal waves illustrated on the array, and for waves arriving at boresight, 30 degrees and 45 degrees. The beamformer used for far field area is implemented in the ABACUS system is a "delay and sum beamformer".

In a simple time domain beamformer summing up the output signal from each transducer element coherently creates a spatial filter. Referring to Figure 11, assuming a signal v propagates in two dimensional spaces as a plane wave at angle Ψ, the resultant signal from the beamformer would be

$$y(r,\Psi)=\sum_{i=1}^{M} v_i(r+d_x(i-1)\sin(\Psi))e^{\frac{j2\pi d_x(i-1)\sin(\Psi)}{\lambda}} \qquad (13)$$

r: Range from the array mid point to the focus point.

M: The total number of sensor elements in the array

d_x: The distance between the centre of two sensors.

v_i: The signal received by the i-th sensor.

Ψ: Angle of arrival in 2-D space.

λ: Wavelength.

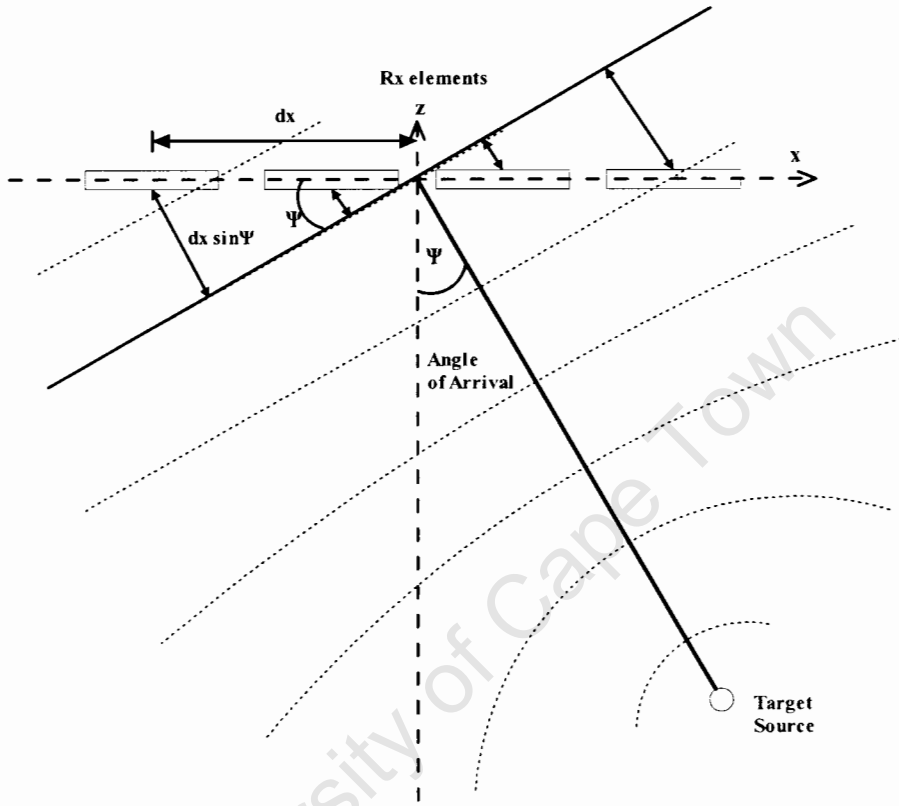

Figure 11: Illustration of far field approximation

The term $\sum_{i=1}^{M} \exp(j\, 2\pi\, d\, (i-1)\, \sin(\Psi) / \lambda)$ is called the beam pattern or field intensity pattern. The magnitude of this beam pattern can be expressed as

$$\left|b(\Psi,\lambda)\right| = \left|\frac{\sin[\pi M d \sin(\Psi-\Psi_0)/\lambda]}{\sin[\pi d \sin(\Psi-\Psi_0)/\lambda]}\right| \qquad (14)$$

Figure 12 uses the ABACUS configuration to simulate the effect of the beam steering on the normalized beam power pattern. The angular range has been displayed between -7° and +7°as beyond this range, spatial aliasing or grating lobe will occur due to the layout of the transducer array. The grating lobe is one of the main features of the ABACUS system, therefore it will be discussed more fully in the Section 2.2.3.

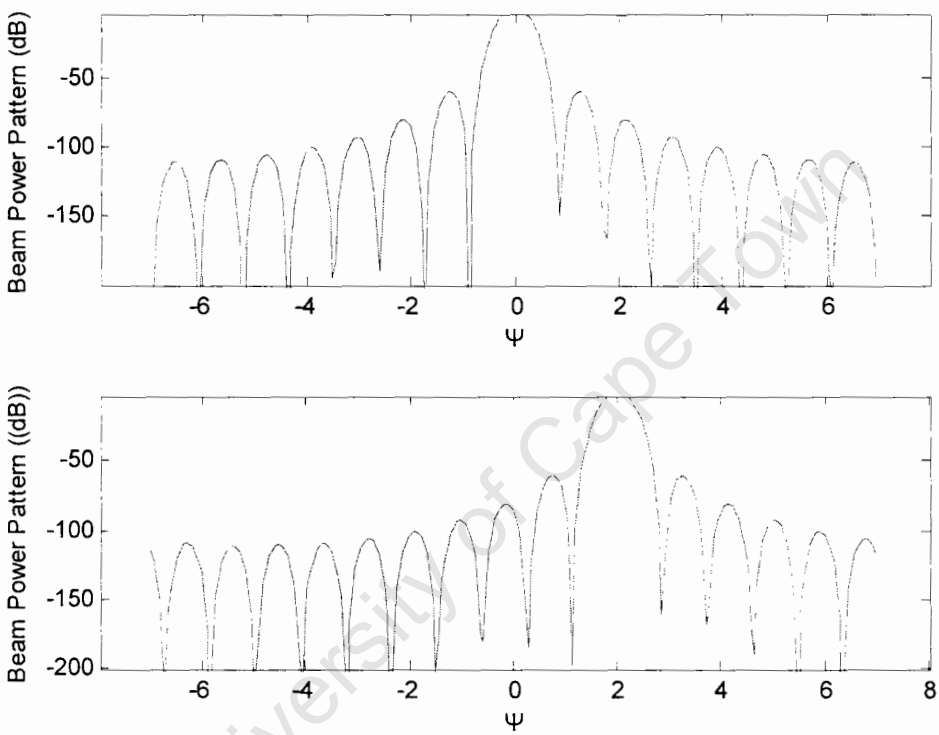

Figure 12: ABACUS' beam power pattern simulator result of beam steering

The beamformer discussed in Equation 13 is only applied in far field region, since in a far field region, the beam spread with a beam angle of $\frac{\lambda}{D}$ is approximately 1 degree. The transition zone S [6] separating the far field and near field region is calculated by

$$S = \frac{D^2}{\lambda}$$

where S is the transition range and D is the length of the transducer array. With ABACUS design where D is 0.237m and λ is 0.0036m, the transition range is at 15.6m. If the far field approximation is applied to target closer than 15.6, poorer performance is resulted. In Section 3.2.4.2, a close field approximation will be discussed.

Although, by using the spatial filtering discussed above, any target in the x-z axis can determined, the ghost target created by the spatial aliasing, which will be discussed shortly, cannot be distinguished. This means that even though the target is not located inside the focused beam, the grating lobe image can still exist inside the focused image. To eliminate targets in the sidelobes perpendicular to the 'plane of fan', interferometry is used. Section 2.4 discusses the concept of interferometry.

2.4.3 Spatial Aliasing (Grating Lobes)

The definition of spatial aliasing or grating lobes is the response peak that is identical to the main lobe [4]. It occurs if the spatial domain is not sampled at a sufficiently fine spacing. Equation 15 helps to explain this phenomenon. The peak of the beam pattern will occur if the denominator tends toward zero, i.e. if

$$\left| \frac{\pi fd(\sin\Psi - \sin\Psi_0)}{c} \right| = \pm n\pi \tag{15}$$

which implies

$$\Psi = \sin^{-1}\left[\pm \frac{nc}{fd} + \sin\Psi_0 \right] \tag{16}$$

Equation 16 indicates that the beam pattern will have more than one peak. The other peaks beside the main lobe at ψ_0 are called the grating lobes or the ambiguous lobe. Since grating lobes are generally undesirable, it is preferable to push them out of the scanning angle, Ψ, which is $\pm\pi/2$.

Firstly, consider the case that no beam steering has been done, which means $\Psi_0 = 0$. Grating Lobes will occur at $\pm\pi / 2$ when $d = \lambda$. Therefore, grating lobes can be avoided if:

$$d \leq \lambda \tag{17}$$

Secondly, consider the case of steering the main lobe to the extreme case which means $\Psi_0 = \pm\pi / 2$. Grating lobes will occur at $\pm\pi / 2$ when $d = \lambda / 2$. Therefore, grating lobes can be avoided if

$$d \leq \frac{\lambda}{2} \tag{18}$$

The following simulation shows the effect of element spacing on grating lobes. Figure 13a is simulating a array of 16 elements which separated by $\lambda / 2$ where λ is 0.0036m (same as ABACUS). Figure 14b is simulating an array of 4 elements which separated by λ x 2 where λ is equal to 0.0036m again. The reason for the decrease in number of elements is to keep the array length (D) constant.

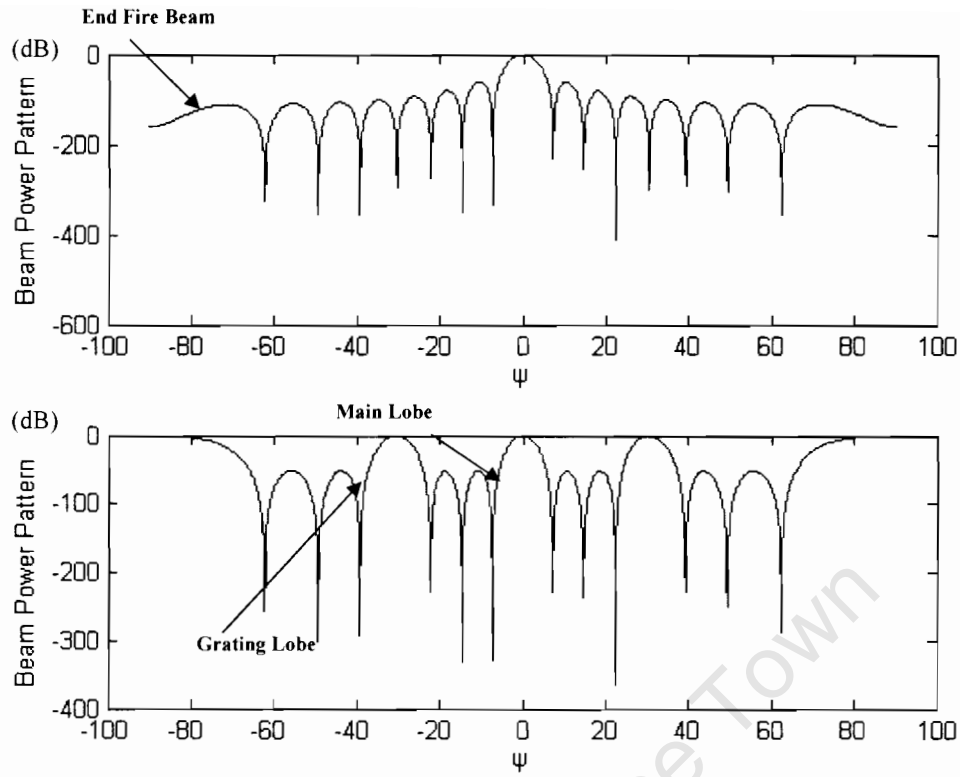

Figure 13: Beam Power Pattern when (a) $d < \lambda/2$, (b) $d > \lambda/2$

2.5 Interferometric

Assume that there are two arrays, which are laid out as shown below in Figure 14:

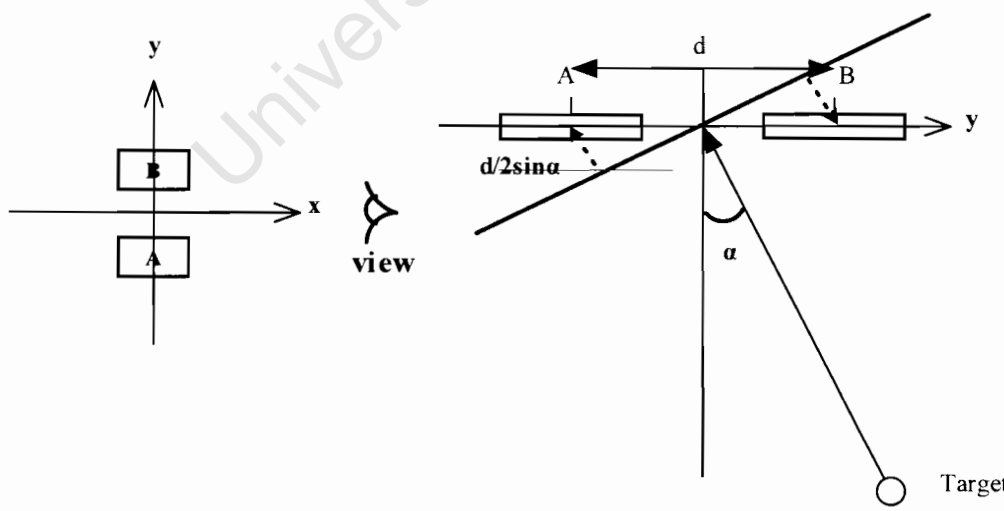

Figure 14: Illustration of interfermetric concept

Since the two arrays are parallel to each other, the echo signal received by the transducers of the two arrays is the same. Assuming that the signal at mid-point between the elements is $S(\alpha)e^{j\omega t}$ [4], the signals received at elements A and B are:

$$y_a(t,\alpha) = s(\alpha)e^{j(\omega t - \frac{\pi d \sin\alpha}{\lambda})} \tag{19}$$

$$y_b(t,\alpha) = s(\alpha)e^{j(\omega t + \frac{\pi d \sin\alpha}{\lambda})} \tag{20}$$

The difference between the two signals is confined to the electrical phase difference caused by the displacement of the two arrays and the angle of arrival, α. The phase difference between the two elements is

$$\Delta\psi = \frac{2\pi d \sin\alpha}{\lambda} \tag{21}$$

$\Delta\psi$ can be found by subtracting the phase of signals y_a and y_b

$$y_\Delta = y_a(t,\alpha)y_b(t,\alpha)^* \tag{22}$$

Combined with Equation 21, it will therefore become

$$\frac{Im[y_\Delta]}{\mathrm{Re}[y_\Delta]} = \tan(\Delta\psi) = \tan\left(\frac{2\pi d \sin\alpha}{\lambda}\right) \tag{23}$$

$$\tan^{-1}\left(\frac{\mathrm{Im}[y_\Delta]}{\mathrm{Re}[y_\Delta]}\right) = \Delta\psi = \frac{2\pi d \sin\alpha}{\lambda} \tag{24}$$

The angle of arrival may be calculated from

$$\alpha = \sin^{-1}\left(\frac{\Delta\psi\lambda}{2\pi d}\right) = \sin^{-1}\left(\tan^{-1}\left(\frac{\mathrm{Im}[y_\Delta]}{\mathrm{Re}[y_\Delta]}\right)\frac{\lambda}{2\pi d}\right) \tag{25}$$

2.7 Summary of the Chapter

Chapter 2 briefly described all the theoretical background of the relevant signal processing techniques such as the pulse compression method, beamformer and interferometry. In the discussion, a special phenomenon called grating lobe is discussed. This phenomenon is caused by the spacing between each transducer element and limits the angle of scanning. All these concepts and factors will be used to derive the image formation algorithm described in Chapter 3.

Chapter 3

ABACUS Signal Processing

In the previous chapter, the theoretical signal processing was described. In this chapter, a development of the ABACUS signal-processing program written in Matlab will be described. Matlab was used both to simulate sonar signals and also to develop the signal processing algorithms which were applied to both simulated and real data. A separate program, written in the Delphi language, was developed to replace the old DOS base Pascal data logging software which used to interfere to the SONAR hardware and to capture data. The Delphi data capturing software will be discussed in Chapter 4.

This chapter starts with the co-ordinate system used in this dissertation. This will lead to the discussion of the ABACUS image formation algorithm. The discussion includes the pulse compression, the range compensation for spreading loss, the beamforming and interferometric algorithm proposed for resolving number of targets with a counting volume. The results of Matlab simulation will be shown.

3.1 The ABACUS Co-ordinate system

There are three co-ordinate systems used in the ABACUS system. These three co-ordinate systems are shown in Figure 15.

The coordinate systems are as follows:

- **Transducer coordinate system**

The origin of the transducer array model is defined at the centre of the two receiving array. This co-ordinate system measure the fish location with respect to the centre of the transducer and it is depicted in Figure 15.

- **Ship co-ordinate system**

This ship co-ordinate system is corresponding to the location of the transducer header with respect to the centre of the ship.

- **Global co-ordinate system**

This co-ordinate system corresponds to the location of the ship in respect to the global aspect.

In this dissertation, only the transducer co-ordinate system is considered in the implementation of the ABACUS Matlab software. The other two co-ordinate system will be considered in future development.

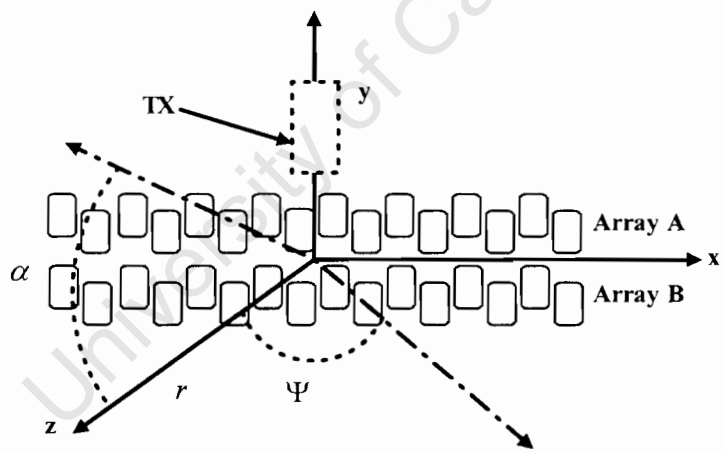

Figure 15: The co-ordinate system of the ABACUS Model

3.2 The ABACUS signal processing algorithm in Matlab Simulation

This section is going to discuss all the concepts and theory used to implement the Matlab simulation.

3.2.1 Signal Detection in Noise

The digital echo received is noisy and most of the desired signals are masked by noise; a typical unprocessed down range profile is shown in Figure 17a below[1]. To detect the signal in noise, a linear filter which can maximize the peak signal to noise ratio is required.

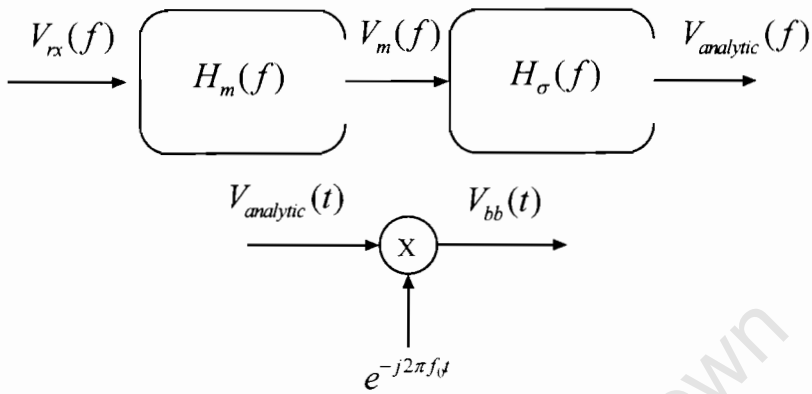

Figure 16: The Matched-Filtering Model

The matched filter $h_m(t)$ discussed in Chapter 2 is suitable for this purpose. Its model is illustrated in Figure 16. The frequency domain receiving signal $V_{rx}(f)$ is passing through a matched filter for compressing the signal. The resulting matched signal $V_m(f)$ is then passing through a filter $H_\sigma(f)$ to eliminate the negative part and form the analytic signal $V_{analytic}(f)$. The analytic signal is inverse transform back to time domain and shift the signal to baseband by multiplying $e^{-j2\pi f_0 t}$. The basebanded signal $V_{bb}(t)$ is resulted.

The output of the matched filter is

$$v_m(t) = v_{rx}(t) \otimes h_m(t) \tag{26}$$

where

$$h_m(t) = v_{rx}^*(-t + t_m) \tag{27}$$

[1] This data was captured in the tank at the Institute of Maritime Technology. The parameters of the chirp signal used in the experiment: B = 10 kHz, K = 1.5 x 10^6, T = 7 ms and f_0 = 420 kHz.

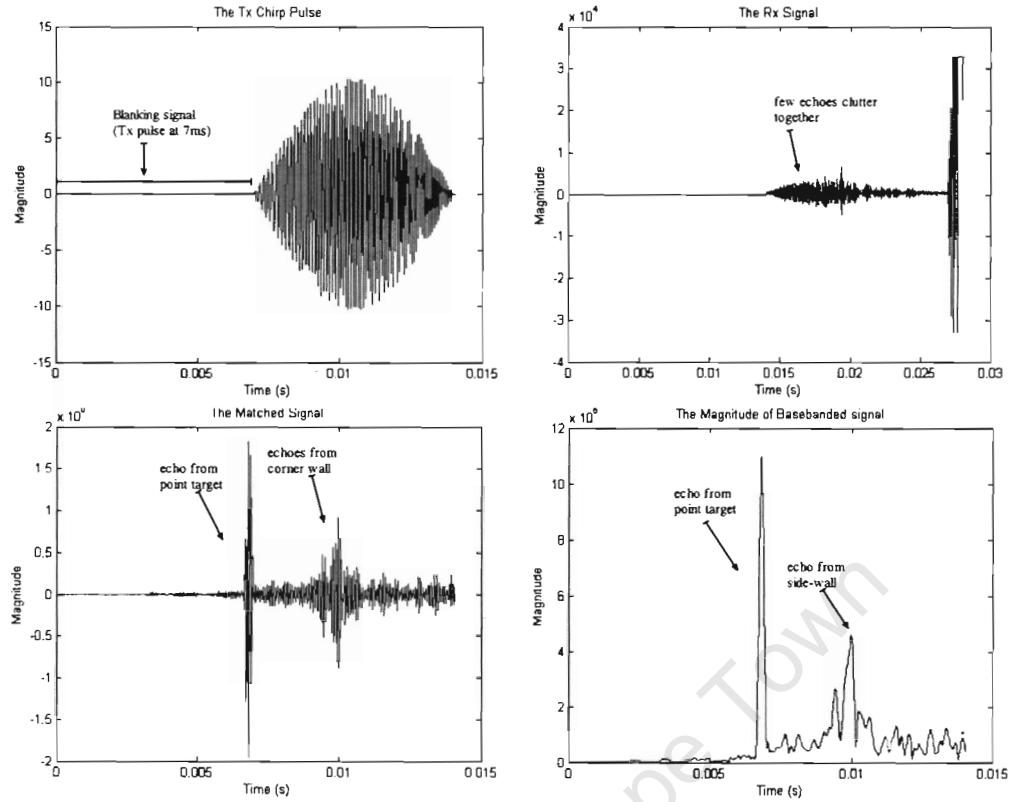

Figure 17: Practical experiment of matched-filtering of point target response from IMT Calibration Experiment result

As in Equation 27, the matched filter used to compress the receiving echo is the conjugate of the transmitted signal (Figure 17a). This filtering action applied to one channel of ABACUS is shown in Figure 17 above.

The transmitted chirp pulse used in ABACUS during this experiment is shown in Figure 17(a) - note that a hanning window (square-rooted) is applied to the chirp pulse. Figure 17(b) shows a return echo from a point target cluttered with other echoes from the water surface and the walls. Figure 17(c) shows the response after the matched filter. As one can see, the resulting signal contains a visible high frequency component related to the centre frequency of the spectrum.

The basebanded analytic version of matched signal is then obtained by zeroing the negative frequency components in the spectrum, inverse transforming to the time

domain, and then multiplying by the factor $e^{-j2\pi f_0 t}$. The relationship is in the time domain as expressed as

$$V_{bb}(t) = \left(V_m(t) \otimes h_\sigma(t)\right) e^{-j2\pi f_0 t} \tag{28}$$

The magnitude of $V_{bb}(t)$ is shown in Figure 17(d). The magnitude of the analytic signal shows the *envelope* of the matched filtered signal in its un-basebanded form (Figure 17(c)). The resolution of the target is approximately 1/B where B is the bandwidth of the transmitted pulse. It is noted that sidelobes are not visible as a result of the hanning window taper applied to the transmitted pulse.

3.2.3 Range compensation

As the acoustic pressure wave propagates outward from the source, the acoustic intensity reduces with respect to the distance. The spreading loss (l_s) is related to the inverse square law.

ABACUS is phased array sonar which the transmitted transducer is an array of 16 elements all driven together by the same signal. A drawing of the layout of the transducer elements is shown in Figure 3.

In very near field, the radiation pattern is uneven due to the superposition action of each transducer element. This is also why the inverse square law cannot be correctly applied in the near field range. As mentioned in Chapter 2, k is a range dependent function in the far field where $k \to 20$.

The spreading loss l_s suggested by Rodney F.W. Coates is only an approximation. To accurately compensate for the transmission loss, it is best to simulate the degradation of the acoustic intensity with respect to range. One thing to note, however, is that the simulation is only concerned with the transmitter array since it is the source of the acoustic pressure.

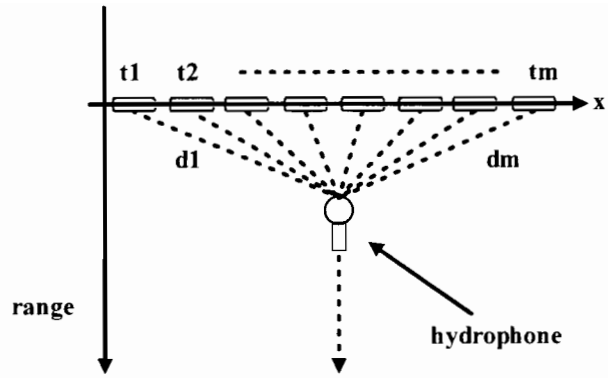

Figure 18: A setup for modeling spreading loss. Note that the microphone is moving away from the transducer array.

To model a more realistic spreading loss, the hydrophone signal level can be simulated as it moves away from the transmitter array as depicted in Figure 18 above. The signal level of the hydrophone with respect to range $V_{spread}(r)$ can be calculated as

$$V_{spread}(r) = \sum_{i=1}^{M} (1/d_i(r)) e^{\frac{-j2\pi d_i(r)}{\lambda}} \tag{29}$$

where the distance $d_i(r)$ measure from the transducer elements to the hydrophone is

$$d_i(r) = \sqrt{(x_{hyrdrophone}(r) - x_i)^2 + (y_{hydrophone}(r) - y_i)^2 + (z_{hydrophone}(r) - z_i)^2} \tag{30}$$

The variables $x_{hydrophone}(r)$, $y_{hydrophone}(r)$ and $z_{hydrophone}(r)$ are the (x, y, z) position of the hydrophone and x_i, y_i and z_i are the (x, y, z) position of the transducer elements.

The result is shown in Figure 19, for the particular case where r is the distance along a line perpendicular to the centre of the array. On the same Figure, a $\frac{1}{R}$ curve is also shown for comparison, where M is the number of transducer elements. From the Figure 19, the deviation between the more realistic spreading loss and the 1/R spread loss is quite significant before 10m; the two curves converge at approximately 15 m with little difference between the two graphs thereafter. Note that simulation only

focuses on the bore sight. The off bore sight compensation has not been investigated and is left for future work.

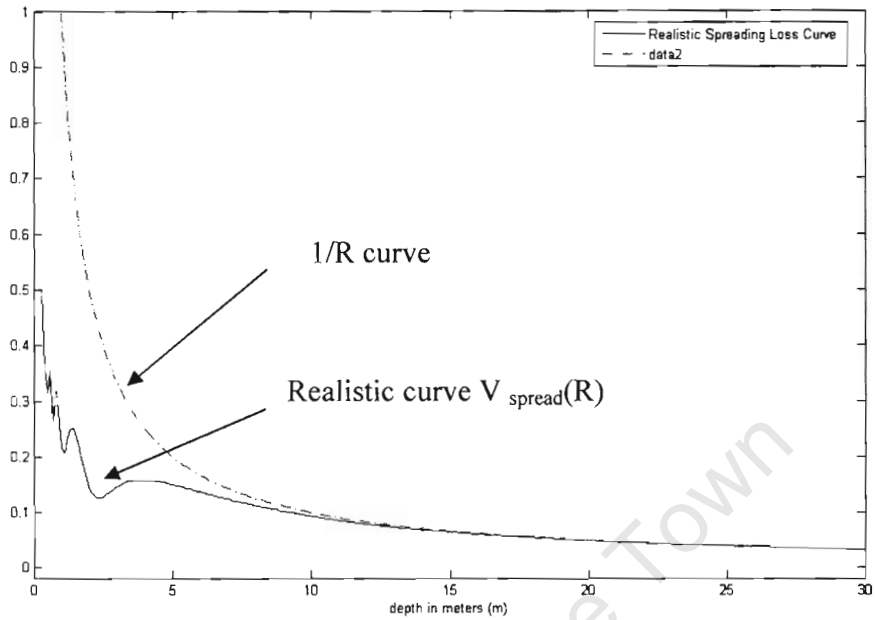

Figure 19: The realistic curve for signal level at the target obtained by simulation and the original 1/R approximation.

From the new result $V_{spread}(R)$, the received signal will vary as a function of range (incorporating both attenuation and spreading in both directions) according to

$$V_{TL} = K\frac{1}{R}\bullet V_{spread}(R)\bullet 10^{-\frac{2\alpha R}{20}}\bullet\frac{1}{M} \tag{31}$$

where R is the range, M is the total number of transmitter elements, αR is the attenuation loss discussed in Figure 2.1.3 and K is a constant. In the transmission loss equation, the $V_{spread}(R)$ described the energy loss for transmitted signal and the 1/R is describing the energy loss for the receiving echo.

3.2.4 Beamforming Algorithm (beamforming.m)

Recall the delay and sum beamformer introduced in Chapter 2, it is a far field approximation beamfomer.

$$y(r,\Psi)=\sum_{i=1}^{M} v_i(r+d(i-1)\sin(\Psi))e^{\frac{j2\pi d(i-1)\sin(\Psi)}{\lambda}} \tag{32}$$

Equation 32 assumes that all the targets are located in the far field range where the arrival wave can be approximated as a plane wave. The reason for the initial far field estimation is this method is very fast. The trade off of this approach is that it only works beyond a certain range.

A concern that arises relates to what occurs if a target is close to the transducer such that the acoustic wave cannot be approximated as a plane wave over the length of the array. This concern is addressed in the following section.

3.2.4.1 Close field approximation vs Far field approximation

Richard O, Nielsen [4], clearly outlines the effect of the wave curvature due to a close field target. His discussion is summarized below.

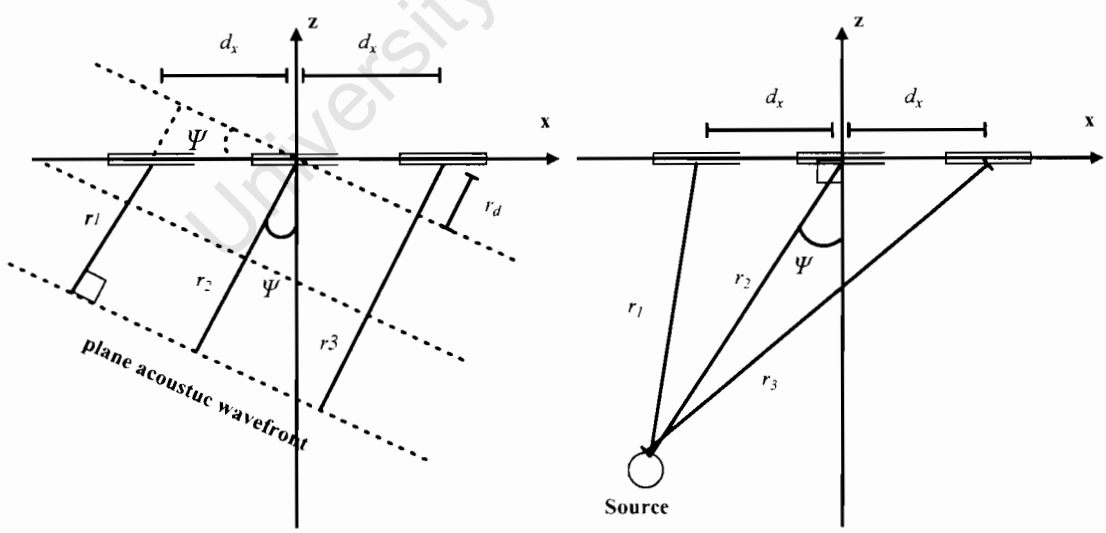

Figure 20: a) This is the illustration of the far field acoustic wave-front. [4] b) This is the illustration of

the close field acoustic wave-front.

Assuming the acoustic wave can be approximated as a plane wave as shown in Figure 20a). The difference in range is r_1

$$r_1 - r_2 = r_d = -d_x \sin\Psi \tag{33}$$

where the symbols are defined in 20.

Figure 20b) illustrates if the acoustic wave-front is not a plane wave. For this case

$$r_1 - r_2 = r_d = d_x^2 + r_2^2 - d_x r_2 \sin\Psi - r_2^2 \tag{34}$$

and

$$r_d = \sqrt{\left(1 + \frac{d_x^2}{r_2^2} - \frac{d_x \sin\Psi}{r_2}\right)} r_2 - r_2 \tag{35}$$

Then since $r_1 >> d_x$, Equation 35 can be approximated as

$$r_d = \left(1 + \frac{d_x^2}{2r_2^2} - \frac{d_x \sin\Psi}{2}\right) r_2 - r_2 \tag{36}$$

$$r_d = -\frac{d_x \sin\Psi}{2} + \frac{d_x^2}{2r_2} \tag{37}$$

Note that, in Equation 37, the first term $-\frac{dx \sin\Psi}{2}$ corresponds to the plane wave approximation. The second term $\frac{d_x^2}{2r_2}$ corresponds to the wave-front curvature. If the target is located in the far field region, where $r_2 \gg d_x^2$, the second term can be

ignored. However, if the target is located in the close field region, the difference between d_x^2 and r^2 becomes significant.

3.2.4.2 Modification of delay and sum beamformer

Recall the relationship between the far field range (S) and the length of the transducer array (D) from Section 2.4.2

$$S = \frac{D^2}{\lambda} \tag{38}$$

For the ABACUS system with D = 0.237m and λ = 0.0036m, by applying Equation 38, S is calculated to be 15.6 m. Therefore any target located before 15.6m is considered as a close field target, and any target beyond is considered as a far field target. In order to correctly focus on targets both in the close field and the far field target certain modifications are required for Equation 37.

In the far field approximation the phase is purely a function of arrival angle, Ψ. For the close field approximation, the phase is a function of both the target arrival angle, Ψ, and the target location in range. A matrix M_p which contains each distance between the transducer elements and the predicted target location is pre-calculated by simple distance equation depicted in Equation 30. The modified delay and sum beamformer is

$$y(r,\Psi) = \sum_{i=1}^{M} v_i(r + r_d) e^{\frac{j2\pi r_d}{\lambda}} \tag{39}$$

where

$r_d = M_p$ for close field region

$r_d = d(i-1)\sin\Psi$ for far field region

To illustrate the importance of this modification, the azimuth cross section of a focused target at 5.2 m has been plotted in Figure 21 using data captured during the IMT calibration experiment, using both the close field approximation and the far field approximation. It is clear that there is significance improvement by using a far field beamformer to focus any close field target.

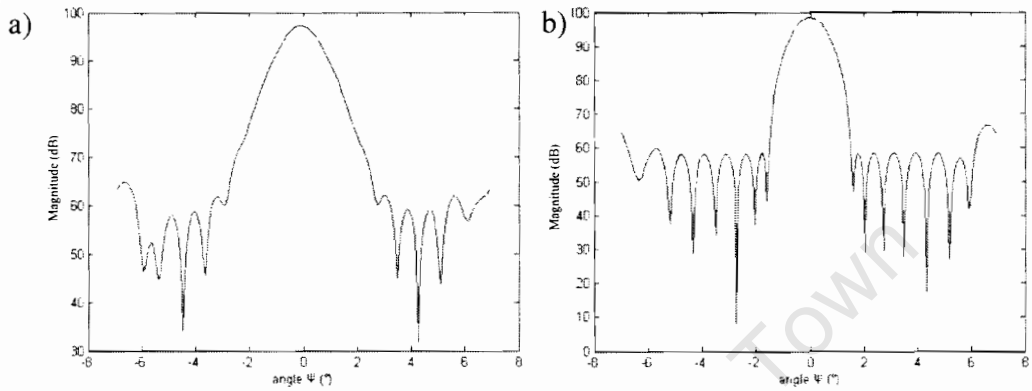

Figure 21: The Cross Section of the measured point target response of a tungsten ball at 5.2 m from IMT of:

a) a target located at close distance but using far field approximation.

b) a target located at close distance but using the close field approximation.

3.2.4.3 Interpolation modified delay and sum beamformer

The scanning angle is determined by the illuminated fan beam and the beamwidth of the receiving elements. The element spacing is chosen such that the lobes are greater than this beamwidth by design. The spatial scanning angle is limited to 14° due to the elevation angle of the transmitter beam and the grating lobes effect. Therefore it is necessary to know how many beams are required to cover the scanning angle. The receiver 3dB beamwidth of the ABACUS system is 1°. It therefore requires 14 beams in order to obtain sufficient spatial coverage.

Recall in Equation 27, that the delay for each sensor is given by $t_d = \frac{d_x \sin\Psi}{c}$. The time shift is limited by the sample spacing.

$$t_d = \frac{n}{f_s} \qquad \text{where } n \in \mathbb{R} \tag{40}$$

The angular sample spacing, ϖ_s is

$$\varpi_s = \sin^{-1} \frac{cn}{d_x f_s} \tag{41}$$

By using the sampling frequency of ABACUS, ϖ_s is calculated to be 120.5°. This means that within the scanning angle, only one sensor signal out of sixteen can be correctly delayed and summed. The other 15 signals are shifting in a non-sample spacing; this will cause beam pattern degradation or so called scalloping loss [13].

A typical acceptable scalloping loss is

$$L_{scalloping} \leq 3dB \qquad \text{at Main Response Axis (MRA)} \tag{42}$$

To minimize the scalloping loss, an increase in sampling frequency is required. The sampling frequency can be increased by the interpolation technique, which was introduced in Appendix D.

3.2.3.4 Windowing function for side-lobe reduction

After the interpolation beamformer, a shading window can be applied to each sensor signal to reduce the spatial sidelobe at the expense of broadening the mainlobe. There are many shading windows and they are tabulated below:

Weighting function	**Peak Sidelobe (dB)**	**Mainlobe width (relative)**	**Sidelobe decay Function**
Uniform	-13.2	1.0	$\frac{1}{t}$
$0.33+0.66\cos^2\left(\frac{\pi f}{B}\right)$	-25.7	1.23	$\frac{1}{t}$
$\cos^2\left(\frac{\pi f}{B}\right)$	-31.7	1.65	$\frac{1}{t^3}$
Taylor ($\bar{n}=8$)	-40	1.41	$\frac{1}{t}$
Dolph-Chebyshev	-40	1.35	1
$0.08+0.92\cos^2\left(\frac{\pi f}{B}\right)$ Hamming	-42.8	1.50	$\frac{1}{t}$

Table 1: Various Shading Window Equation [18]

The Dolph-Chebyshev function was chosen for its significant sidelobe reduction whilst still minimizing mainlobe broadening. The Dolph-Chebyshev polynomials are defined by the following Equations

$$T_n(x)=\begin{cases}\cos(n\cos^{-1}x) & |x|\le 1;\\ \cosh(n\cosh^{-1}x) & |x|>1;\end{cases} \tag{43}$$

where

$$T_0(x)=1,\quad T_1(x)=x \tag{44}$$

$$T_n(x)=2xT_{n-1}(x)-T_{n-2}(x),\qquad n\ge 2 \tag{45}$$

Figure 22 below shows the results of applying different window functions, such as uniform, hanning, hamming and Dolph-Chebyshev shading window, to the recorded tungsten ball target response at 5.2 meter away from the transducer head.

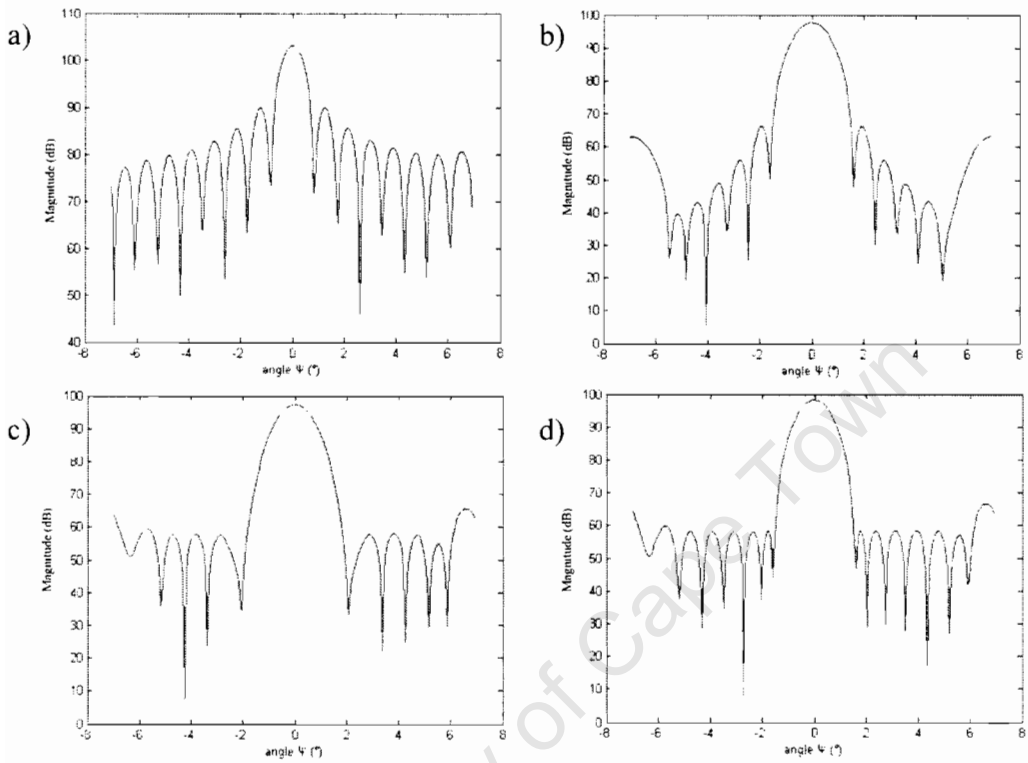

Figure 22: The resulted beam pattern of various shading Window function:

a) Uniform
b) Hanning
c) Hamming
d) Dolph-Chebyshev

The result shown in Figure 22 verified that Dolph-Chebyshev function has the best performance compared to Hanning and Hamming. The Hanning window gives a high sidelobe response with an acceptable mainlobe broadening. The Hamming window gives a low sidelobe response, but with a much wider mainlobe response. The Dolph-Chebyshev has the best sidelobe response but with increased mainlobe broadening.

In his paper, Peter Lynch [18] clearly analyses the performance of the Dolph-Chebyshev function and in text book [4], the author has also recommended the Dolph-Chebyshev function as the optimal window for detecting weak targets in the presence of strong targets. In order to separate closely spaced targets of similar strength, a uniform window is preferred. Since return echoes from fish vary significantly depending on target type, size and orientation, a window function should be used in practice with the ABACUS system.

3.2.3.5 Block diagram of the modified interpolation beamformer

In Figure 23, the flow diagram of the modified interpolation beamformer algorithm is shown. The compressed signal of each channel is first interpolated by the factor D; the signal is then passed through a close field approximation phase shift module which processes images in a range from 0 m to S m. Record Equation 38, S is dependent on the length of the array. If only 8 elements are used, S will be smaller and vice verse.

The region between S m to maximum meters is then processed by far field approximation. At the end, all signals will be shaped by a weighting window before summing them up and passing through a low pass filter to eliminate duplicate components. More discussion on interpolation and anti-imaging filters can be found in Appendix D.

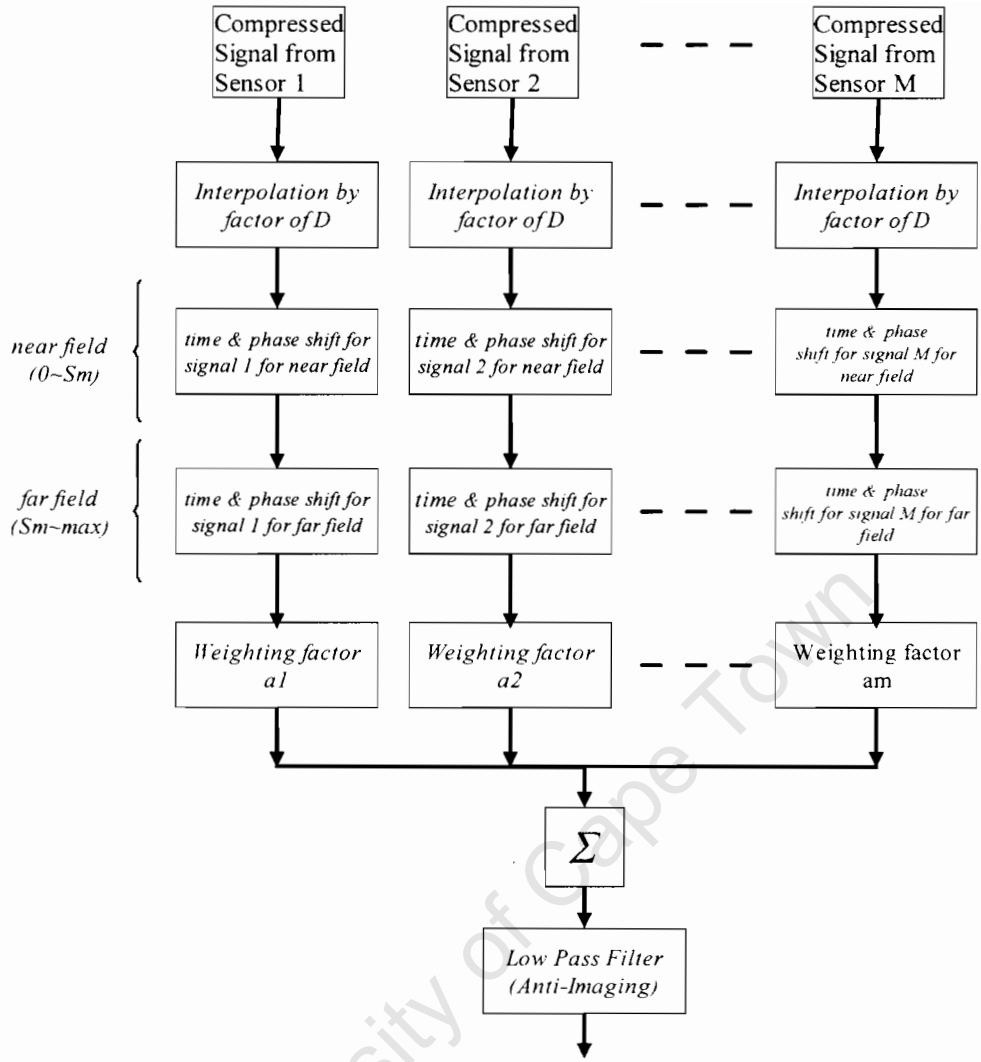

Figure 23: Modified Beamformer Flow Diagram

3.3 Interferometry

As mentioned, in Chapter 2, interferometry can be used to differentiate between a target in the main transmitter beam (1 deg by 10 deg), and one which is in the sidelobes of the beam in the "cross-receiver-array" direction (i.e. $\alpha>+0.5$ or $\alpha<-0.5$deg in Figure 15). The spacing between the two receiving arrays in the y-axis is 0.02m which is greater than the half-wavelength "element spacing requirement" as specified in Equation 18. The ambiguous angle spacing is $\arcsin(\lambda/d) = 10.2$ degrees, at which the sidelobe levels of the transmitter beam should be well down; the receiving element beam should also offer some suppression at this angle and beyond.

For each detected target, the phase difference can be calculated and used to infer the direction of arrival α. Targets for which $\alpha>0.5$ or $\alpha<-0.5$ are discarded, as they are not in the counting volume. This technique is used to make sure that the number of targets within a counting volume (i.e. the main lobe of the transmitter beam) is accurate.

A simulation has been written to prove the concept of interferometry and the result is shown in the following image in Figure 24.

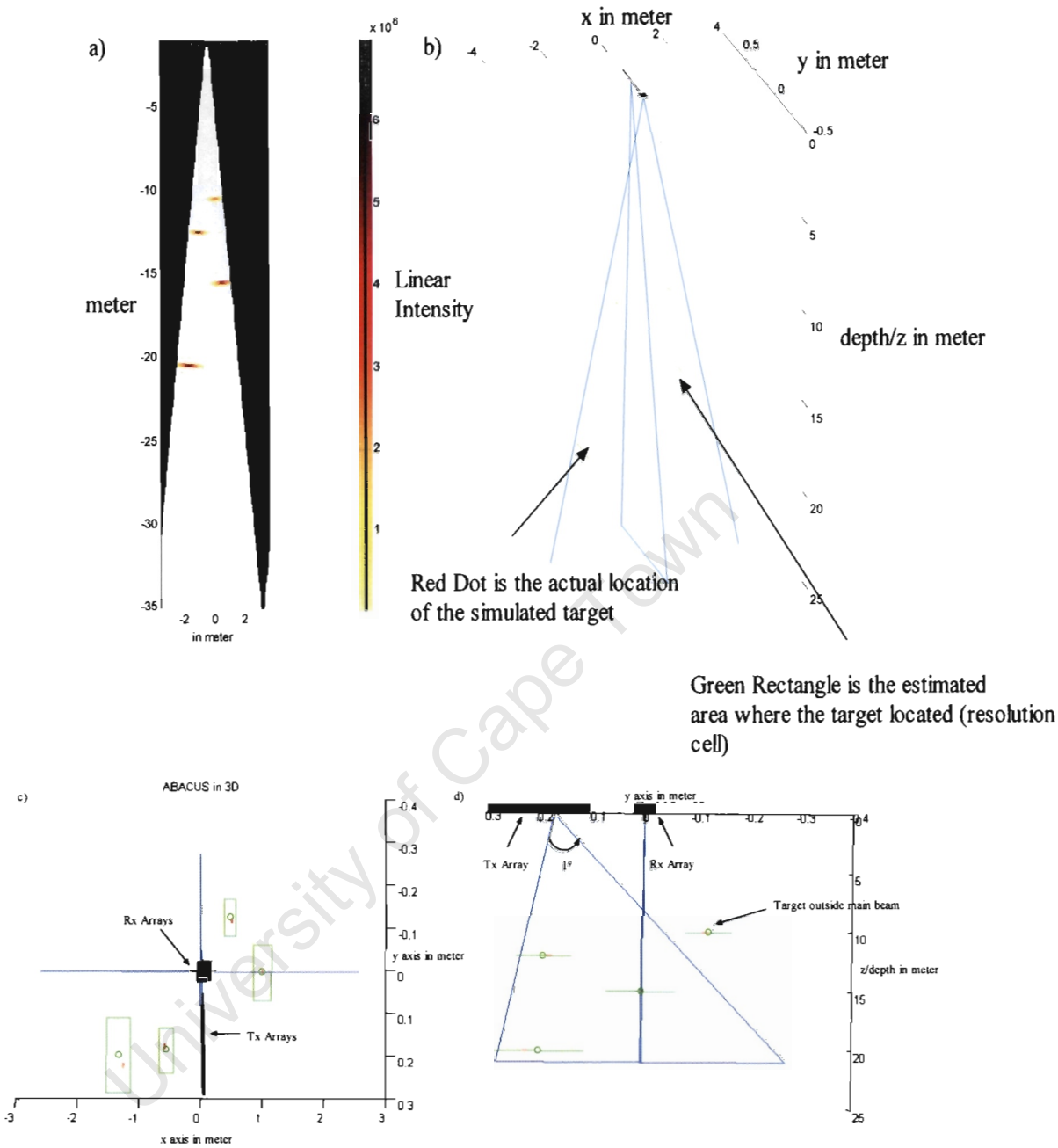

Figure 24: The simulated target location and the result of interferometry from various angles: (a) fan beam image with four targets (b) 3-D view (c) top view showing targets intentionally displaced from the x-axis to be in the sidelobes of the 1deg transmitter beam spread (d) side view looking in the x-direction.

y direction, (i.e. targets at some non-zero α angle will still appear in the fan beam image). The target at 10m range is actually out of the main lobe of the transmitter beam in the α direction.

By using Equation 25, one can deduce the targets' angle of arrival α ("in the y direction"). If α angle of arrival is outside of the main lobe of the transmitter beam, the detected target is in the sidelobes and should be eliminated from the counting process. To prove that the interferometry can deduce the angle of arrival in α direction, Equation 25 is applied to the simulated results in Figure 24a, allowing targets to be located in spherical coordinates (R, α, ψ).

The result of interferometry is shown in the Figure 24b (3-D view), 24c (top view), 24d (y-z plane view). The red dot is the actual location of the simulated target and the green rectangular block is centred on the estimated target location, obtained by interferometry. The target at 10m located outside the main lobe is a sidelobe response and should be eliminated. These simulations verified that interferometry can allow one to deduce the position of the targets in α direction.

3.4 The ABACUS Matlab Data Processing Algorithm

This section discusses the overview of the required input files and the algorithm of ABABUS Matlab data processing algorithm program. The flow graph is illustrated in Figure 25.

3.4.1 Input file for the ABACUS Matlab software

There are three input files that must be required to be placed in the same directory as the ABACUS software. They are as follows:

- **ABACUS setup file (setup.m)**

This is a setup file for the ABACUS software. It stores the system parameters, such as carrier frequency and bandwidth. The user can enter the preference setup parameters for the visual display including, for example, the display area, log or linear scale etc.

- **ABACUS data files (*.dat, *.tim)**

This is the binary file. It stores the ABACUS transducer digital echo data collected by the Delphi data capturing front end. The Delphi software will be discussed in Chapter 4. There are two formats of the data file; the extension "tim" is created by the old Pascal software and the extension "dat" is created by the new Delphi software. These two format structures can be found in Appendix A.

- **ABACUS transducer model file (transducer.m)**

This transducer model file stores the co-ordinates for each transducer element. This information is important in the beamforming process; this aspect is discussed in Section 3.2.4.[2]

3.4.2 ABACUS data processing algorithm

The flow graph of ABACUS data processing algorithm is shown in Figure 26. Each process is discussed below:

1. *Input Files*

   Three inputs are required for the software. They are the setup file which consists of all the settings such as the depth display or which window function is used etc. The transducer model contains the transducer element position and the ABACUS files contain the data set that was captured during the sea trial or the calibration experiment.

2. *Pulse Compression Module*

[2] This data was captured in the tank at the Institute of MariTime Technology on 22nd of Oct, 2004.

The signal data will then be extracted from the file and stored in memory. The signal passes through a matched filter module which then compresses the data and increases the signal to noise ratio.

3. Range Compensation

A bore sight only range compensation curve will then be applied to the data set to compensate for the spreading loss. This curve has been simulated and is shown as red curve in Figure 19.

4. Phase and Time Compensation Module

The data set will then pass through another correction factors module. This module is used to correct the phase error due to the inaccuracy of the element position and the gain error due to the variation of the amplifier. The phase and gain corrections factors were obtained from the IMT calibration experiments and will be discussed in more detail in Chapter 5.

5. Beamformer Algorithm

The data set will then pass through the Beamformer that was discussed in section 3.2. The resultant data set will then pass to the display module which will render the image into a suitable format.

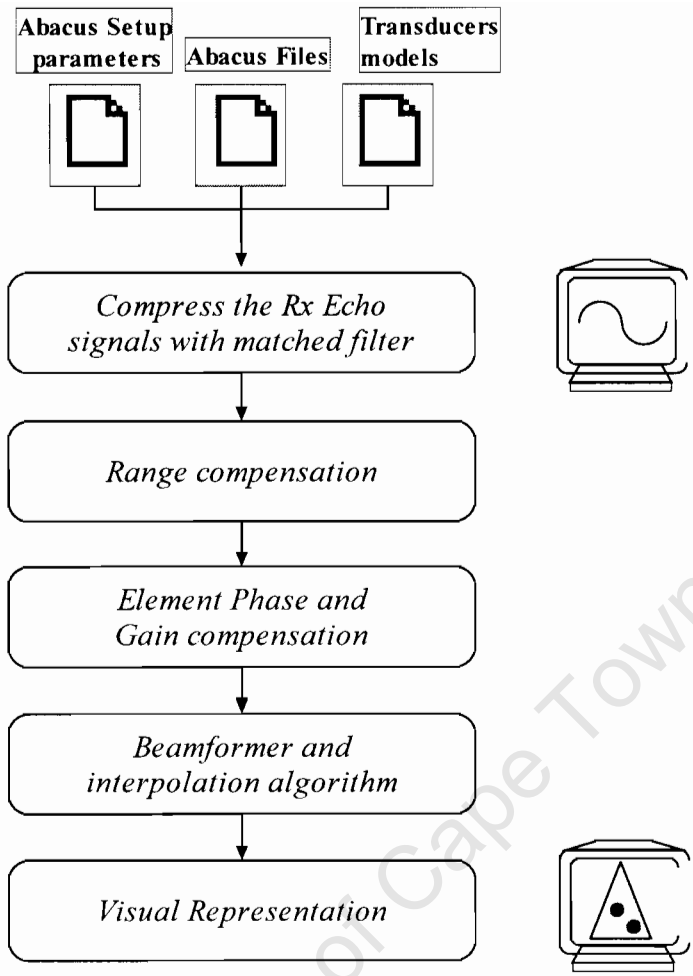

Figure 25: An algorithm used to implement the Matlab software for ABACUS processing real data set

3.5 Summary

This chapter discussed the co-ordinate system used in this dissertation and the algorithm used to implement the Matlab image formation software for ABACUS. The discussion includes various shading windows, spread loss compensation and beamforming and interferometric algorithm. This algorithm is also build into the Delphi data capturing front end, which will be discussed in the next chapter.

Chapter 4

Delphi Data Capturing Front-End

The original data capturing system, developed in the mid 1999's was written in Borland Turbo Pascal and ran in a DOS environment. Pascal is a language, which works under a 16-bit DOS OS environment. Commonly used Microsoft Windows is a 32-bit OS, and the present Windows 2000 and XP are not based on DOS OS, therefore certain commands in the original Pascal code that communicate with the Parallex DSP cards would not work. The original Pascal software was limited in functionality and extensibility, and an improvement in the existing program was therefore essential to take advantage of features offered by a modern OS.

The possibility of continually adding features onto the existing software has become limited since Borland has unfortunately already stopped maintaining Pascal. Therefore with respect to future developments, a new development environment is clearly required. Borland's new generation of Pascal, Delphi 7, was selected for the following reasons:

1) Delphi is the next generation of inheritance of Pascal, which simplifies the process of translation of the existing code.
2) Delphi is one of the industrial standard 32-bit compilers.
3) Delphi supports a useful GUI development environment.

This chapter will describe the criteria for designing the new software. It will then lead to the discussion of the development, the structure of the program and its features.

4.1 Criteria for the software development

The basic requirements for the ABACUS system are listed below.

- All processing and graphical display updates must be completed within one second, corresponding to the desired ping repetition rate.
- It must work in all versions of the Windows environment.
- A client-server model builds in to the system.

4.1.1 Background of the ABACUS hardware

ABACUS was originally developed in mid 90's with a 100 MHz PC. The original intention was to use dedicated DSP processing, on ISA cards, developed by Peralex in mid 90's, at a time when PC's were too slow.

In 2003, PC power had reached sufficient speed to allow all processing to be done on PC. The problem however, was that we needed a PC with ISA slots, and the only one available was an old 300 MHz PC. Although this was used this MSc project for data capture, it was considered a bit slow for real time processing.

The solution was to use two PCs: one being the 300 MHz PC purely for data capture; the second being a modern 2.8 GHz PC for signal processing and display. The two PCs would be linked via Ethernet for data transfer.

4.1.2 Problems encountered during the development.

There were a few problems encountered during the development of the software that had to be solved. They are as follows:

1) Insufficient space in normal PC Case for DSP ISA slot

The two DSPs are based on ISA slots with a circuit board piggy backed onto it. Therefore a case with two ISA slots far enough apart was required. The ISA bus standard has now been replaced by the faster PCI bus and recent motherboards only come with a one or two ISA slots positioned right next to each other.

2) Limited CPU resources

Due to above mentioned limitation, the most powerful PC available was a 300 MHz AMD K6 with sufficient space for the two ISA DSP cards. For a real time system, the resources are quite tight.

3) Microsoft disabled Windows I/O Port Access

The driver written in Pascal, which talks to the DSP cards has to rewritten in Delphi because of the recent versions of Microsoft Windows (including Windows 2000 and Windows XP) have a restriction on the I/O port access. If anyone attempts to access any port in any Windows NT environment, a privileged instruction exception will occur as shown below in Figure 26:

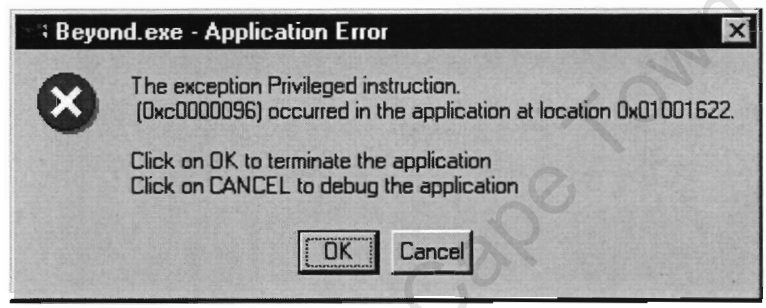

Figure 26: An error message shown when the old Pascal program runs in a Windows NT, 2000 or XP

This exception is caused by un-trusted software trying to access the supervisor mode or trying to access trusted software. Trusted software, such as kernel module, is a piece of software which has been carefully written and debugged, and conversely un-trusted software is software that has not been through such careful analysis and its correctness cannot be depended upon. In recent computers, such as 80486s or Pentiums, in order to enforce this resources isolation and prevent conflict, a mode bit has been incorporated to distinguish between supervisor and user instructions and port access falls under user mode.

Under Windows NT, if an I/O instruction is executed, the OS will first check the mode bit to see if it is privileged enough to access the ports. If it is valid, the instruction will be executed immediately, otherwise, the processor will check the I/O

permission bitmap. If the port's bit in the I/O permission bitmap is disserted, which means it has permission to access the port, the instruction will be executed also. On the other hand, if it is asserted, a privileged instruction exception will occur.

The difference between Windows 98 and Windows NT is the I/O permission bitmap. In Windows 98, the I/O Ports are disserted, which means it will gain permission to any request for port access. For security reasons, in Windows NT, only the supervisor mode can access ports. If anyone wants to access the port, there has to be a driver running in kernel mode to execute the I/O port access on behalf of the user mode software. [14] had a more detail discussion on how the OS operated..

As a result, a very useful function called "port" had to be removed from any version of Delphi after version 1.0. Unfortunately, the two DSP cards (Falcon and SIP) drivers originally written in Pascal relied heavily on this function to access the DSP cards. The following section will discuss the approach used to eliminate this problem.

4.2 Enable the Windows I/O Port Access

To fix the privileged instruction exception, a two step approach was required.

4.2.1 Step one: modify Windows NT/2000/XP OS

There are two solutions for allowing the Falcon and SIP DSP cards driver to work correctly in all versions of Windows.

1) One approach would be to re-write the device driver for the ABACUS system running in supervisor mode. Unfortunately, the writer does not have enough information on the two DSP cards.
2) Another approach would be to manipulate the I/O permission bitmap in the OS, which gives the I/O permission for accessing a specific port. .

4.2.2 Step two: implement a port access function in Delphi

As mentioned earlier, Delphi had not included any I/O port function since Delphi 2. One therefore has to implement one`s own Delphi version of port access function in

low-level assembly language. This would allow the old Pascal driver to work on the new Delphi environment with minor modifications.

4.3 Design and structure of the software (Block Diagram)

The hardware used in the structure included two PC stations (PC01 for data capture and PC02 for signal processing and display) and the ABACUS System Hardware. The overall structure layout is shown in Figure 27. The design of the ABACUS software is divided into two parts:

- The PC to ABACUS Hardware section.
- PC to PC section.

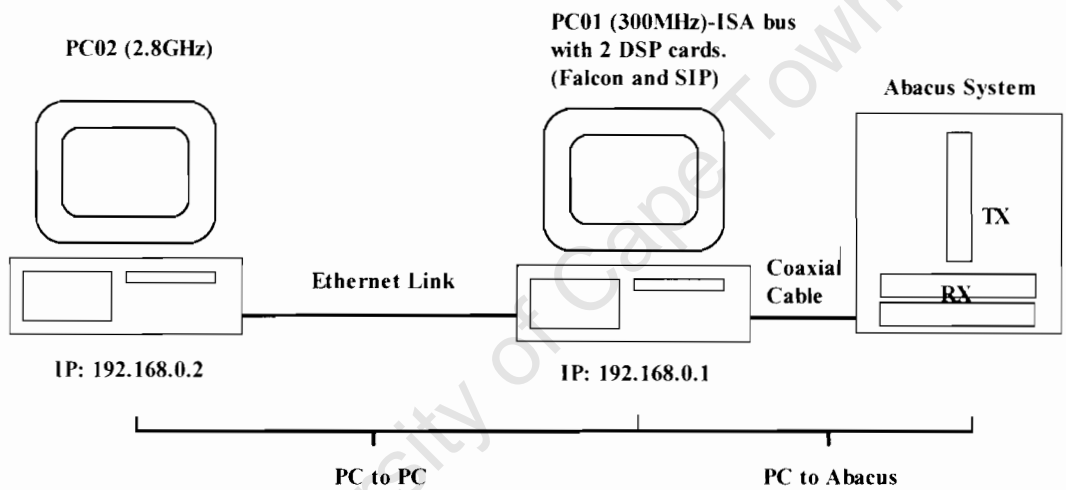

Figure 27: The connection setting of the ABACUS system

4.3.1 Data Capturing Server

PC01 is a data server shown in Figure 28, which listens on port 12000 for any control request from PC02. The motherboard of PC contains two ISA slots for the two DSPs cards (Falcon and SIP), which it uses to pass information from or to the ABACUS system. The Falcon card is responsible for generating the time varied gain (TVG) control signal and transmitted chirp pulse. The SIP card is responsible for receiving the digital data stream from the 16 data logging cards in the ABACUS system through the TAXI chip and storing them in the SIP card's memory.

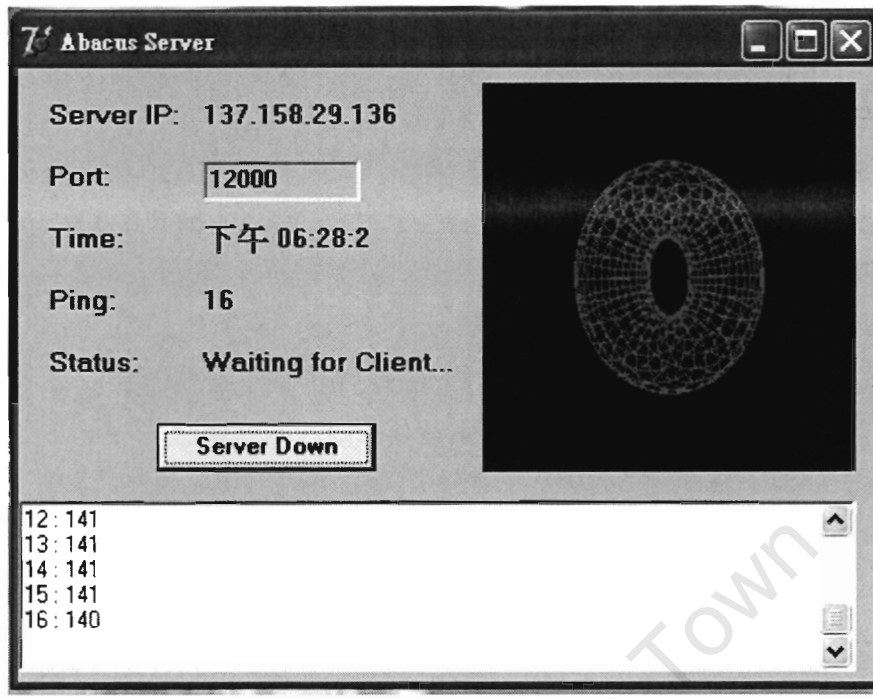

Figure 28: The Delphi Capturing Server Front-end

The data server builds on top of a DSP interface component, which is used to communicate with the two DSP cards. Two functions within the DSP interface component "TriggerFalcon" and "ReadAbacus" are used respectively to trigger the hardware to send out a chirp pulse and to collect digital echo data from the hardware respectively.

When the PC01 server starts up, it preloads the chirp pulse data, TVG data and gain setting into the Falcon DSP card's internal memory. If the server receives a control message for data capturing, it calls the TriggerFalcon function to tell the hardware to send out a chirp pulse. Immediately, the ReadABACUS will be executed and echo data will be collected. All the collected echo data will then be routed to the client program through the Ethernet for further data processing and visual representation.

4.3.2 Data Processing Client

The data processing client resides in PC02 and is responsible for signal processing, visual representation, system controlling and data capturing (File format can be found in Appendix C).

System controlling

A new protocol layer was implemented on top of the network layer (TCP) for communication between the ABACUS server and the client. It provides services to the application layer such as:

- Passing hardware control commands (e.g. changing the gain setting) between server and client.
- Passing the received echo data from the ABACUS server to the client application as shown in Figure 29, a complete stack is shown in Figure 32.

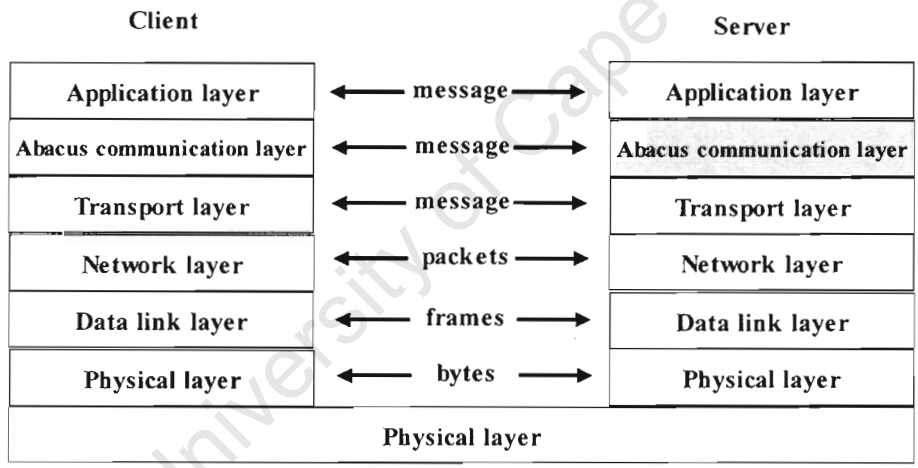

Figure 29: The communication stack between the ABACUS server and client

- **Signal processing**

The PC02 sends out an ABACUS triggering command message to PC01 in fixed time duration (e.g. every second). The ABACUS echo data collected by PC01 will send back to PC02 through Ethernet connection. The received data matrix in PC02 will pass to the signal-processing unit. The signal processing unit (SigProcTools.pas)

implements the algorithm discussed in Chapter 3. This unit will then compress the signal and carry out the beamforming. Since Delphi has not got a built in FFT library, the software developed used the FFT component written by Nils Haeck [14].

The beamformed matrix is then being passed to the visual representation unit for GUI display.

- **Visual representation**

The client program shown in Figure 30 and 31 allows the user to view two kinds of signal representation: a raw linear display and a polar display.

The plot display allows the downrange profile to be viewed. The plot display makes use of plotting components in a library created by Mat Ballard [15]. The plotting component has a built in zoom and an auto-scale function.

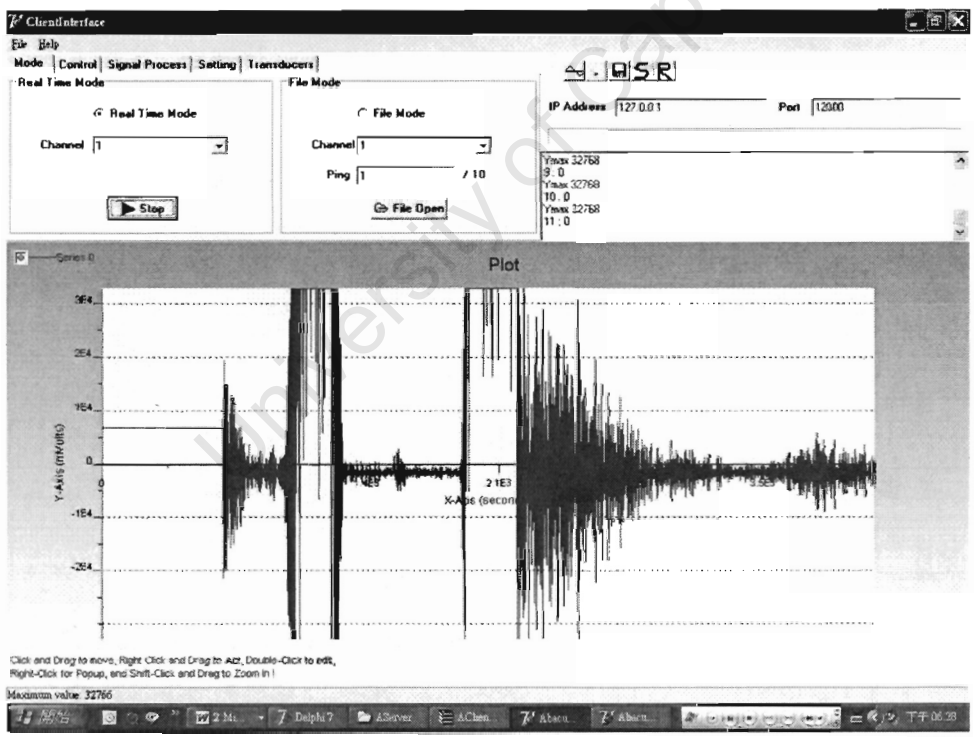

Figure 30: The Delphi Data Capturing Client Front-end in raw linear display

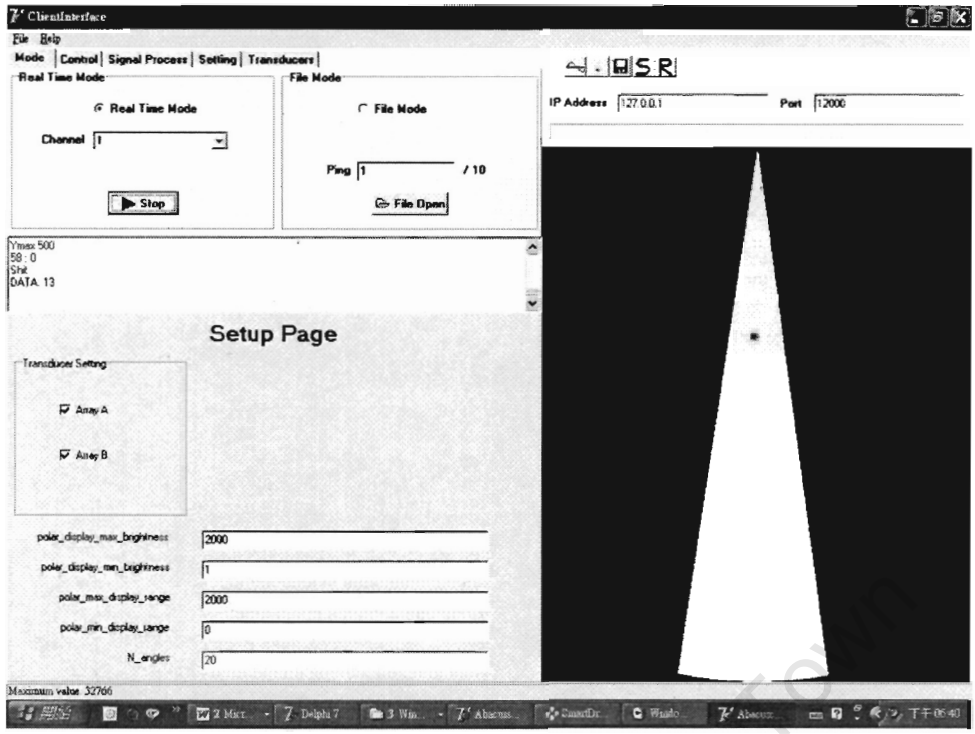

Figure 31: The Delphi Data Capturing Client Front-end in beamformed polar display

The polar plot was implemented using the OpenGL graphical engine. The OpenGL interface library is hardware independent and has direct interfacing with the graphics hardware, which makes drawing of both 2D and 3D graphics more efficient. Although at the moment, only 2D figures have been created. For future development, OpenGL allows further 3D development. More snapshot of the program can be found in Appendix D.

4.4 The advantages of Server-Client architecture

There are two advantages with this dual PC structure:

1) Since PC01 is a bottleneck due to the limited resources for a data processing environment, by sharing the workload between the two PCs, the bottleneck can be opened up, achieving a system with better performance.

2) The Ethernet uses Internet standard IP as a transport protocol and this increases the compatibility and extendibility of with the system. It can also extend across the platform server to communicate with any client interface. There is another MSc research project concerned with implementing a C++ client interfacing with Delphi server for data capturing and hardware control.

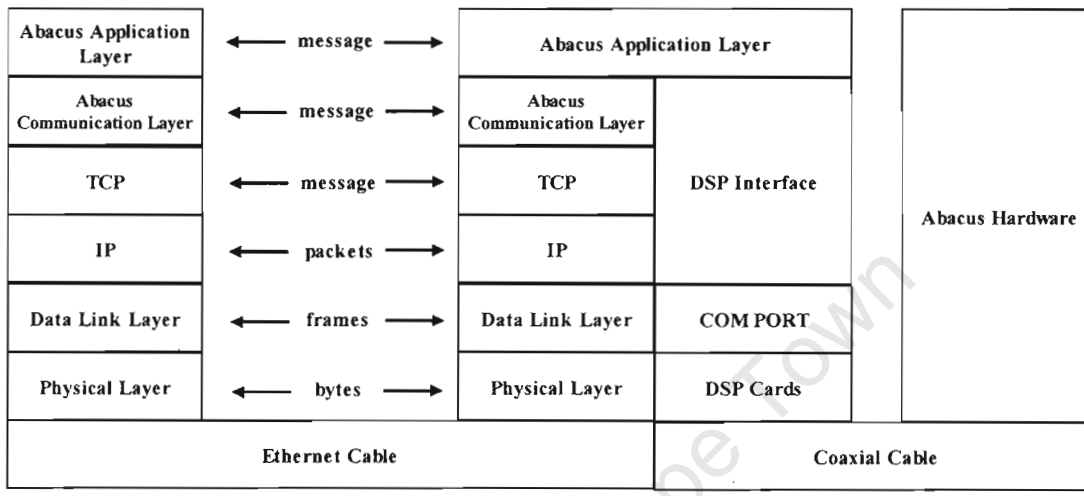

Figure 32: A complete stacks of the Delphi ABACUS capturing software

4.5 Summary of the Chapter

This chapter outlined the architecture and essential problems experienced during the Delphi software implementation. Some snapshots of the software are also shown. The architecture makes use of the client and server model, which removed the performance bottleneck of processing power in the underpowered hardware interfacing PC. This software was used in various calibration trials and sea trials, which will be discussed in Chapter 5 and 6.

Chapter 5

IMT Tank Calibration Experiment

On the 22nd of October, 25th of October and 2nd of November 2004, three tank measurements took place at the Institute of Maritime Technology in Simons Town, Cape Town. The set-up of the experiment is illustrated in Figure 34 and a photograph shown in Figure 33. The aim of this calibration exercise was to obtain measurements in a controlled environment, which would then allow the performance of the system to be studied as well as the transducer response. This chapter will start with the limitation of the experiments in the IMT tank. It will then lead to the methods for deriving phase and gain correction factors for each transducer elements. Finally the improvements resulting from the compensation factors will be shown.

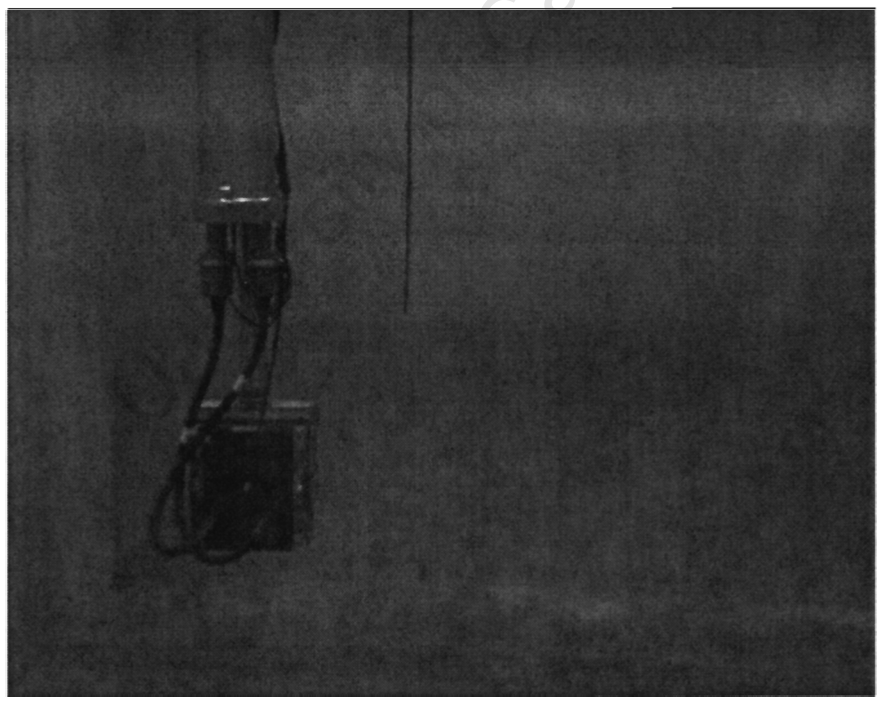

Figure 33: A photo from IMT shows the setting of the ABACUS system and the tungsten ball

5.1 IMT Tank Measurements Setup

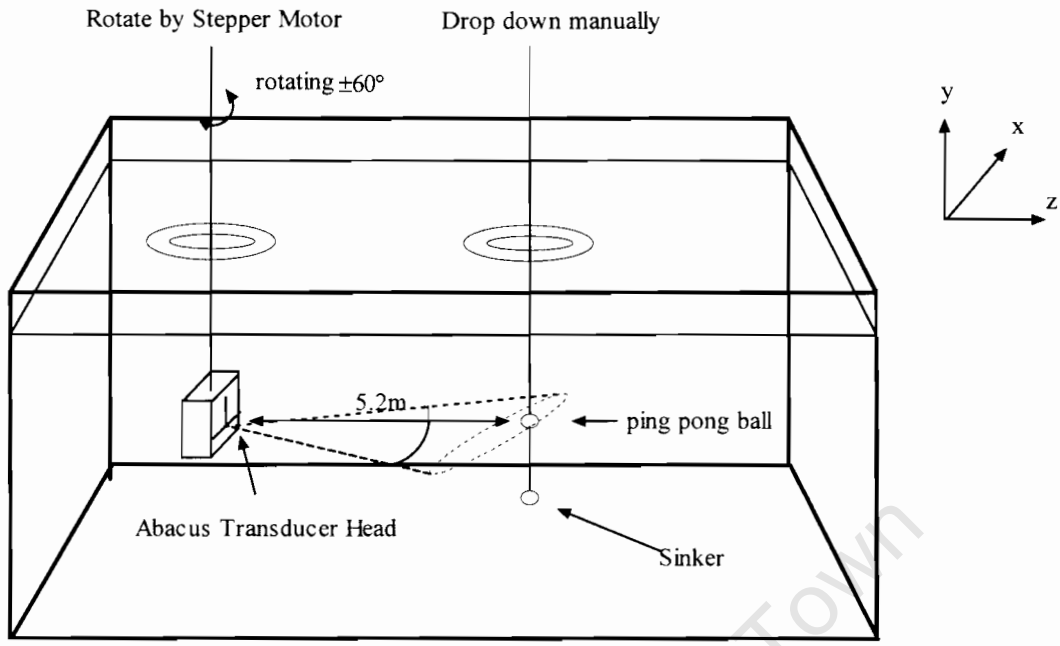

Figure 34: IMT tank calibration setup

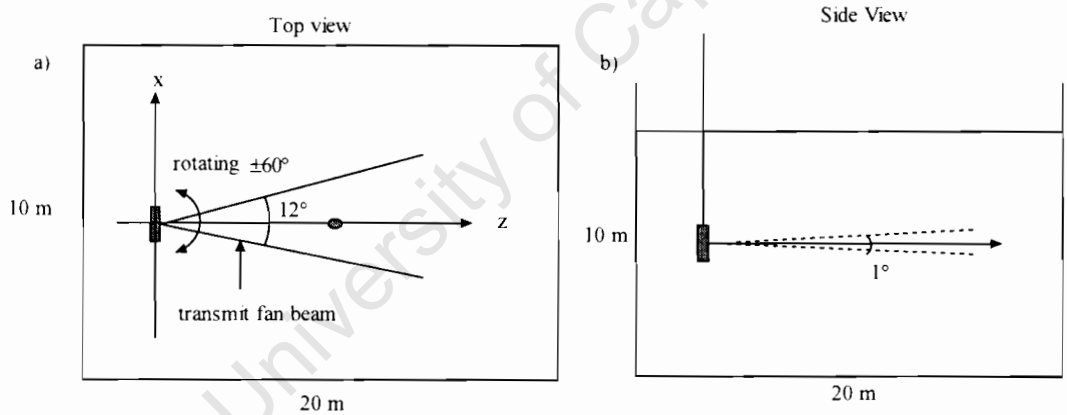

Figure 35: The side view and top view of the IMT tank calibration setup

The basic layout of the tank is shown in Figure 34 and Figure 35. The dimensions of the IMT tank are 20m x 10m x 10m. The ABACUS transducer head is attached to a stepper motor which allows the transducer head to scan the transducer horizontally within ±60° angle in steps of half a degree. During the tank measurement, only one array B was activated, the array A was not used. There were two kinds of point target

used in this measurement, a ping-pong ball (diameter = 4cm) and a tungsten ball (diameter = 4 cm). The two "point" targets were suspended using 0.6 mm monofilament fishing line and a sinker was suspended several metres below the ping-pong ball, which was manually dropped down to the desired position.

5.2 The Limitation of the calibration experiments

During the measurement, the point target was manually lowered to the desired depth. Since the transducer head can rotate horizontally using the stepper motor, inaccurate positioning of the target in the horizontal plane is not a concern. The main problem is the location in the vertical plane.

The transmitter beam had a 3dB beamwidth of 1-degree elevation and 10-degree azimuth given by calibration [26]. According to the previous calibration on the ABACUS system by Runciman [26], the azimuth 3dB focused beamwidth is 1°. If the target is located at 5.2m away from the transducer face, the movable depth is ± 8 cm.

As mentioned previously, the ping-pong ball is 4cm in diameter. If the ball is off centre by ± 2 cm, the target will be out of the 3dB beamwidth, which means that a small movement will result in a large variation in target strength. In the case of the tungsten ball, the chance is the same since its size is relatively the same. To support the limitations mentioned above, the radiation pattern of the transmitter array, was simulated.

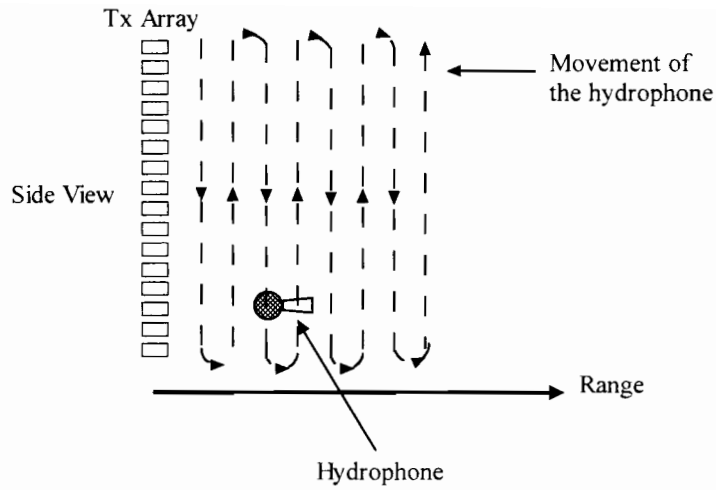

Figure 36: ABACUS transmitter array radiation pattern simulation setup

The simulation set-up is illustrated in Figure 36. The setting of the transmitter array is following the ABACUS set-up (such as element spacing, transmitter signal etc). This simulation is the extended version of the simulation for range compensation discussed in Section 3.2.3. The transmitted radiation level in voltage is collected by moving a simulated hydrophone around the area as shown in the above figure. The resulted radiation pattern matrix is then recorded and plotted in Figure 37 and 38. Note that the resulted radiation matrix is looking at the side view, which is the same perspective as Figure 35b and it is a dissection of the centre of the transmitter element.

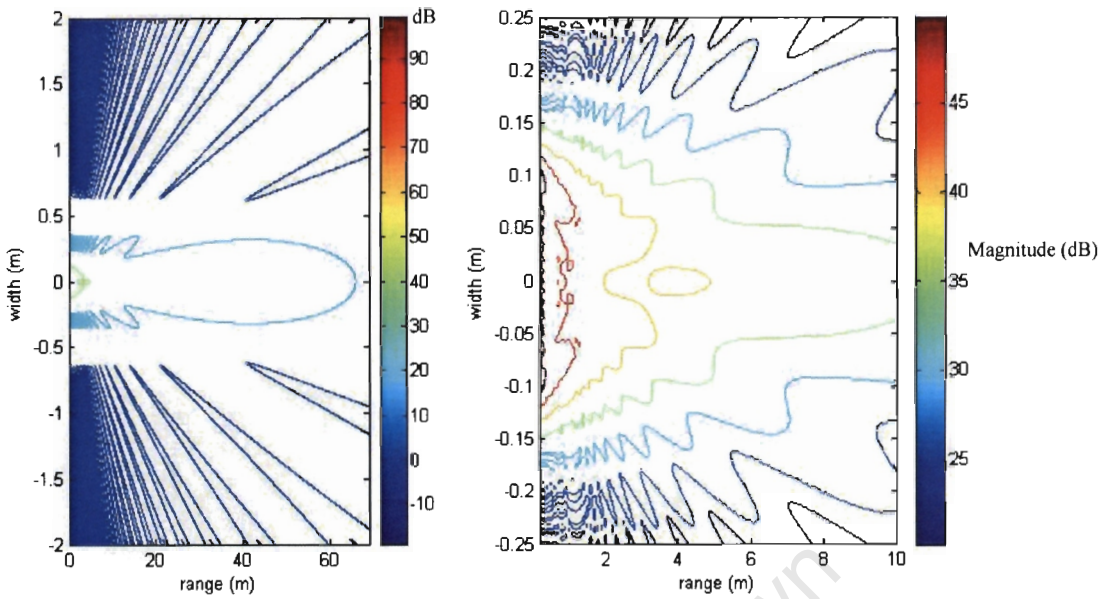

Figure 37: Simulated log scale beam pattern of ABACUS transducer during IMT Calibration

a) Overall Beam Pattern

b) Zoom into 0 to 10 m version of the beam pattern

Figure 37a is the radiation pattern in the area of 4m elevations x 70m in range. Since the calibration experiment only takes place in the range from 0m to 10m. A zoomed version of the radiation pattern is shown in Figure 37b. The irregular radiation pattern is the result of superposition of the radiation signal of the 16 elements.

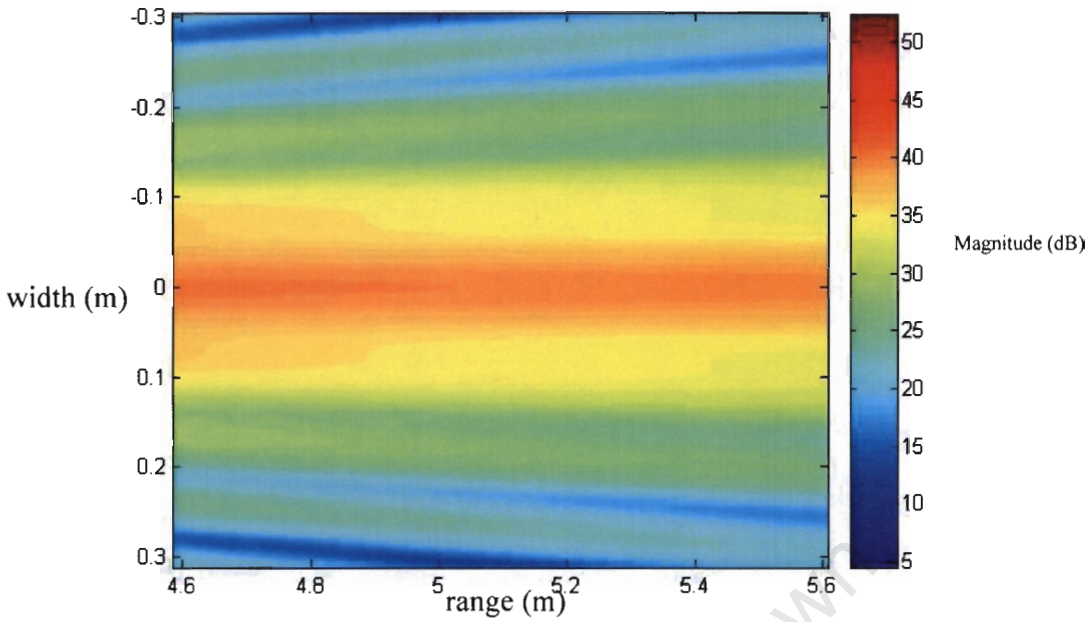

Figure 38: Zoomed Simulated log scale beam pattern of ABACUS Tx Transducer with colormap display.

As discussed in calibration setup in Section 5.1, the calibration target is located at 5.2 meters away from the transducer head. A zoomed version of the simulated transmitter radiation pattern at 5.2m is shown in Figure 38.

Another major problem experienced during with the tank experiments were interfering echoes from the sidewalls and corners of the tank. The down range profile of one of the IMT datasets is shown in Figure 39. The interfering echoes are clearly visible are limited the placement of point targets to within 5.2 meter of the transducer head.

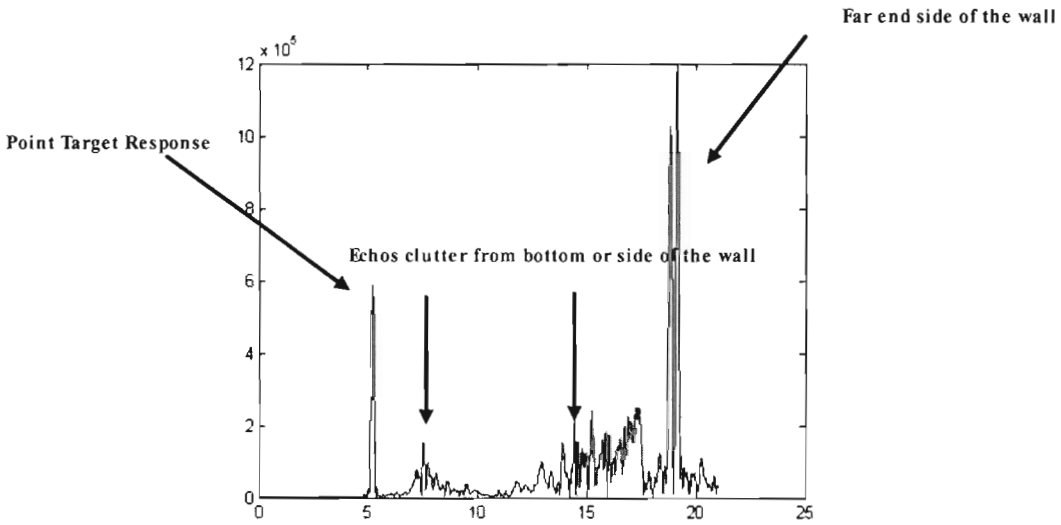

Figure 39: Range-compressed Down range profile of the data from IMT calibration experiment

Finally, the interferometric capability was not investigated during these experiments due to the fact that only one array was active, but this work was planned for a later date.

5.3 Phase correction of the transducer elements

The beamforming algorithm used in this dissertation assumes that the positions of the transducer elements are accurate. In the practical sense, nothing in the world is perfect, so when the transducer header is manufactured, the element position record in [28] will contain some tolerance. There will also be gain and phase mismatches in the receiver filter and amplifiers. This tolerance will affect the performance of the beamforming algorithm. Therefore the correction factor for each element for these errors must be found out.

5.3.1 The effect of target inaccurate positioning on phase response

Before discussing the phase correction factor determination algorithm, it is better to investigate the effect of different positions on the phase response. The receiver element layout is shown in Figure 40.

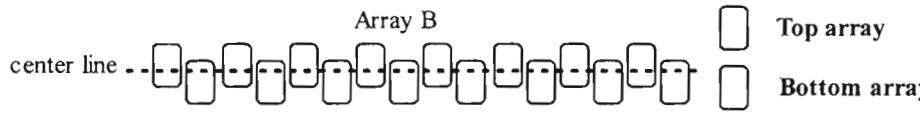

Figure 40: The arrangement of the receiver transducer array

Figure 40 illustrates the receiver element layout. As one can see, the elements are layout in a strange staggered fashion. The writer does not fully understand the reason for it and it could be a design error, which we cannot change without making a new head. A linear array would be preferable.

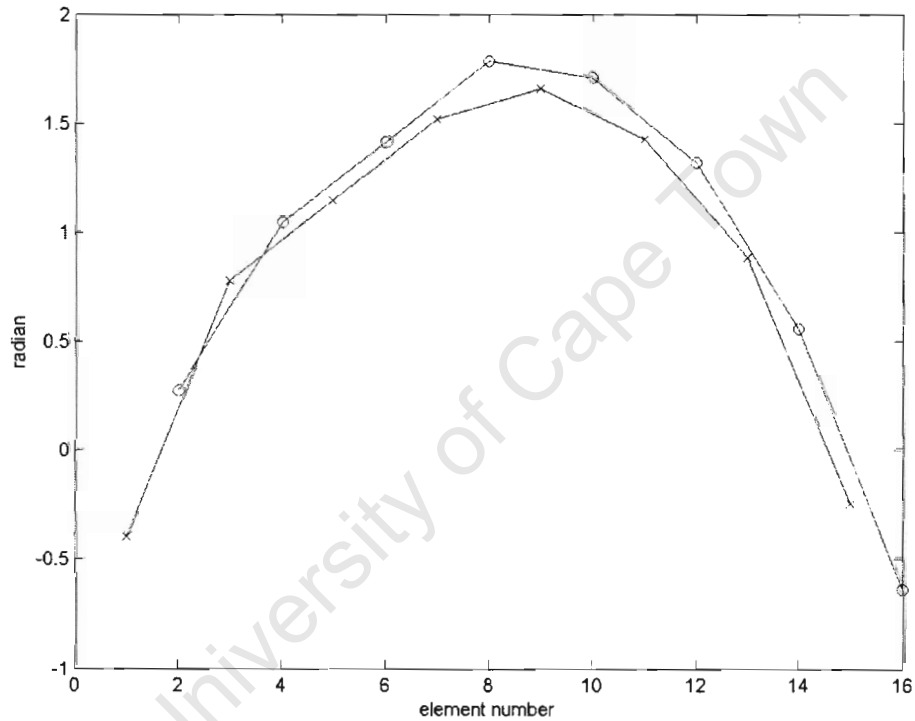

Figure 41: The measured phase of the ABACUS transducer element from the result of IMT

After studying the layout of the transducer, an experiment was carried out at calibration target was placed at the centre of the transmit beam 5.2m away from the transducer head. The phase of the resulted captured data set is shown in Figure 41. The 'crosses' line represents the top array (every 2nd element) and the circles line represents the bottom array.

With the same set-up used for the calibration experiment above, a simulation is implemented. Assuming that a simulated point target is located at 5.2 m, the theoretical phase response of array B is plotted in Figure 42a. In this figure, all points are precisely located on a hyperbolic locus (This is a result well known for linear array). In Figure 41 however, the measured phase of the top and bottom arrays is separated, and does not lie on a hyperbolic locus. The phases are also shifted downwards.

Figure 42b indicates the effect on the phase if the simulated point target is moved in the x-axis direction (horizontal displacement). Figure 42c shows the effect for displacement in the y-direction (vertical displacement), and 42d show the effect for displacement in the z-direction (increasing range). It is clear that the movement in the y and z directions will make the phase locus shift up and down, whereas horizontal displacement shifts the locus left and right.

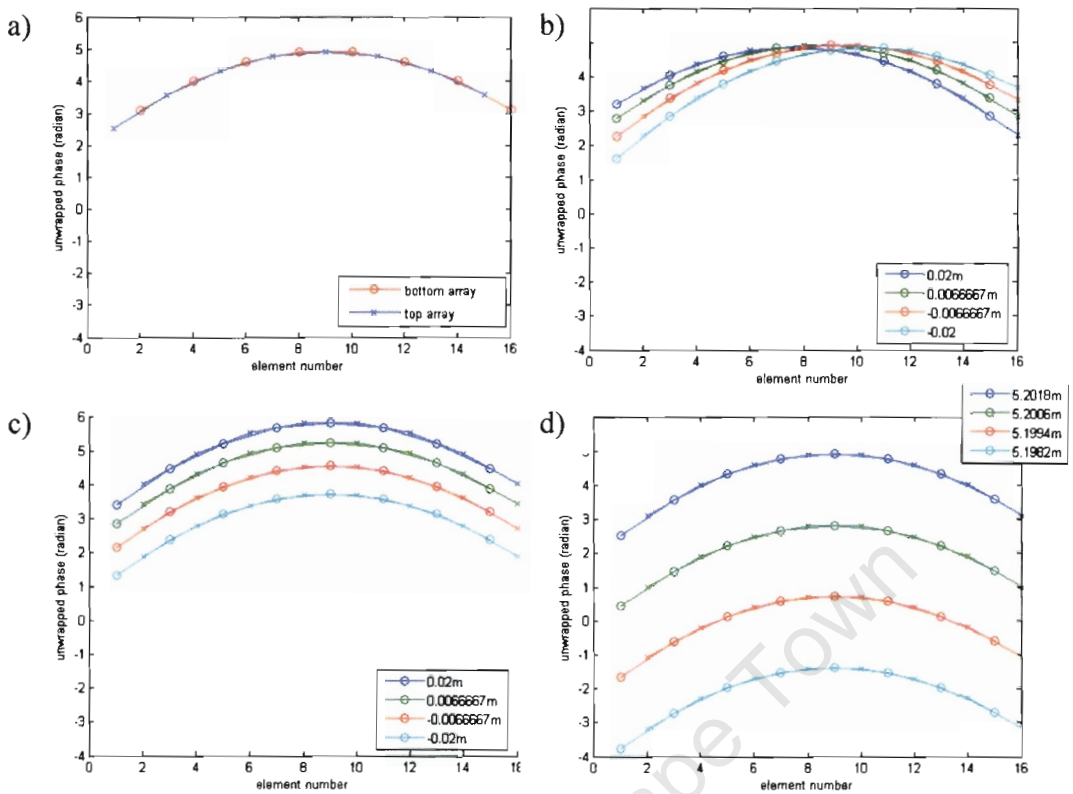

Figure 42: The simulated result of the effect of moving at x, y and z direction

a) The point target at the center of the beam

b) The point target is moving in x-axis.

c) The point target is moving in y-axis.

d) The point target is moving in z -axis.

5.3.2 Phase correction factor determination method

Since the beamforming algorithm relies on shifting all elements in phase and summing up the signal at the desired direction, it is necessary to make sure the phase response of each element is correct.

The phase correction factor can be found by calculating the difference between the predicted phase response (assuming the target location is known) and the actual phase response. The method of finding the phase correction factor is illustrated in Figure 43.

The method is simple. The real target response $V(p_{rx}, p_{pt})$ can be obtained by taking the measurements of a point target inside the 3dB beamwidth at position p_{rx} from the receiver element positions p_{pt}.

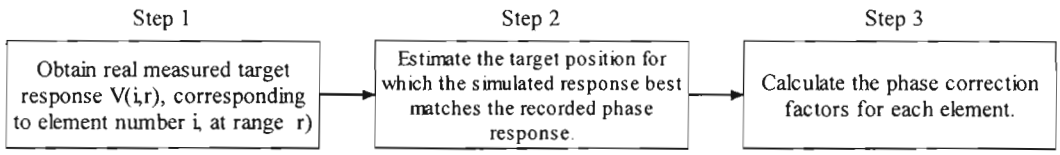

Figure 43: The flow model for finding the phase correction factors

As the true position of the point target is not precisely known, an iterative method [19] was derived in order to estimate the target position from the measured data itself. The target-positioning algorithm involved searching within a constrained search space being the dotted cube in depicted in Fig. 44 right diagram, to obtain the location for which the simulated phase response best matched the measured response.

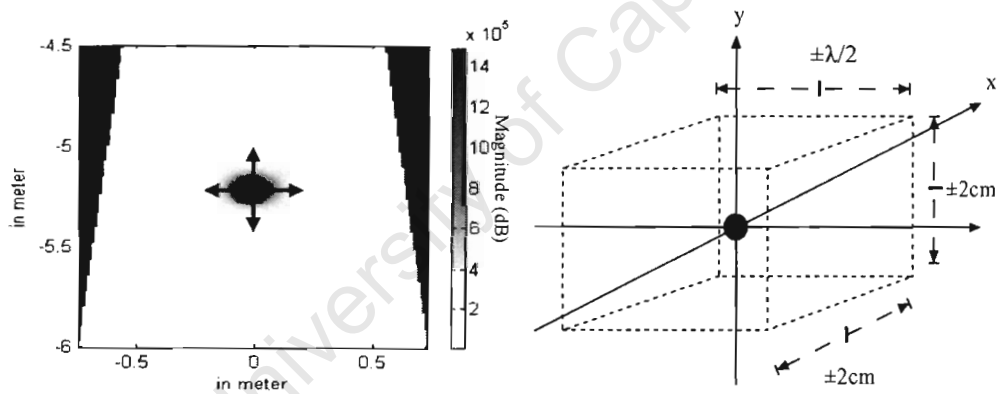

Figure 44: An illustration of the method of obtaining the phase compensation factors

The *magnitude* of the complex correlation coefficient (c) was used as a measure of fit.

$$c = \frac{\sum_{i=1}^{16}(V_i - \bar{V})(U_i - \bar{U})^*}{\sqrt{\sum_{i=1}^{16}|V_i - \bar{V}|^2 \bullet \sum_{i=1}^{16}|U_i - \bar{U}|^2}} \qquad (47)$$

where $0 \leq |c| \leq 1$

and Vi and Ui are the measured and predicted complex values for the i'th element.

The phase correction factors were then calculated as the difference between the measured results $V_1..V_{16}$ and the predicted phase values $U_1..U_{16}$.

By using the above method, the phase correction factors were estimated and are plotted in Figure 45. The phase errors were surprisingly low, with a worst case error of 0.18 radians, being just 2.9% of a wavelength. Such small phase errors would not significantly affect the main lobe, but some degradation in sidelobe level could result.

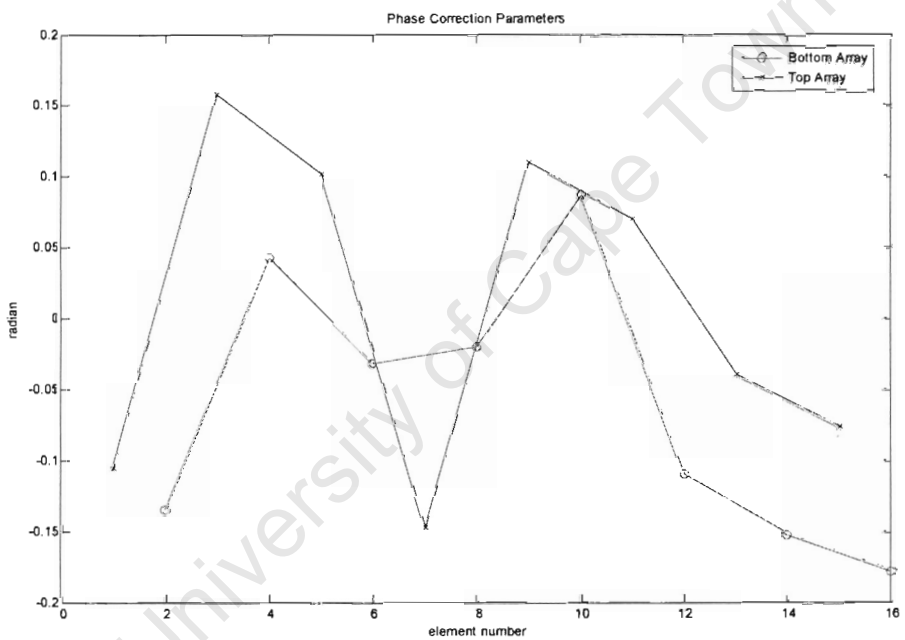

Figure 45: The resulted phase correction factors for ABACUS Receiving Array B.

In the following sections, the effect of this phase correction factors and the gain compensation factors will be shown and discussed. Section 5.4 it will first look at the application of phase compensation to the set of experimental results set. It will then lead on to the application of gain compensation only. After that the result of applying

both phase and gain compensation will be shown and discussed. Finally, the results of the compensation factors on different targets at different ranges will be shown.

5.4 The effect of phase and gain compensation

The data sets that used to compile the resulted in this section are chosen, where a point target (tungsten ball) is located at the right side, the left side and in the middle of the focused beam. The locations of tungsten ball are shown in Figure 46.

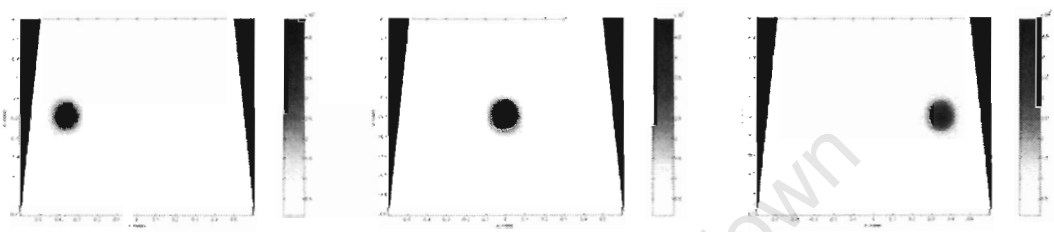

Figure 46: A tungsten ball in left, middle and right side of the beam

During this data capturing, a whole array-B of 16 elements is used. A chirp pulse of 420 kHz, 10 kHz bandwidth and 7 ms chirp pulse are used. A Hanning window is applied in range and Dolph-Chebyshev is applied in azimuth.

5.4.1 Improvement of the phase correction factor (excluding gain)

This section shows the resulted of applying phase correction factor only to the selected data set. Figure 47 to 49 shows the contour map of received power of tungsten ball at various angle located at 5.2 meter away from the transducer head in log scale. The left images are without the phase correction factors and the right images include the correction factors. A Dolph-Chebyshev window was applied. The results show that there is only a slight improvement in some of the side-lobe (mainly close to the main-lobe). This shows that the transducer elements are very well assemble and matched.

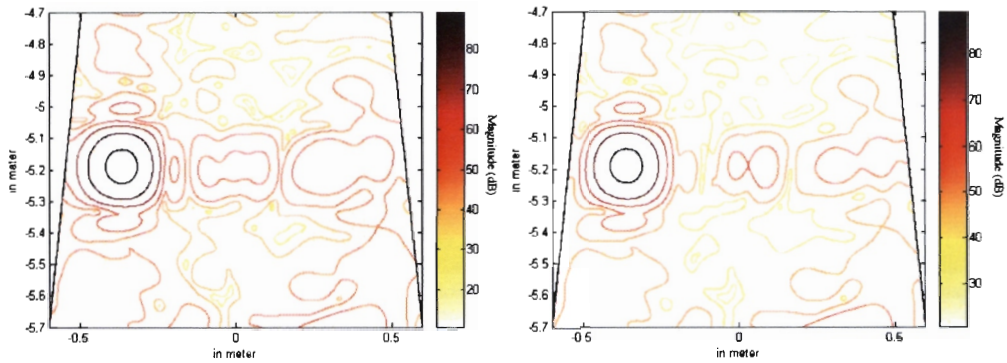

Figure 47: dB contour map results of point target situation on the left side of the beam. The left image is the result without the phase correction factor. The right image shows the result with phase correction factor.

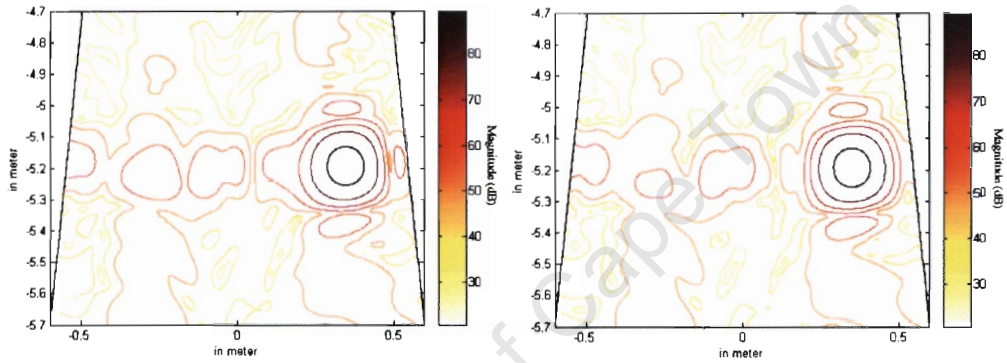

Figure 48: dB contour map results of point target situation on the right side of the beam. The left image is the result without the phase correction factor. The right image shows the result with phase correction factor.

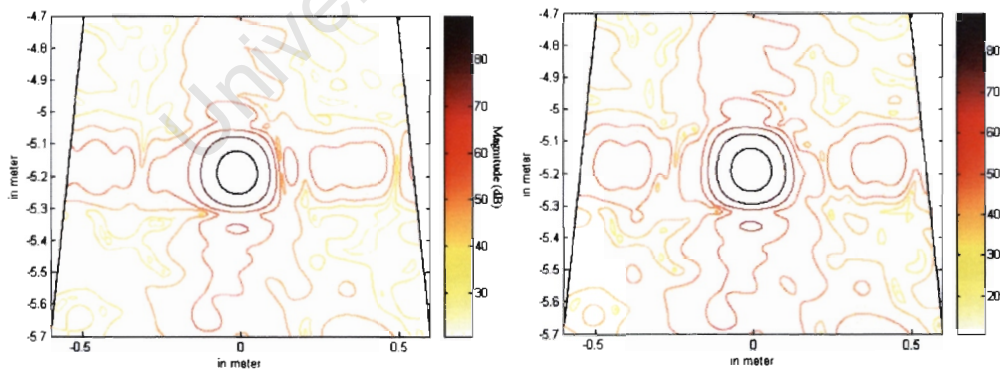

Figure 49: dB contour map results of point target situation on the center of the beam. The Left image is the result without the phase correction factor. The right image shows the result with phase correction factor.

To gain more insight, in Figure 50 to 52, the azimuth cross-section of the tungsten ball at 5.2m away from the transducer head is shown in dB scale. The target response with no phase compensation is shown as a dotted line and the target response with phase compensation is shown as a solid line. The results show that only a slight improvement in the second side lobe, but a significant dropped of approximately 8 dB in the third side lobe when applying the phase correction factors. These results also show that by applying the same phase correction can improve the sidelobe for targets at different angular position in the beam.

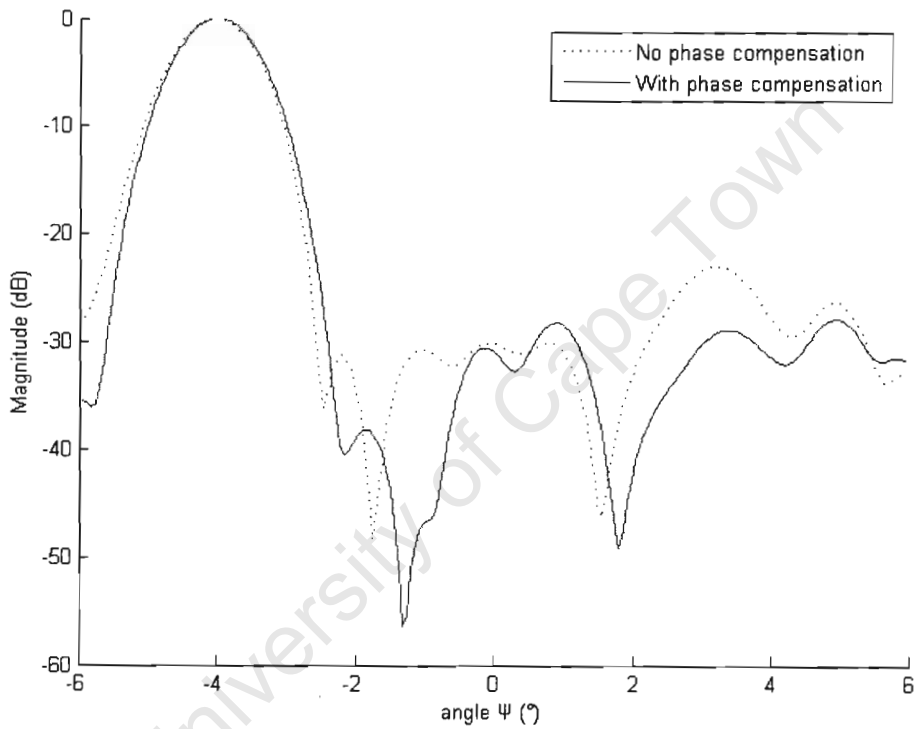

Figure 50: The effect of phase compensation using data set from IMT calibration (left target)

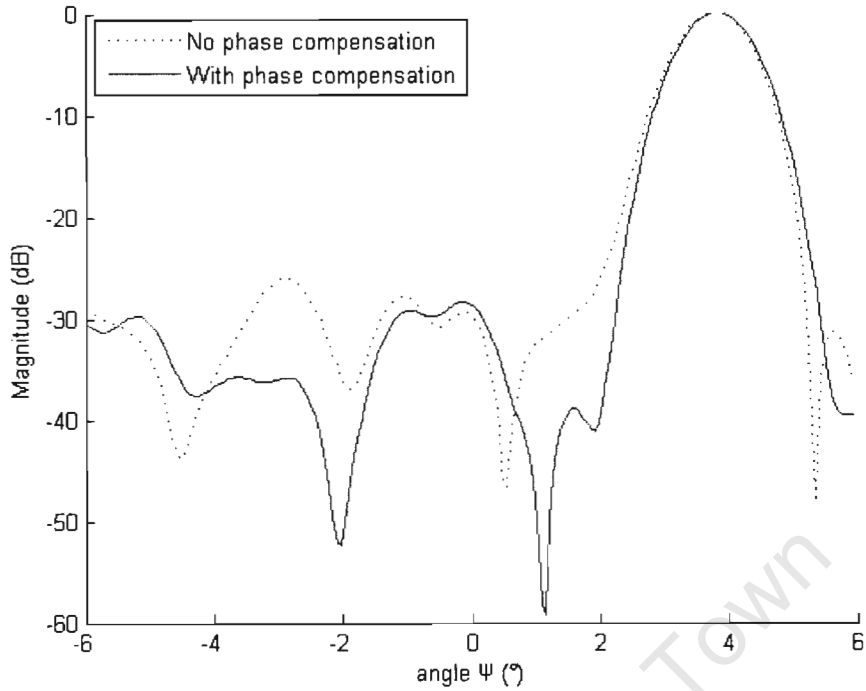

Figure 51: The effect of phase compensation using data set from IMT calibration (right target)

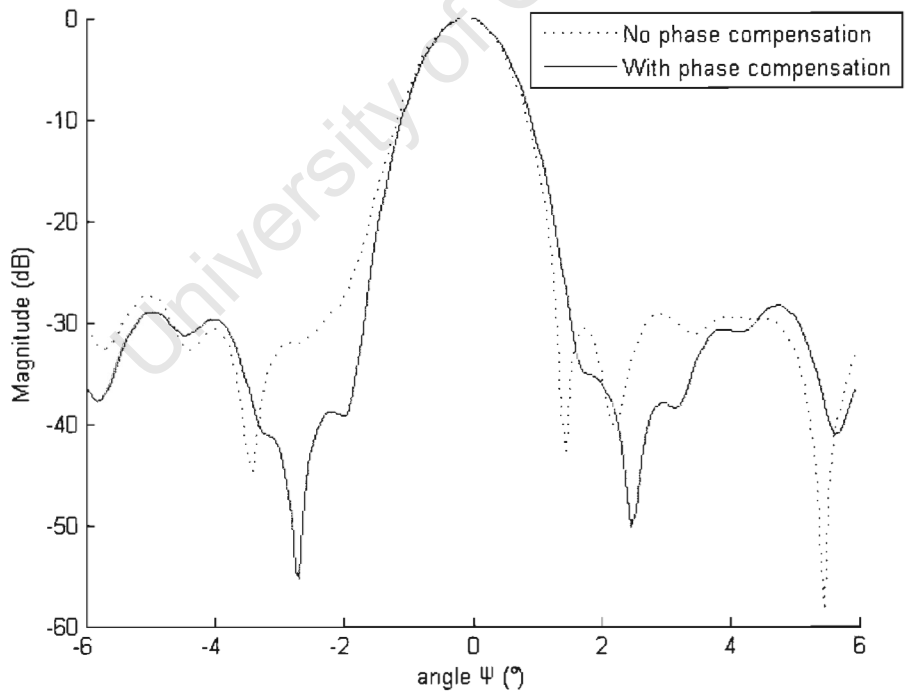

Figure 52: The effect of phase compensation using data set from IMT calibration (center target)

5.4.2 Gain Compensation (without phase correction)

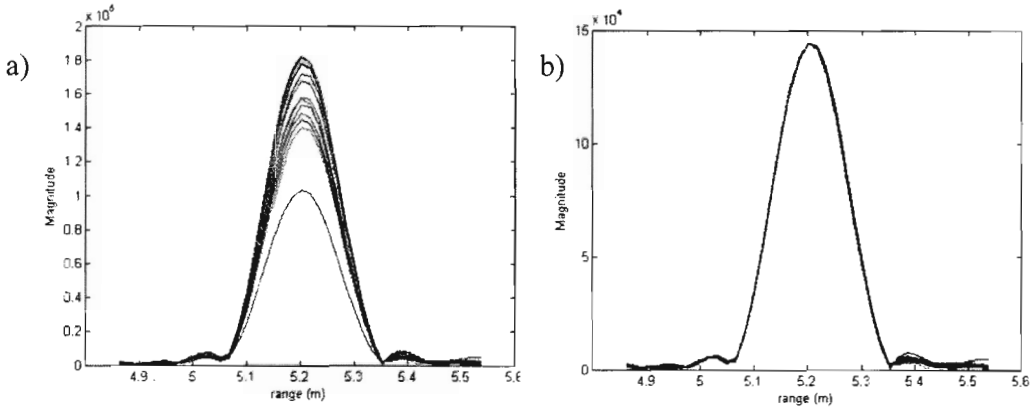

Figure 53: close look at down-range profile of a ball target response with gain compensation and without gain compensation.

In the real world, electronic components such as the ceramic elements in the transducer and the amplifiers used in the A/D converters will never be perfectly matched. This will inevitably result in different gain and phase responses for each channel, which will degrade the performance of the SONAR system.

These mismatches will result in a different signal level for each transducer element as depicted in Figure 53a. As shown in this figure, the channels are not well matched and the amplitudes of the return echoes vary quite significantly. To compensate for these gain errors, a scaling factor was applied to each channel such that the peak responses all equalled that of the centre element of the array, as shown in Figure 53b. A practical compressed point response (from a tungsten ball), to which the gain compensation factors were applied, is shown in Figure 54 to 56 for various angles. The display is a contour map in log scale. In such a display, it is difficult to quantify the improvement. To show the detail, azimuth cross-sections of the target response are shown in Figure 57 to 59. The narrowing effect of applying gain compensation factors is clearly visible in the main lobe. It is clear that the side-lobes also show improvement.

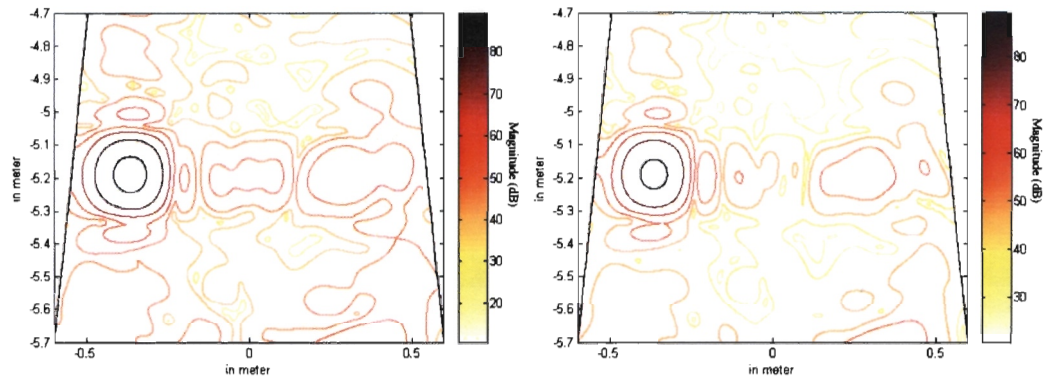

Figure 54: An azimuth cross section of tungsten ball response on the left of the beam.
a) no gain compensation. b) with gain compensation.

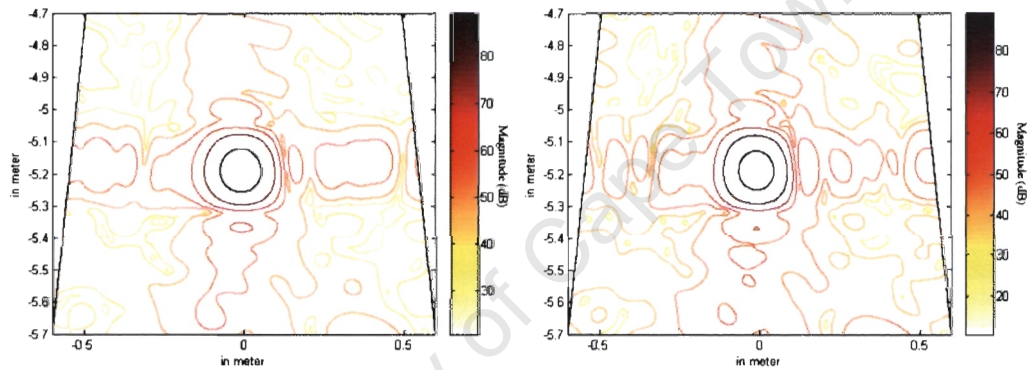

Figure 55: An azimuth cross-section of tungsten ball response in the centre of the beam.
a) no gain compensation. b) with gain compensation.

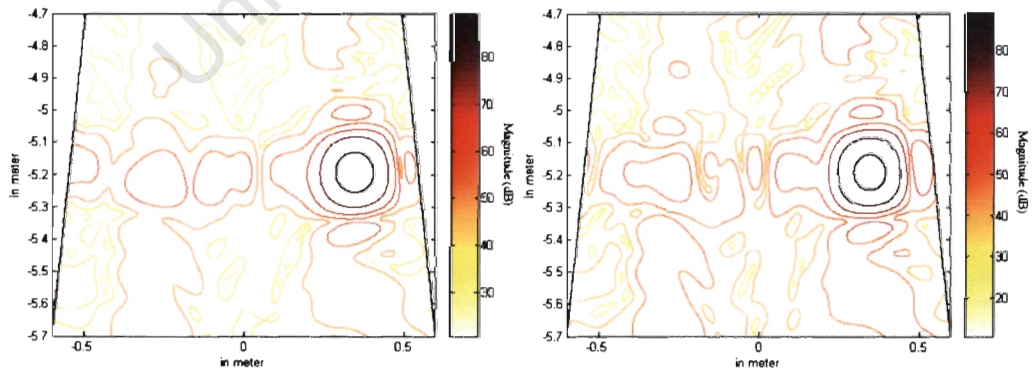

Figure 56: An azimuth cross section of tungsten ball response on the right of the beam.
a) no gain compensation. b) with gain compensation

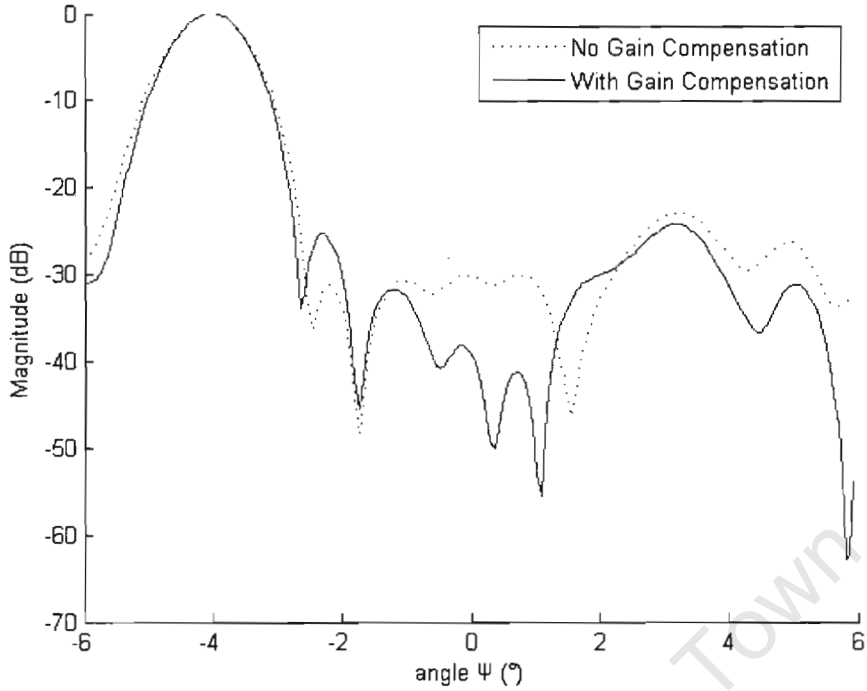

Figure 57: The effect of gain compensation on the data set (target on the left)

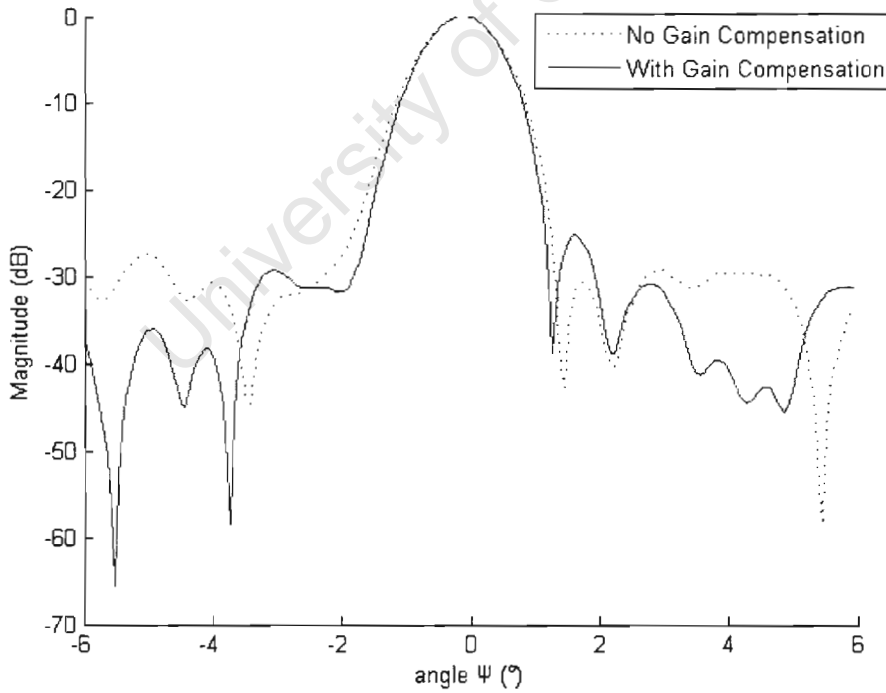

Figure 58: The effect of gain compensation on the data set (target in the centre)

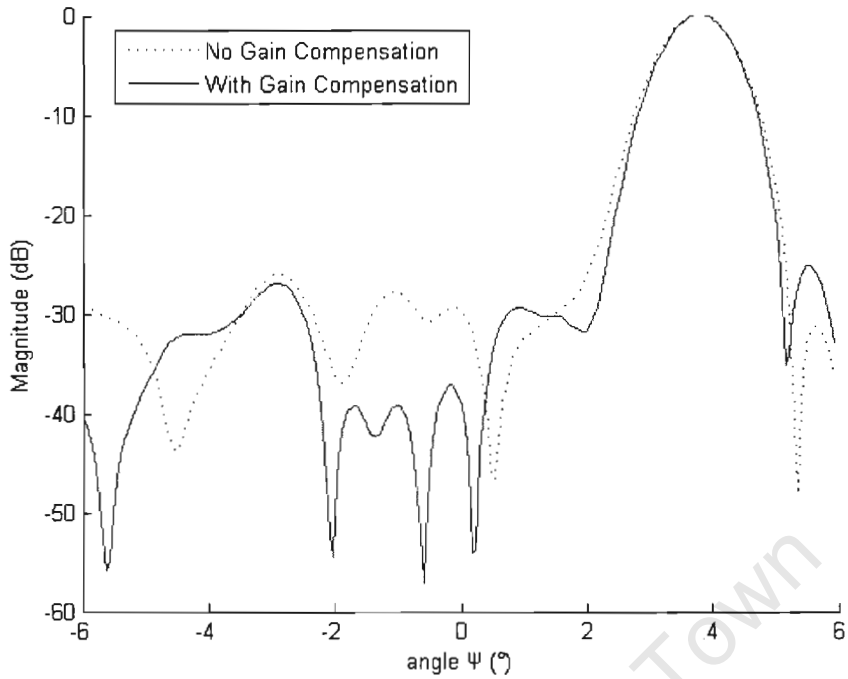

Figure 59: The effect of gain compensation on the data set (target on the right)

5.4.3 The effect of combined Gain and Phase Compensation

This section shows improvement with gain and phase compensation. Figure 60 to 62 shows a contour map of target response between 4.7 to 5.7 m at various azimuth angle in the fan beam (left, right and middle). The left images have no phase or gain compensation applied, while the right images are compensated with phase and gain compensation. From these images, the improvements to the images are not easily seen.

In Figure 63 to 65, the azimuth cross sections of target response at 5.2 m is shown. The dotted line shows the target response with no gain or phase correction at all. The dashdotted line shows the response with only the phase correction factor. The sidelobes show only a slight improvement in some regions. This shows that the transducer elements are very well assembled (previously we determined that the worst case phase error was only 3%), and the phase correction factors can only improve it slightly.

The solid line shows the case of both gain and phase compensation applied. The 3-dB beamwidth and the sidelobe are significantly improved. The results show that with both gain and phase correction factors, there is an improvement in the beamwidth and the sidelobes drop by 10 dB over most of the sidelobe region.

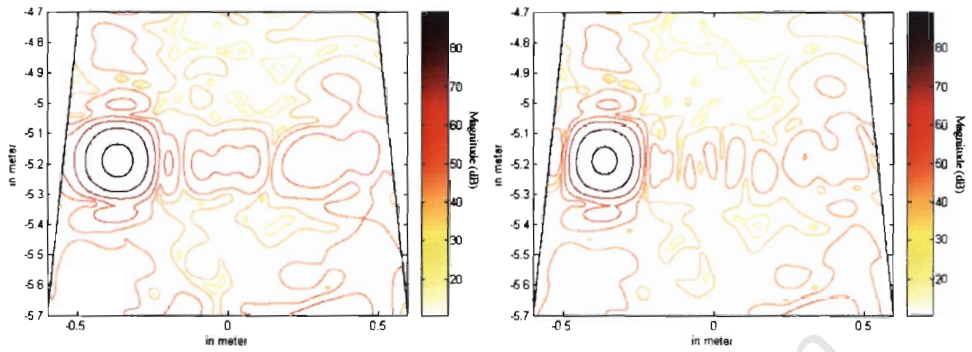

Figure 60: The gain and phase compensation effect on the tungsten ball at 5.2 m located on the left of the beam.

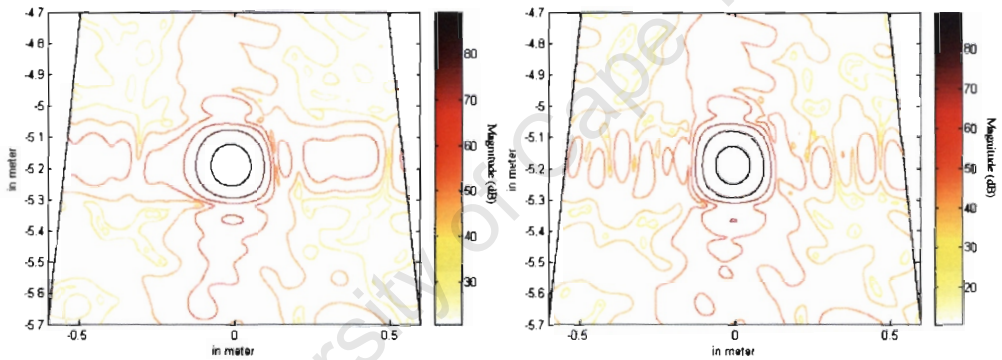

Figure 61: The gain and phase compensation effect on the tungsten ball at 5.2 m located in the centre of the beam.

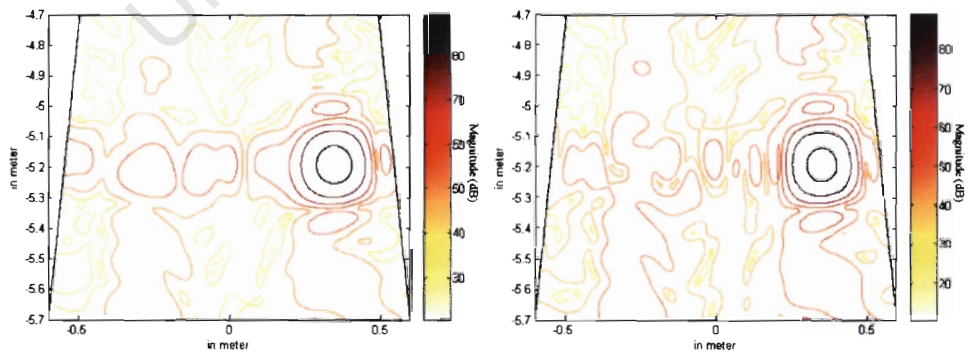

Figure 62: The gain and phase compensation effect on the tungsten ball at 5.2 m located on the right of the beam.

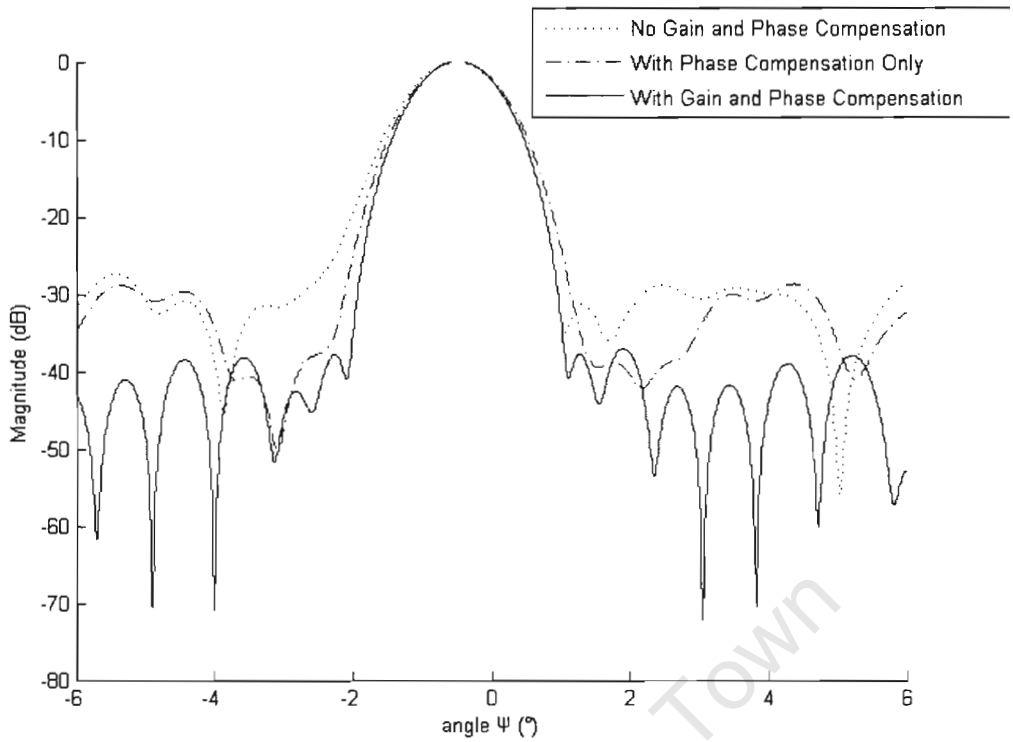

Figure 63: The effect of gain and phase compensation (center target)

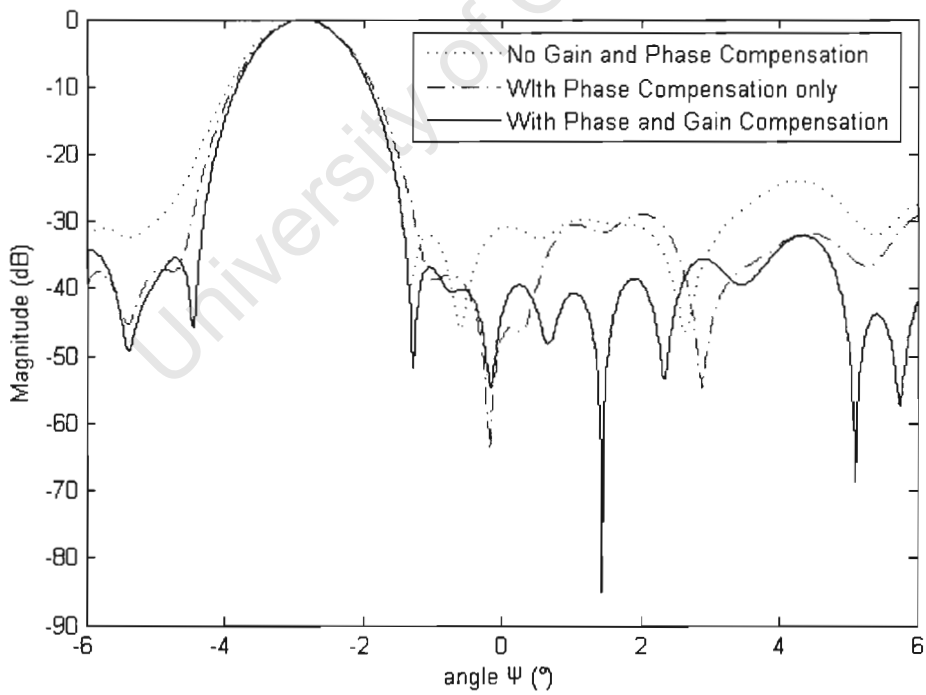

Figure 64: The effect of gain and phase compensation (left target)

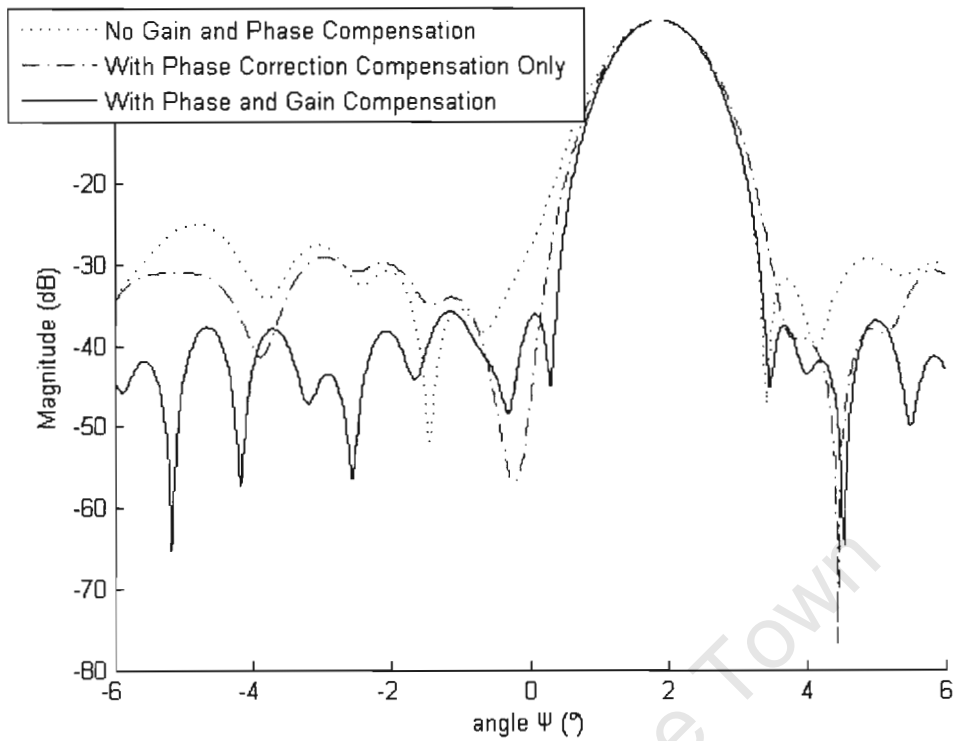

Figure 65: The effect of gain and phase compensation (right target)

5.4.4 Applying Gain and Phase Compensation on T-Shape Rod at 9.2 m

The previous results only use the tungsten ball as the target point response. In order to prove that the compensation factors will improve the images for different targets at different ranges, the gain and phase compensation factors are applied to a T-shape aluminium rod located 9.2 m away from the transducer head. Figure 66 to 68 shows the result in contour map of target response (between 9 and 10 m in depth) in dB scale and Figure 69 to 71 shows the azimuth cross section of the target response at 5.2 m. The result shows that the same phase compensation factors and gain compensation can achieve an improvement in side-lobe and beamwidth.

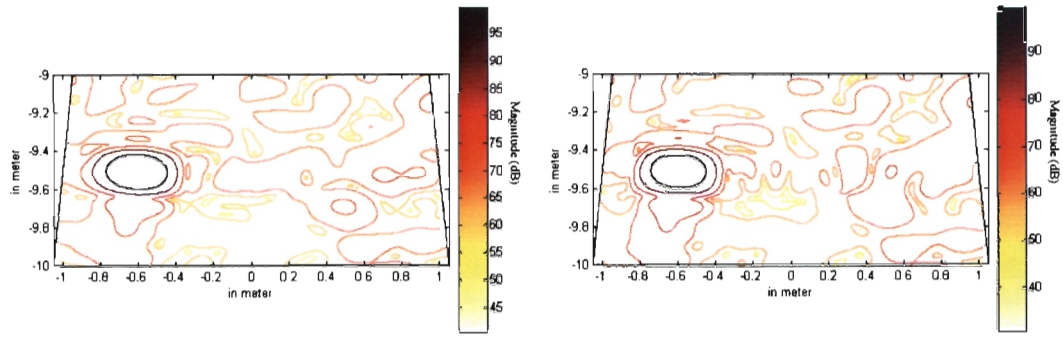

Figure 66: An azimuth cross section of T-shape rod response at 9.2m on the right of the beam.
a) no gain compensation. b) with gain compensation.

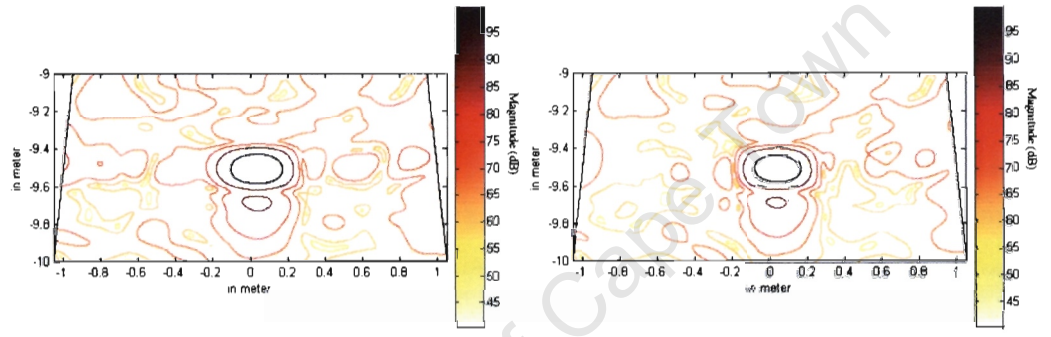

Figure 67: An azimuth cross section of T-shape rod response at 9.2m in the center of the beam.
a) no gain compensation. b) with gain compensation.

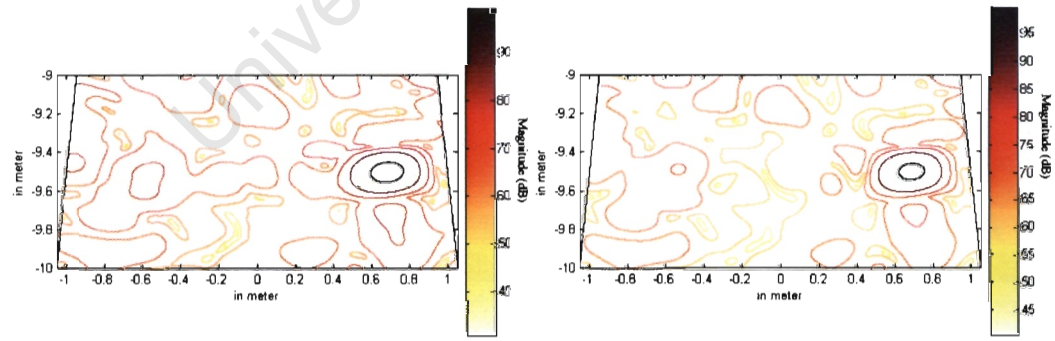

Figure 68: An azimuth cross section of T-shape rod response at 9.2m on the right of the beam.
a) no gain compensation. b) with gain compensation.

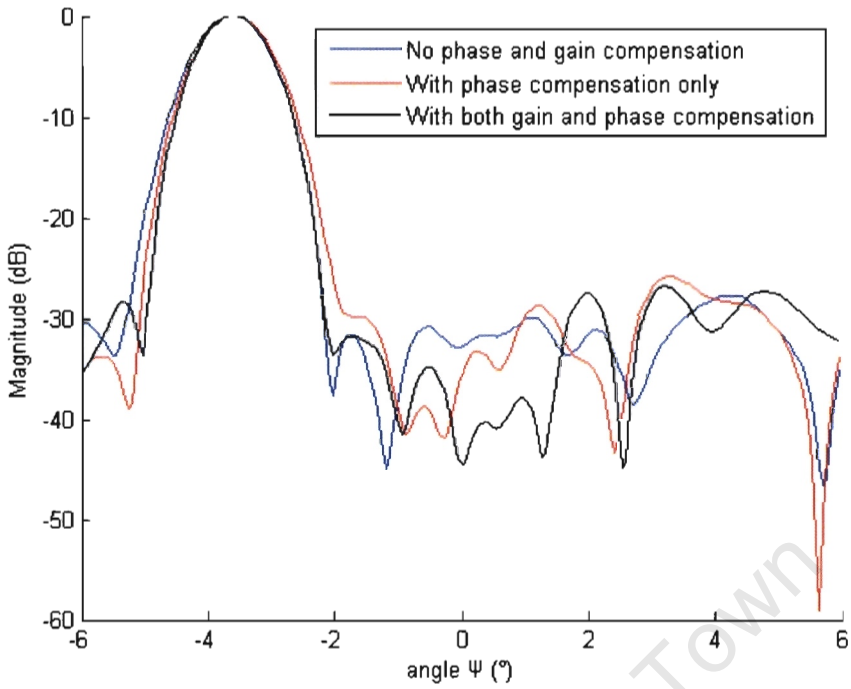

Figure 69: The gain and phase compensation effect on the T-Shape rod at 9.2 m located on the left of the beam.

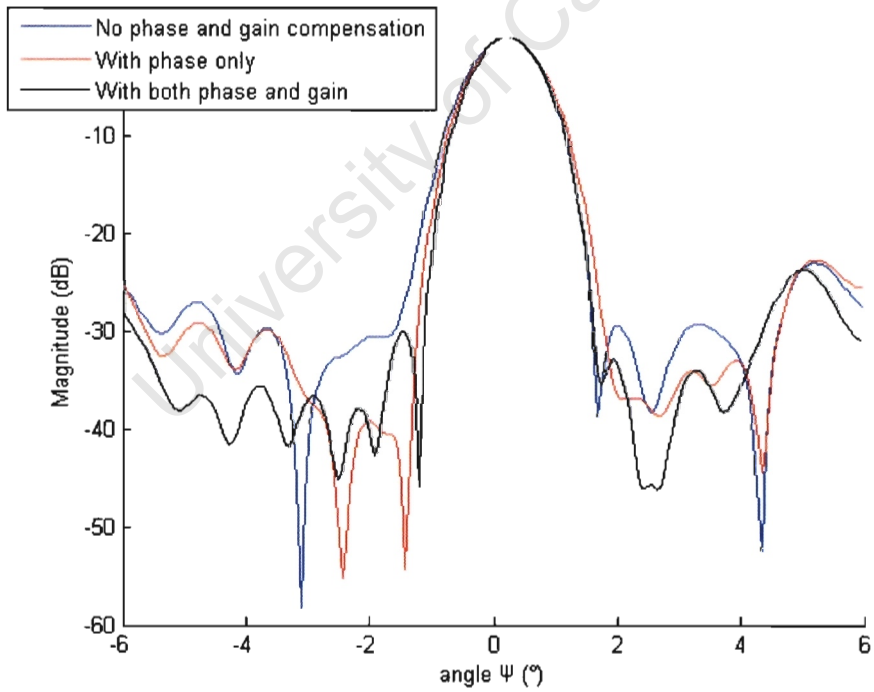

Figure 70: The gain and phase compensation effect on the T-Shape rod at 9.2 m located in the center of the beam.

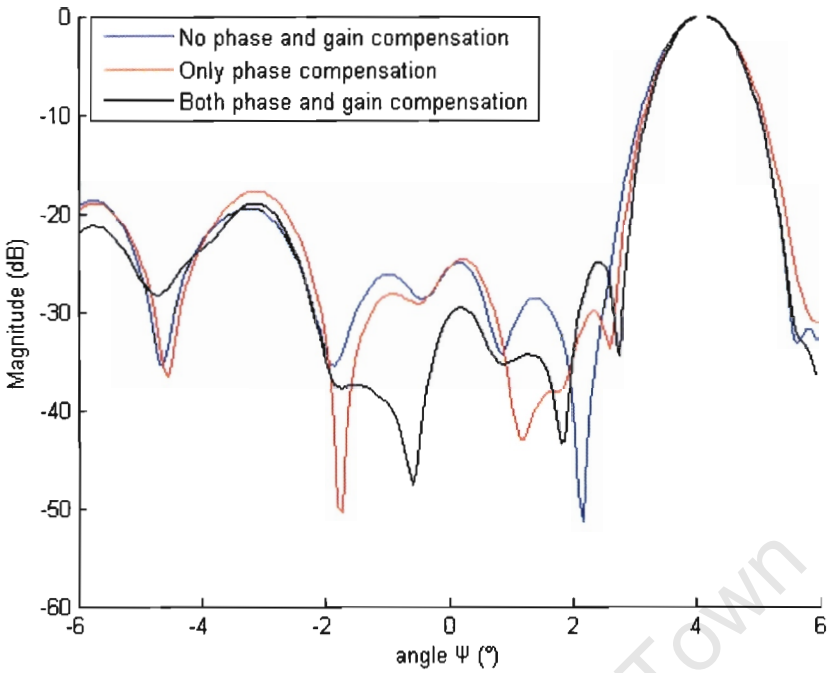

Figure 71: The gain and phase compensation effect on the T-Shape rod at 9.2 m located on the right of the beam.

5.5 Other performance Aspects of the ABACUS System

After looking at the compensation factor (phase and gain) performance of the phase and gain compensation on the image formation, this section is going to study other aspects relating to performance. The first aspect is the chosen matched filter performance in practical environment. The second aspect is the separation of targets in azimuth direction.

5.5.1 The performance of the matched filter

Figure 72 shows the down range profile and the phase of a compressed tungsten ball response. It is captured by ABACUS at a distance of 5.2 m from the transducer head. This result shows that the matched filter that was used to compress the data is suitable since the phases are flat in the 3 dB bandwidth and the sidelobe is relatively low.

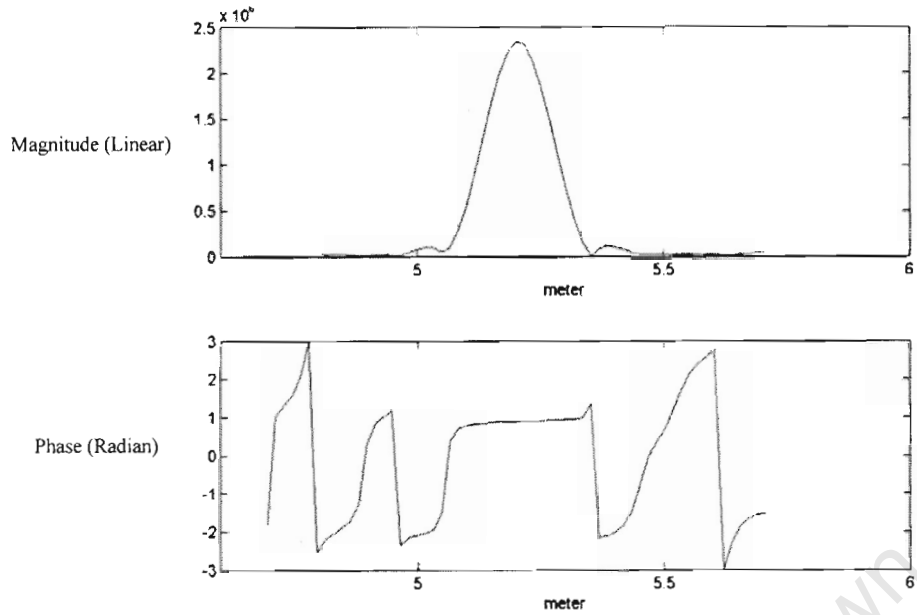

Figure 72: Down-range profile and phase of a tungsten ball response obtained from IMT.

5.5.2 The performance on separation of targets in azimuth direction

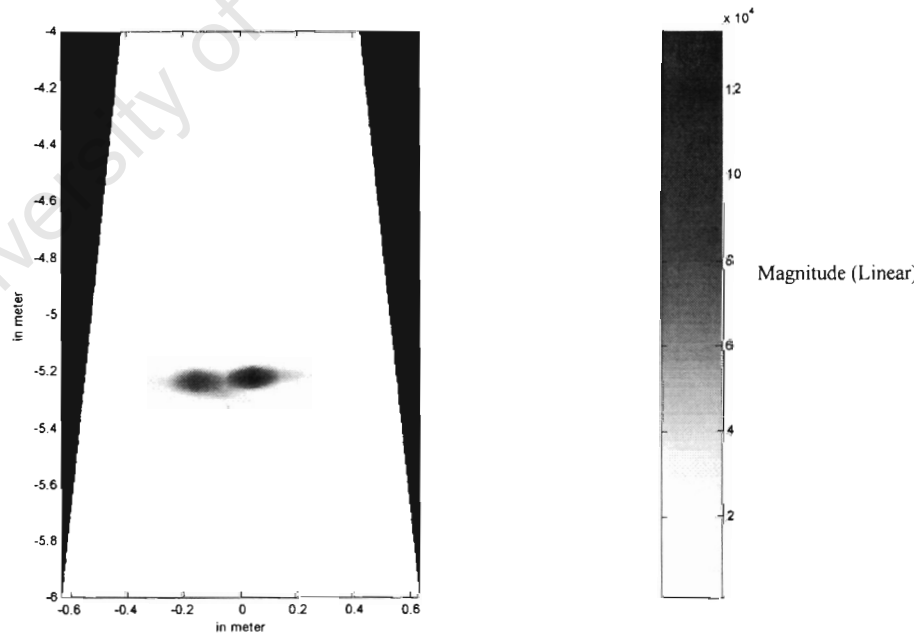

Figure 73: Two ping-pong balls separated from each other by 10 cm

Figure 73 shows the result image of the dataset where two ping-pong balls are hanging side by side separated by a distance of 10 cm. These two targets are located 5.2 m away from the transducer head. The full receiver array B is used and the transmitted chirp signal is 420 kHz, 10 kHz bandwidth and 7 ms chirp length.

From the measurement of beamwidth [26], the full array focussed beam-width is 1° azimuth. At 5.2 m, any targets must separate azimuthally by 12.6 cm (using trigonometric relationship) to be resolved. Figure 50 and the zoomed version in Figure 74 prove that although the two targets are joined and 10cm apart, each target can still be separately distinguished.

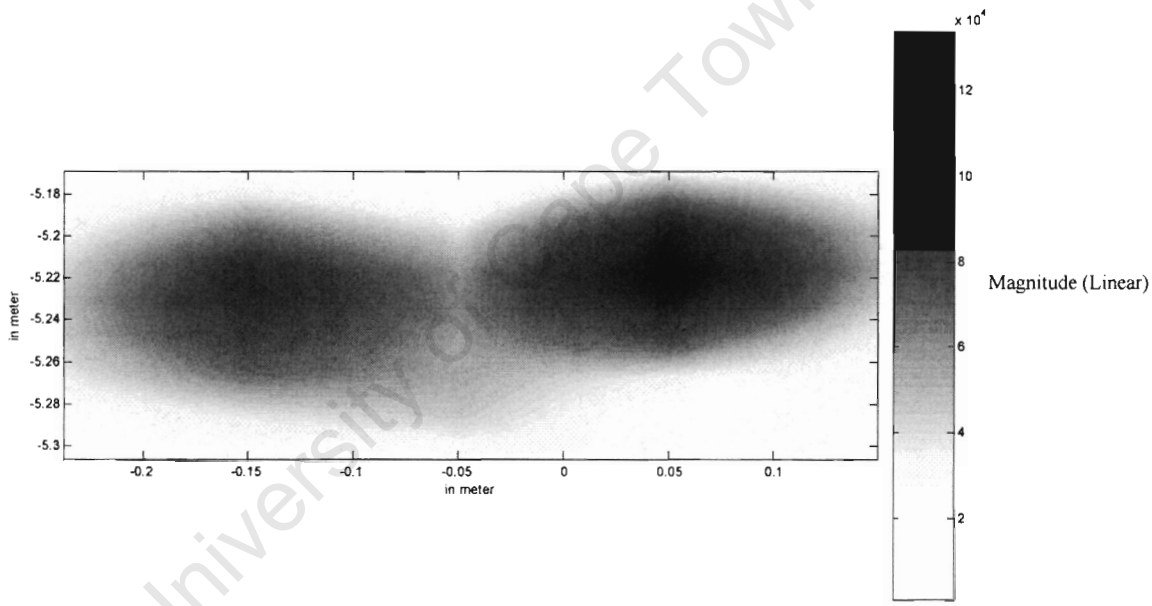

Figure 74: A close view into the two ping pong balls

5.5.3 An azimuth beam pattern of ABACUS transducer array

Figure 75 shows the azimuth beam pattern of ABACUS receiving array B captured during IMT tank calibration.

The experiment is started with locating a tungsten ball at the range of 5.2 m away from the transducer head; the transducer head is then attached to a stepper motor and rotate 180° at a step of 1° per second.

One can then plot the following graph using the maximum value of target response at 5.2 m with respect to scanning angle.

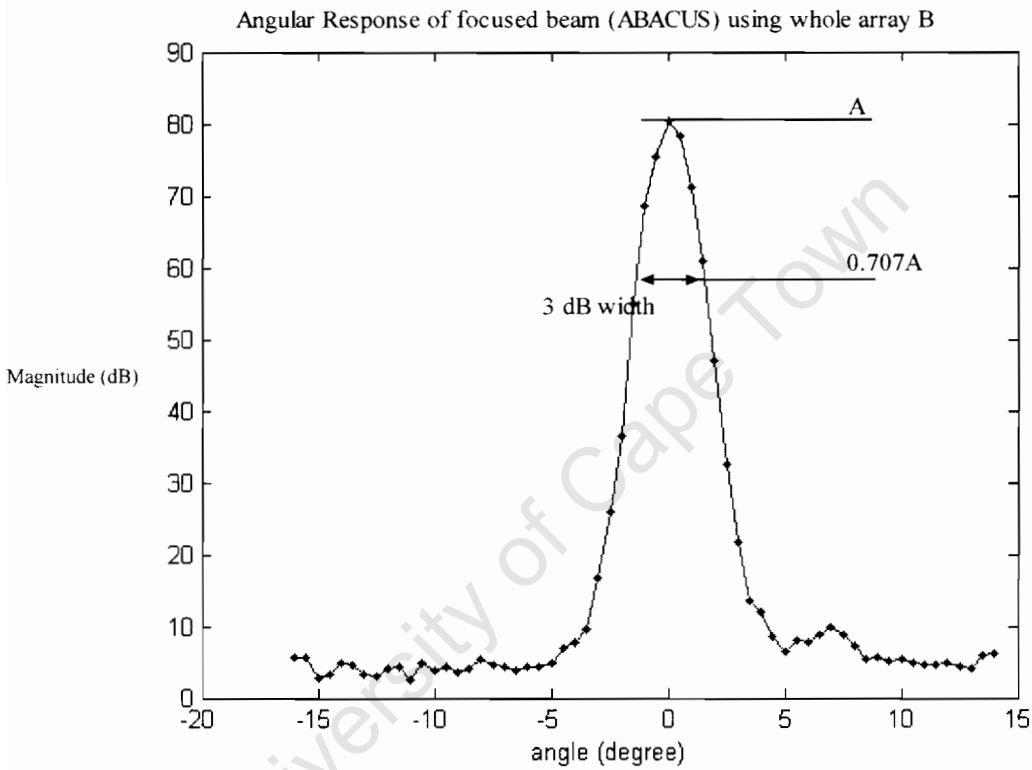

Figure 75: Azimuth beam pattern of ABACUS receiving array obtained in IMT tank calibration experiment. the beamwidth is 4 degree.

5.6 Summary of the Chapter.

This chapter described the method and the results of the calibration during the IMT calibration experiment. Gain and phase errors were studied. and a method was implemented to correct for these errors. The result clearly showed that the phase correction factors and the gain correction factors do provide a significant

improvement on the image formation process. The phase correction factors can also significantly improve the sidelobe response and the gain correction factors can significantly improve the 3-dB beamwidth.

Chapter 6

Field Trip Results

After all the discussion on the image formation algorithm and the derivation of the gain, phase and spreadloss compensation, this chapter will show the results from an experiment conducted in a large swimming pool, and the results from three sets at sea trials. Each section will first describe the setup of the experiment and then present the image results. Finally, the results from the most recent sea trial, in 2004, will be compared with the output from a SIMRAD EK500 echo sounder.

It is note that due to the reason that only array B is connected during IMT calibration, the writer only obtains the compensation factors for array B. Unfortunately, in Newlands Pool Test, Algoa Sea Trial 2003 and Africana Sea Trial 2004 where both array A and B each with 8 elements are connected, the results in those sections are therefore no phase compensation factors applied.

6.1 The Newlands Pool Test

The Newlands Pool Test was the first trial of the ABACUS system since the project was terminated in 1995 and it was the first experience using the ABACUS system for the Signal Processing Research Group led by Dr. Wilkinson. The aim of the experiment was to verify the status of the hardware. Mr M. Soule of Fisheries Resource Surveys, Dr. A.J. Wilkinson and Ferdinand Ng from UCT, were involved in this activity (Figure 76).

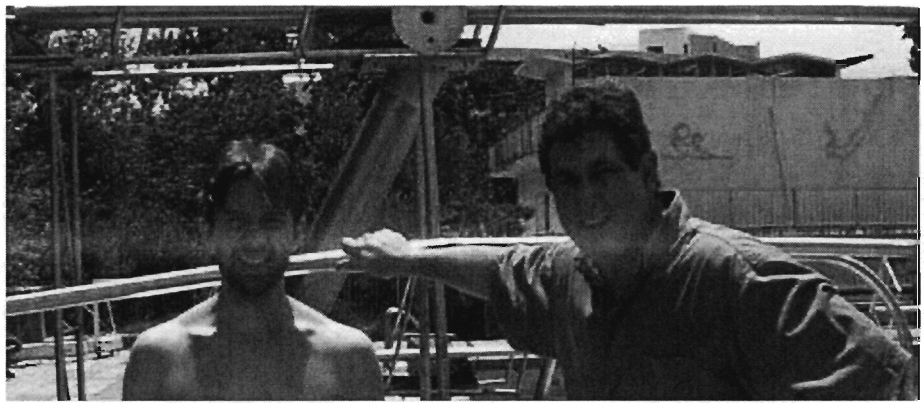

Figure 76: Dr A.J Wilkinson (Left) and Mr M. Soule (Right)

6.1.1 Experimental Environment Setup

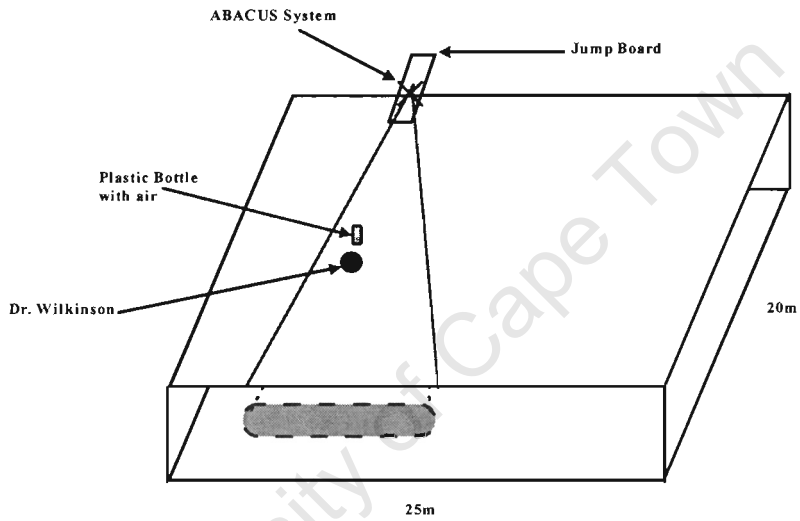

Figure 77: An illustration of Newlands Swimming Pool

The experience took place in the Newlands swimming pool in Cape Town. The dimensions of the pool are 25m by 20m and 4m in depth. There is a diving board located on the side of the pool. The ABACUS transducer head was suspended by a rope in front of the diving board. Horizontal scanning is used in this experiment because of the depth of the pool. That is the transmitter "fan beam" was orientated horizontally pointing across the pool as illustrated in Figure 77. Mike Soule did the steering manually.

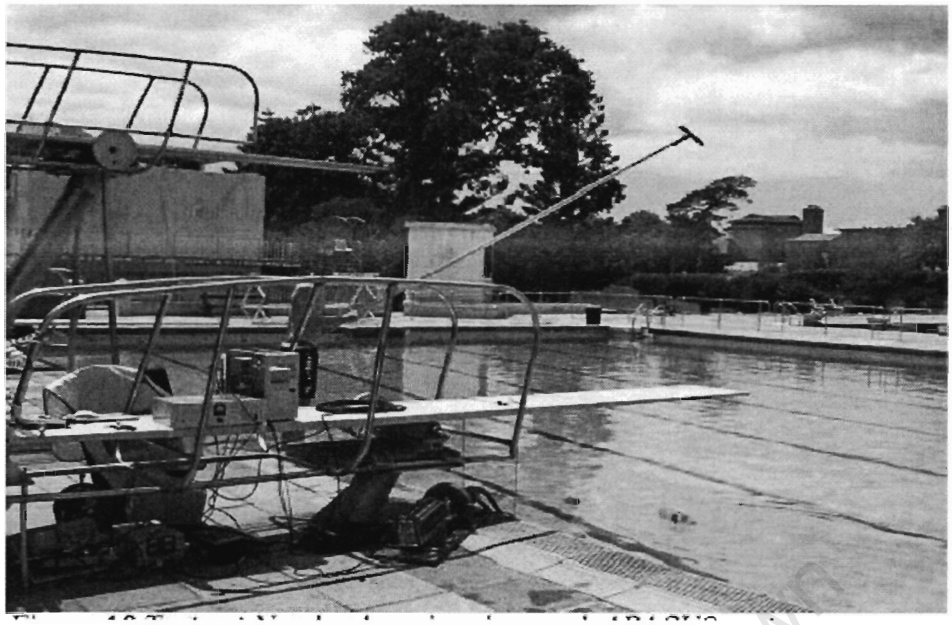

Figure 78: Newlands Swimming Pool with ABACUS on the side of diving board.

The targets used in this experiment were a swimmer (Dr. A. J. Wilkinson) and a half filled bottle hanging on a long rod which shown in Figure 80. The set-up of the experiment is illustrated in Figure 77. One of the data capture cards malfunctioned during the experiment therefore, only 15 channels were used.

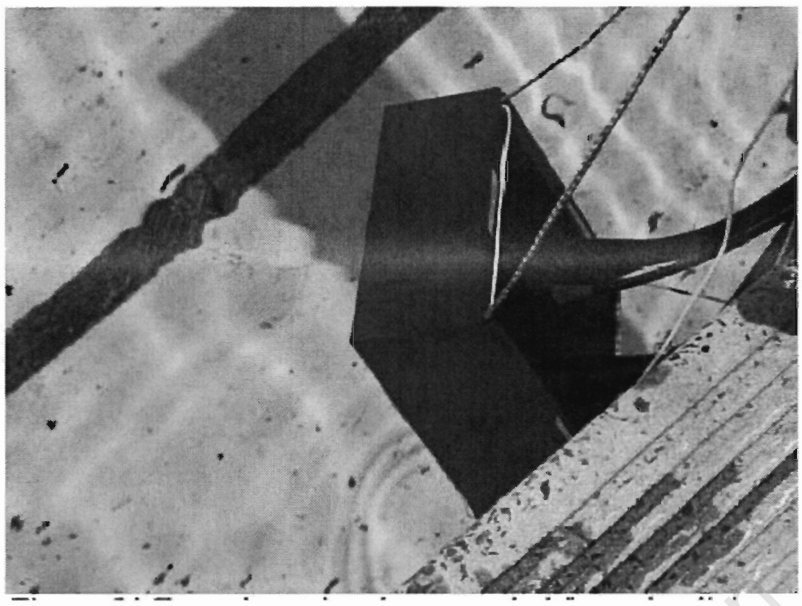

Figure 79: The ABACUS transducer head is holding by rode on the side of the pool

6.1.2 ABACUS Experiment Settings

Location:	*Newlands Swimming Pool*
Time:	*afternoon*
Number of Channel:	*15*
Ping Rate:	*1 ping per second*
Transmit Chirp Bandwidth:	*10 kHz*
Chirp Length:	*7 ms*
Window:	*hanning in range and Dolph-Chebyshev in azimuth*
Compensation Factor:	*Only gain compensation (discussed in Section 5.4.2) is applied. For the reason that only array B is calibrated during the calibration process discussed in Chapter 5. In this experiment, both arrays are being used. The phase compensation is therefore not applied.*
Team Members:	*Mike Soule, Dr. A. J. Wilkinsons and Ferdinand Ng.*
Main Target Objects:	*Human swimmer and half filled water bottle (Figure 79).*
Data Capture Software:	*Peralex Pascal Data Capturing Software.*

Element Channel Mapping: *Configured as two arrays of 8 elements per array of length 0.1185m, the channel 1 (element A5, refer to Figure 3) is not working.*

Direction of transducer head: *The transducer head is scanning horizontally for the reason that the limitation of the pool depth.*

Channel	***1***	***2***	***3***	***4***	***5***	***6***	***7***	***8***	***9***	***10***	***11***	***12***	***13***	***14***	***15***	***16***
Element	N/A	A6	A7	A8	A9	A10	A11	A12	B5	B6	B7	B8	B9	B10	B11	B12

Note: The metal case for the data capturing unit pod is not fitted.

Figure 80: Dr Wilkinson and the bottle are the targets during the experiment.

6.1.3 Image Results

Figure 81 is a series of linear images from the ABACUS system of target swimming across the beam from left to right.

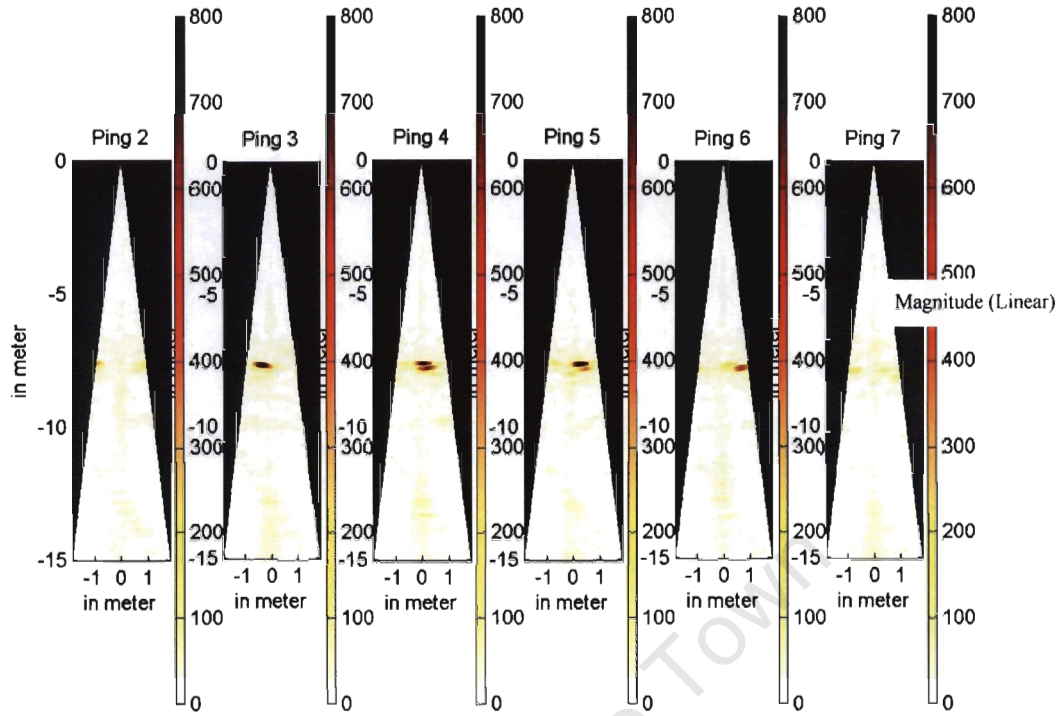

Figure 81: Target Swimming across the ABACUS Beam

The images are taken at one-second intervals. A clear target appeared at around 7.5m from the transducer. The swimmer is then moved from left to right. In pings 4 and 5, two distinct targets can be seen, which believed is coming from different body parts.

If the images are studied closely, a strip of yellow mud in the middle of the beam can be seen. This is a parasitic oscillation (present in the pre-amplifier), which was present in the hardware. The oscillation level does not cause a significant corruption of the data in these images for the reason that the metal case for the metal case for the data capturing pod is not assembled together, but in the first sea trial discussed in the next Section, this oscillation became a significant issue in the next experiment, ALGOA sea trial 2003.

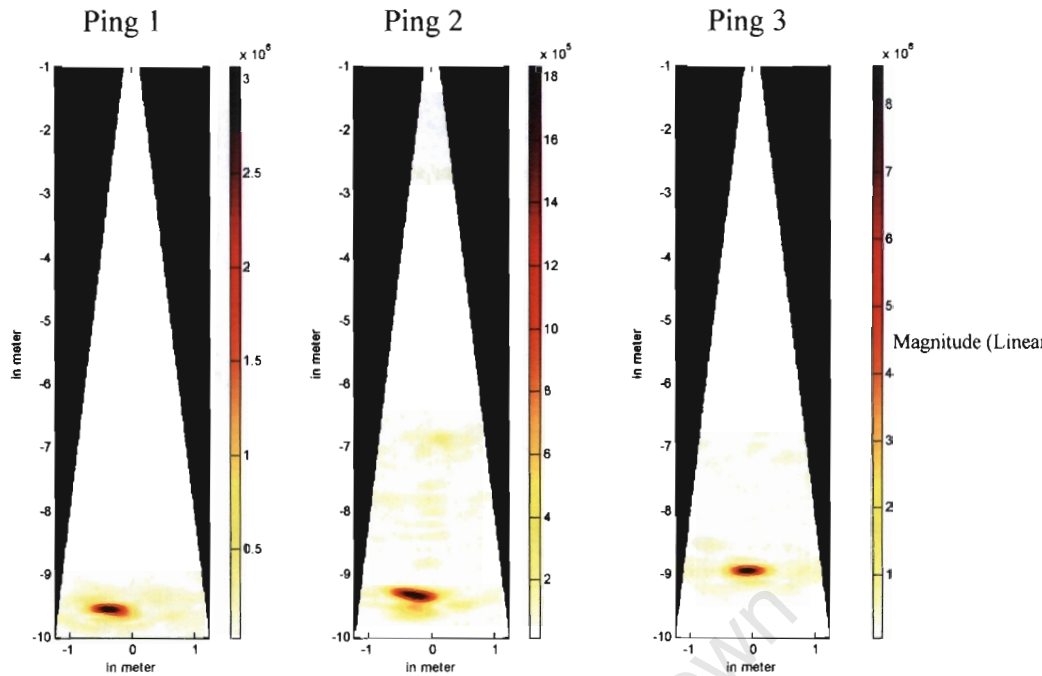

Figure 82: Images of targets swimming toward the ABACUS Transducer (first three pings)

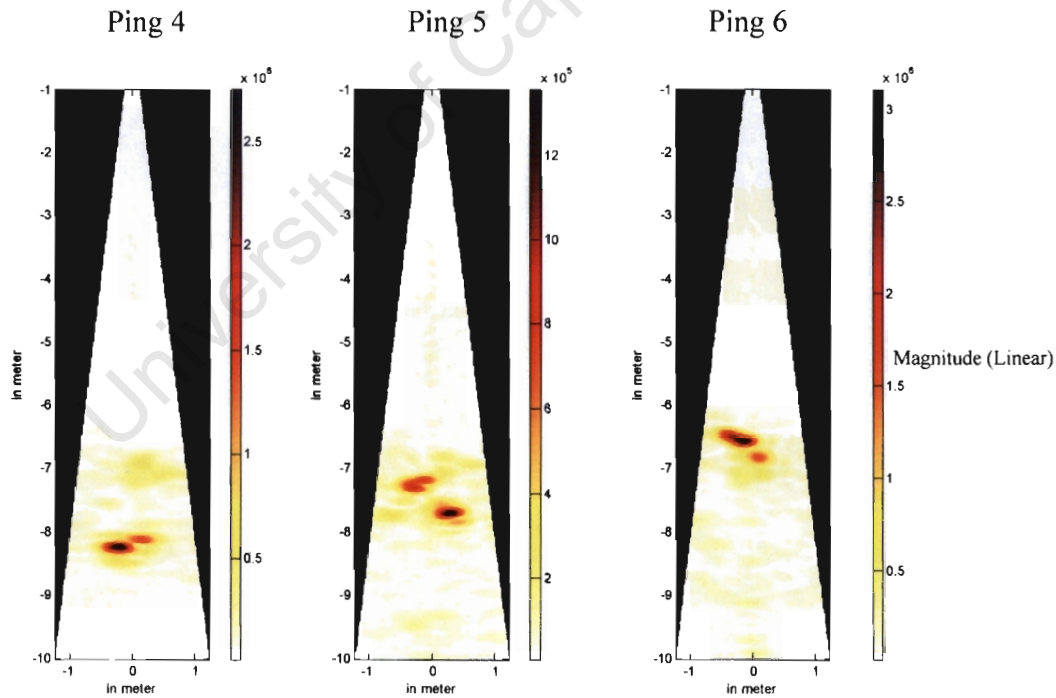

Figure 83: Images of targets swimming towards the ABACUS Transducer
(one second between pings)

Figure 82 and 83 are a set of linear scale images of two targets moving towards the transducer head. In ping 1 to 3, only one target is being picked up by the system. Only in ping 3 to 6, is second target (the bottle) visible. The reason is that at the time of the experiment, the data logging software cannot display and record received signal at the same time; and the hanging of both the transducer head and the target bottle are controlled manually. The bottle is relatively small; it is therefore very difficult to locate the bottle at the centre of the beam throughout the experiment. This results in the disappearance of the bottle in some of the images.

6.2 Algoa Sea Trial Nov 2003

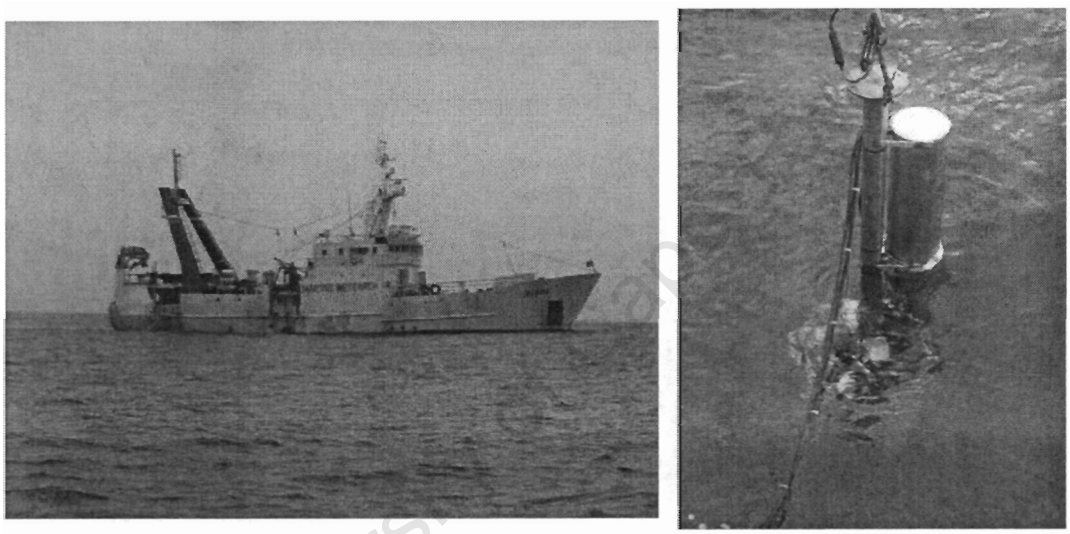

Figure 84: Photos of the ALGOA and the ABACUS deployment

The first ABACUS sea trials took place in November 2003 on the MCM research vessel, FRS ALGOA, during the annual squid survey off the eastern Cape coast. At this time large spawning squid concentrations are found between Plattenberg Bay and Port Alfred, providing reasonably stable targets for investigations. The data capturing for this experiment took place in the open sea near Oyster Bay. This is shown in Figure 84.

The aim of this experiment was to collect data from real targets and therefore to validate the operation of the hardware in a practical environment. This was ABACUS's first sea launch. The data-capturing card was repaired prior to departure and all 16 channels were functional for the survey.

6.2.1 Experiment Environment Setup

The measurements were conducted from the mid section of Algoa. The squid targets imaged tended to concentrate in large mushroom shaped during the day, but dispersed at night. The experiment took place from late afternoon until at night.

The ABACUS PC and power supply were located in the starboard laboratory as shown in Figure 85. The transducer and data capturing electronics were suspended about 3m from the gunwale of Algoa by means of a crane and a rope. The transducer head was facing vertically downwards, with the beam pointing towards the bottom, and cutting though the squid aggregation, as illustrated in Figure 85. The head was typically 2m below the sea surface, but this varied depending on the sea conditions and the movement of the vessel.

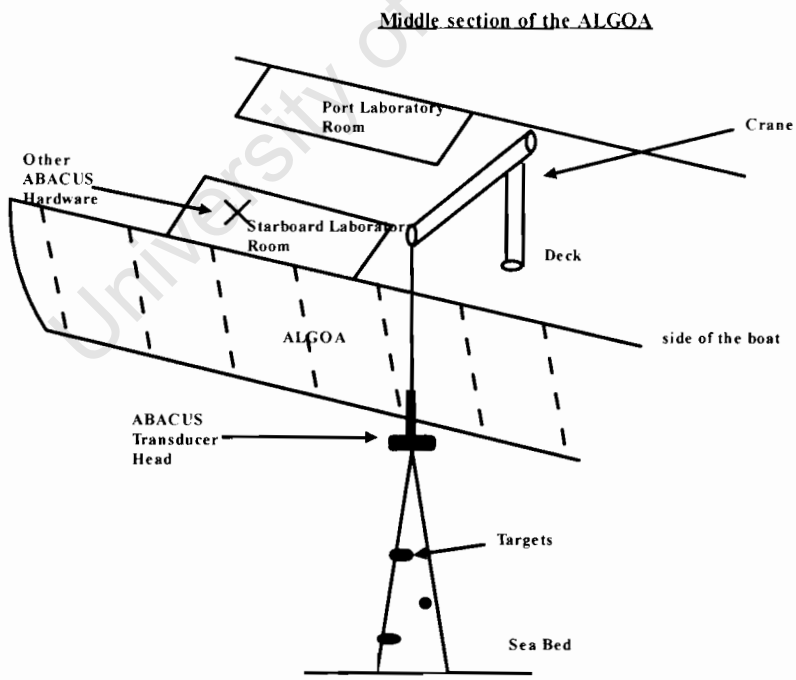

Figure 85: Illustration of the experiment setup on the Algoa 2003

Unfortunately, the weather conditions were not good which meant that the time available for experiments was limited. The main concern was that rough seas could cause the transducer to hit the side of the ship thus damaging the hardware.

6.2.2 ABACUS System Setting

Location: *Oyster Bay near Port Elizabeth*

Time: *Evening*

Number of Channel: *16*

Ping Rate: *1 ping per second*

Transmit Chirp Bandwidth: *10 kHz*

Chirp Length: *7 ms*

Window: *Hanning in range and Dolph-Chebyshev in azimuth*

Compensation Factor: *Only gain compensation (discussed in Section 5.4.2) is applied. For the reason that only array B is calibrated during the calibration process discussed in Chapter 5. In this experiment, both arrays are being used. The phase compensation is therefore not applied.*

Team Member: *Mike Soule, Dr. M. Lipinski, Dr. A. J. Wilkinson, every member on Algoa and Ferdinand Ng.*

Main Target Objects: *Squids.*

Data Capturing Software: *Modified Parallax Pascal Data Capturing Software*

Element Channel Mapping: *Configured as two arrays of 8 elements per array of length 0.1185.*

Direction of transducer head: *Transducer head is hanging on the side of the ship and pointing downward to perform vertical imaging.*

Channel	***1***	***2***	***3***	***4***	***5***	***6***	***7***	***8***	***9***	***10***	***11***	***12***	***13***	***14***	***15***	***16***
Element	A5	A6	A7	A8	A9	A10	A11	A12	B5	B6	B7	B8	B9	B10	B11	B12

6.2.3 Image Results

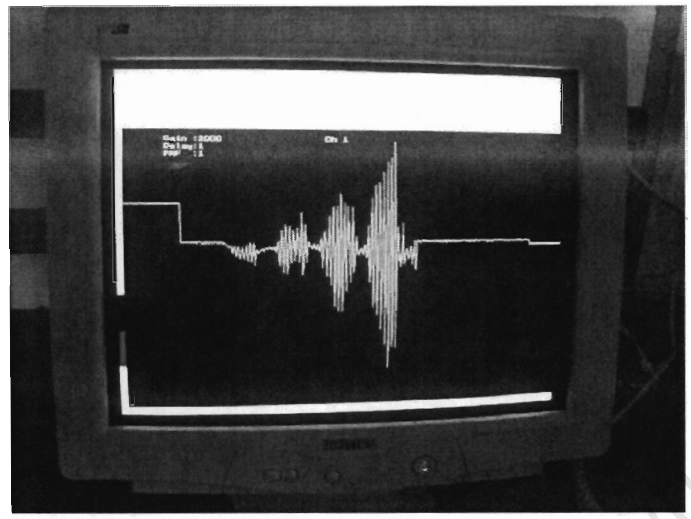

Figure 86: Images from the Algoa November. 2003 Sea Trial

At the beginning of the experiment, a periodic oscillation signal was picked up by the system, which in turn dramatically affected the data. This unknown periodic signal is shown in Figure 86. The gradual increase in amplitude was due to the TVG control. It was found that grounding the metal case reduced the amplitude of the oscillation to a level that was acceptable.

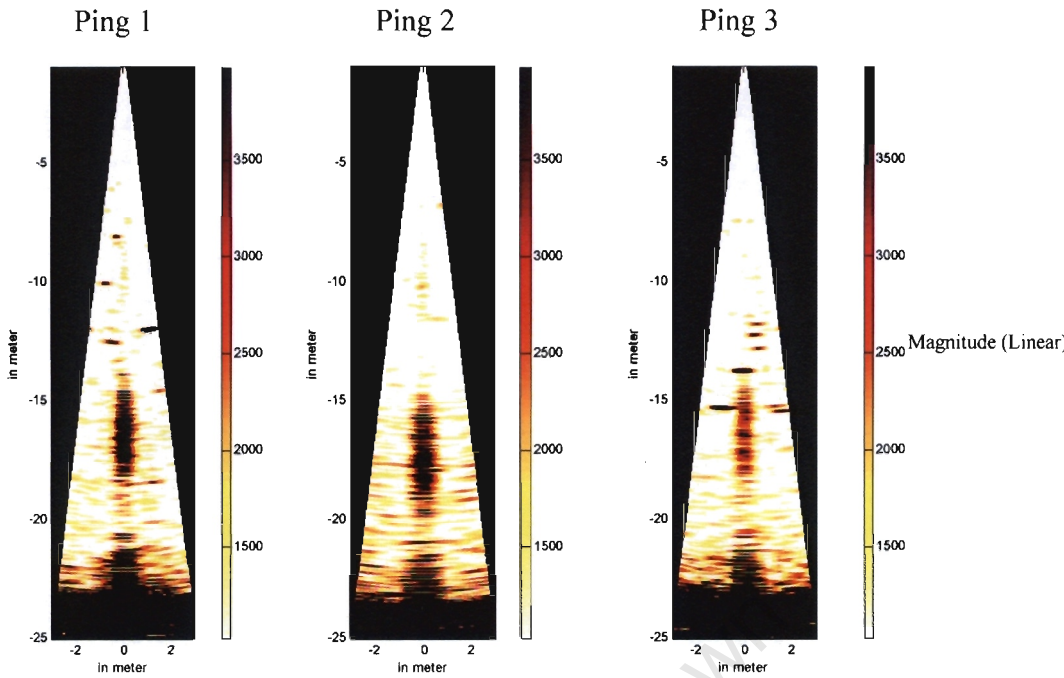

Figure 87: The resulted images from the ALGOA Sea Trial 2003

Looking at linear scaled images in Figure 87 where a dark central band is clearly shown in the middle of the images due to the periodic oscillation described in the previous paragraph.

To gain more knowledge on what the images are showing, an initial idea was to use an underwater camera to video the targets. Unfortunately, this was not possible for the following two reasons:

1) The data capturing took place at night when the sea was too dark to be able to observe anything.

2) Spot lights or underwater lights would have affected the behaviour of the squid, which would have interfered with simultaneous target strength experiments being conducted with the EK500 scientific echo sounder.

As shown in the Figure 87, the bottom echo is visible at around 24 meters and many targets were concentrated at a level of 15m and deeper, although a few targets were present in the upper half of the sea. The bottom range varies between pings as a result of the rocking movement of the ship.

6.2 Africana Sea Trial Aug 2004

Figure 88: The Africana Research Ship

The Africana experiments took place in August 2004 during an acoustic survey cruise in False Bay. The Africana is the largest research scientific survey vessel in South Africa and is shown in Figure 88. Generally Africana is used to collect statistical data relating to pilchards and anchovies to allow biologists to estimate the size of pilchard and anchovy stocks.

The aim of this experiment was to gather sample data for different targets and to test the newly developed Delphi data capturing software. A tungsten ball was used in this experiment to act as a reference target for resulting images. Every part of the ABACUS' hardware was thoroughly checked and grounded. The internal oscillation noted earlier was reduced a level which was acceptable for the experiments being conducted.

6.3.1 Experiment Environment Setup

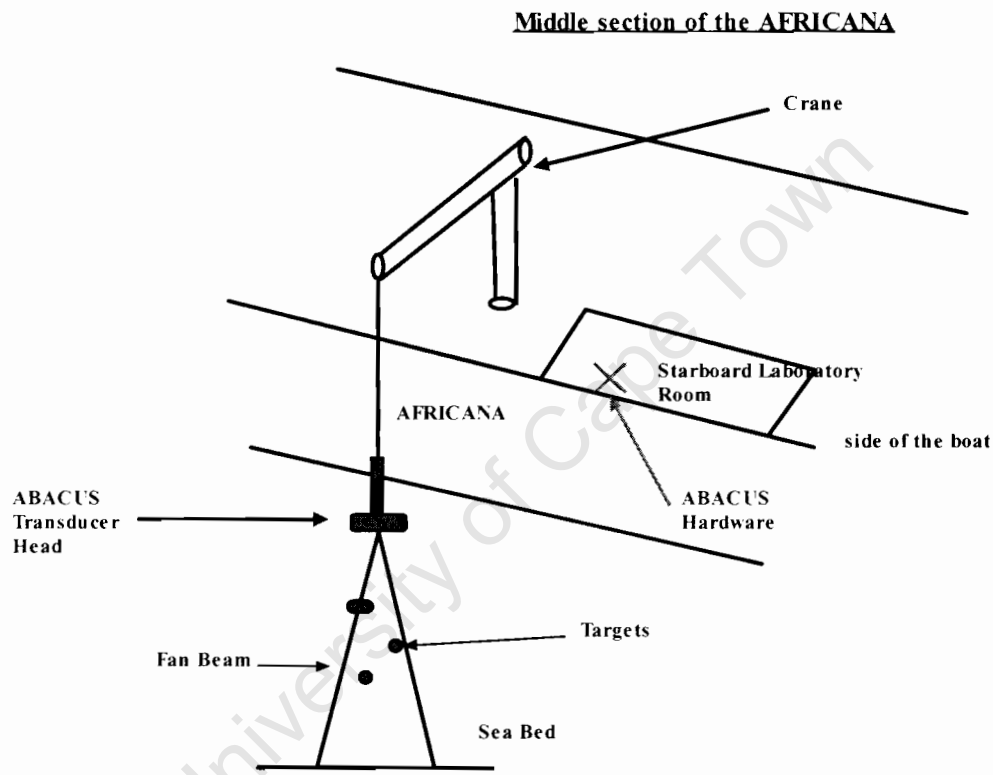

Figure 89: The illustration of experiment setup on Africana 2004

The weather conditions were good for both experiments conducted. As with the ALGOA field trip, the experiment took place in the evening. The imaging targets for the experiment were pilchards and anchovies.

The ABACUS PC and hardware equipment were located in the starboard laboratory near the crane. The ABACUS transducer head was hanging on the side by the rope

and the crane. The transducer head was facing vertically downwards, with the beam pointing towards the bottom, and cutting though the fish aggregation, as illustrated in Figure 89.

6.3.2 Experiment Environment Setting

Location:	*False Bay, Cape Point, Cape Town*
Time:	*Evening*
Number of Channel:	*16*
Ping rate:	*1 ping per second*
Transmit Chirp Bandwidth:	*10 kHz*
Chirp Length:	*7 ms*
Window:	*hanning in range and Dolph-Chebyshev in azimuth*
Compensation Factor:	*Only gain compensation (discussed in Section 5.4.2) is applied. For the reason that only array B is calibrated during the calibration process discussed in Chapter 5. In this experiment, both arrays are being used. The phase compensation is therefore not applied.*
Team Members:	*Mike Soule, Dr. A. J. Wilkinson, every member on the Africana and Ferdinand Ng.*
Main Target Objects:	*38.1mm Tungsten Carbide ball, pilchards and anchovies.*
Data Capturing Software:	*New Delphi Data Capturing Software*
Element Channel Mapping:	*ConFigured as two arrays of 8 elements per array of length 0.1185m:*
Direction of transducer head:	*Transducer head is hanging on the side of the ship and pointing downward to perform vertical imaging.*

Channel	***1***	***2***	***3***	***4***	***5***	***6***	***7***	***8***	***9***	***10***	***11***	***12***	***13***	***14***	***15***	***16***
Element	A5	A6	A7	A8	A9	A10	A11	A12	B5	B6	B7	B8	B9	B10	B11	B12

6.3.3 Images from the experiment

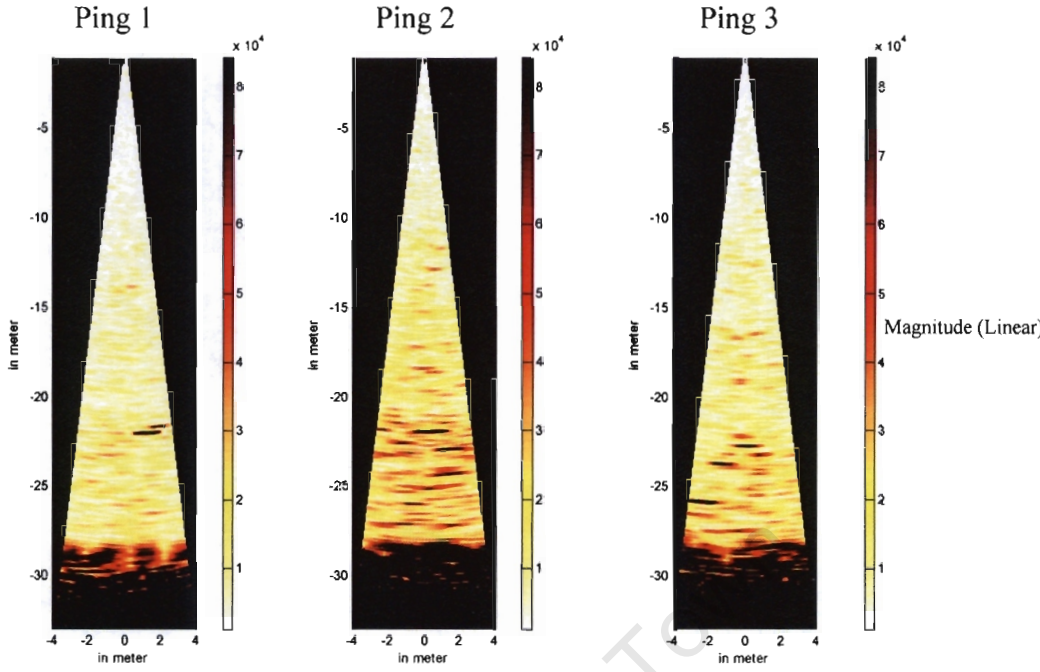

Figure 90: Images from the Africana August, 2004 Sea Trial

Figure 90 shows the linearly scaled images from the first section of the experiment. The result indicates that the central band created by the internal oscillation had been eliminated by grounding the metal case of the data capturing pod. The images were significantly clearer than those obtained during the ALGOA 2003 survey. The range from the transducer head to the bottom was approximately 28m. A high density of fish was concentrated at 22 meter below sea level. There was a medium density fish at 10 to 20m below the surface.

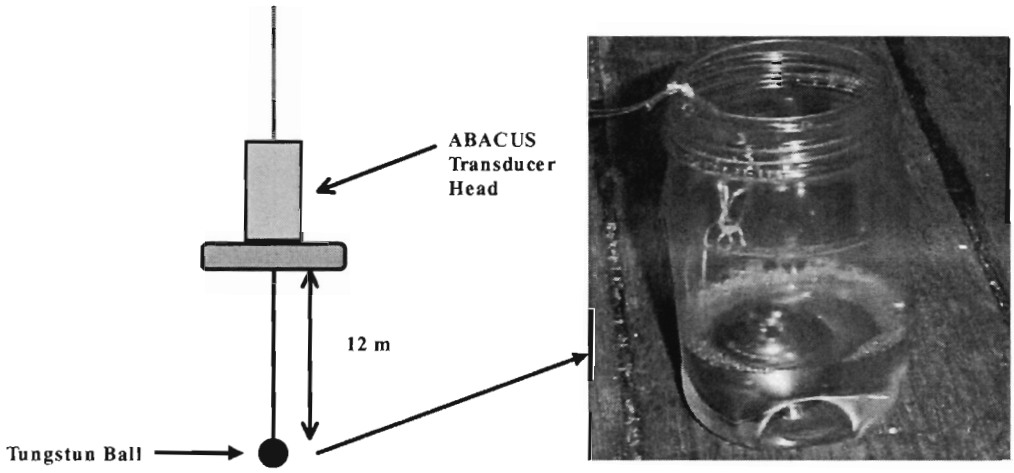

Figure 91: The illustration of the Tungsten ball on the ABACUS transducer head

For the second part of the experiment, a tungsten ball, 3.81 cm in diameters (Figure 91), was hung on the transducer head as shown. The tungsten ball was soaked in soapy water to prevent air bubbles from being trapped on the surface, which could affect the signal. The results are shown in Figure 92. The tungsten ball was clearly identified at a depth of 12m, although it tended to swing in and out of the beam. Its echo was sufficiently strong that during some pings, the amplitude was clipped. The first and third pings were clipped, which caused a mudded target as shown in Figure 92.

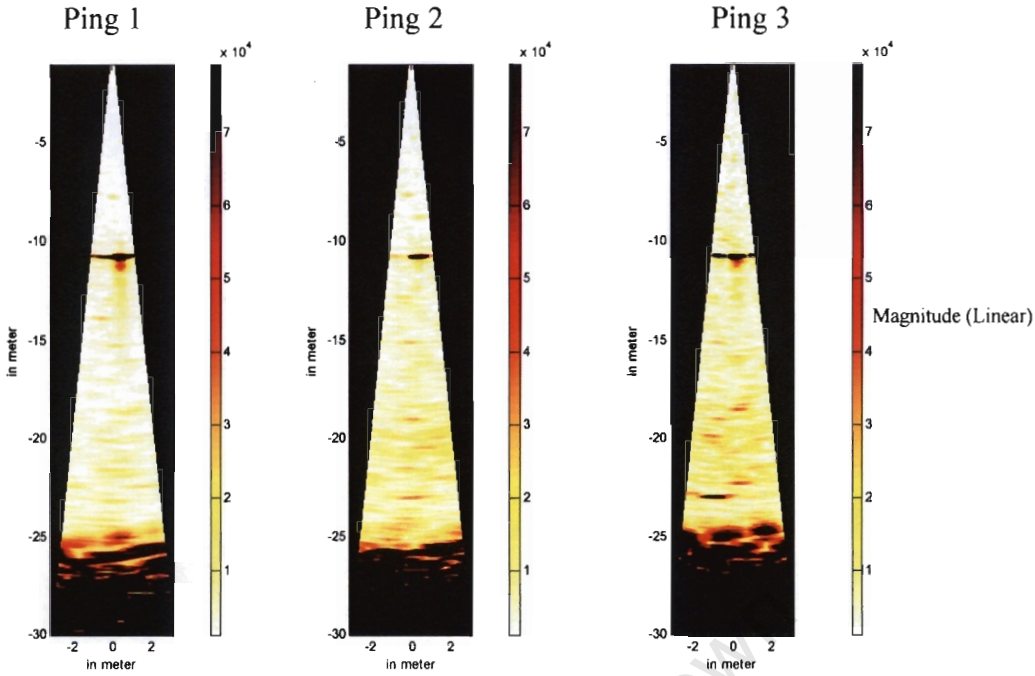

Figure 92: Images from the Africana August. 2004 Sea Trial with Tungsten ball attached as a reference target.

6.3.4 Interferometric Result from the Africana Sea Trial

Interferometric measurements require the use of both A and B receive arrays. For the reason that the first Algoa Sea Trial data set are polluted by unknown oscillation and the subsequent Algoa Sea Trial used only one receiving array (array B), the Africana Sea Trial data sets are therefore the only data sets that are suitable to test the performance of the Interferometric technique.

In Africana Sea Trial, a tungsten ball was attached at approximately 5 m below the transducer head as a reference calibration point target. Using the delay and sum beamformer (for x and z direction location) and interferometric technique (for y direction location) discussed in Section 2.5 and 3.3, the results are shown in Figure 93 and 94.

In Figure 93a, a strong target is apparent at a depth of approximately 4.7 m, slightly toward the left side of the beam. At that time, we don't know if this target is a true

tungsten ball response. Figure 94b, c and d show the interferometric results plotted in 3-D spaces. It is clear that the target is located inside the primary beam and its position is approximately at 4.5 m, -0.2m toward the left (x-z plane) and 0.02 m forward (y-z plane) and the target is located inside the focused beam.

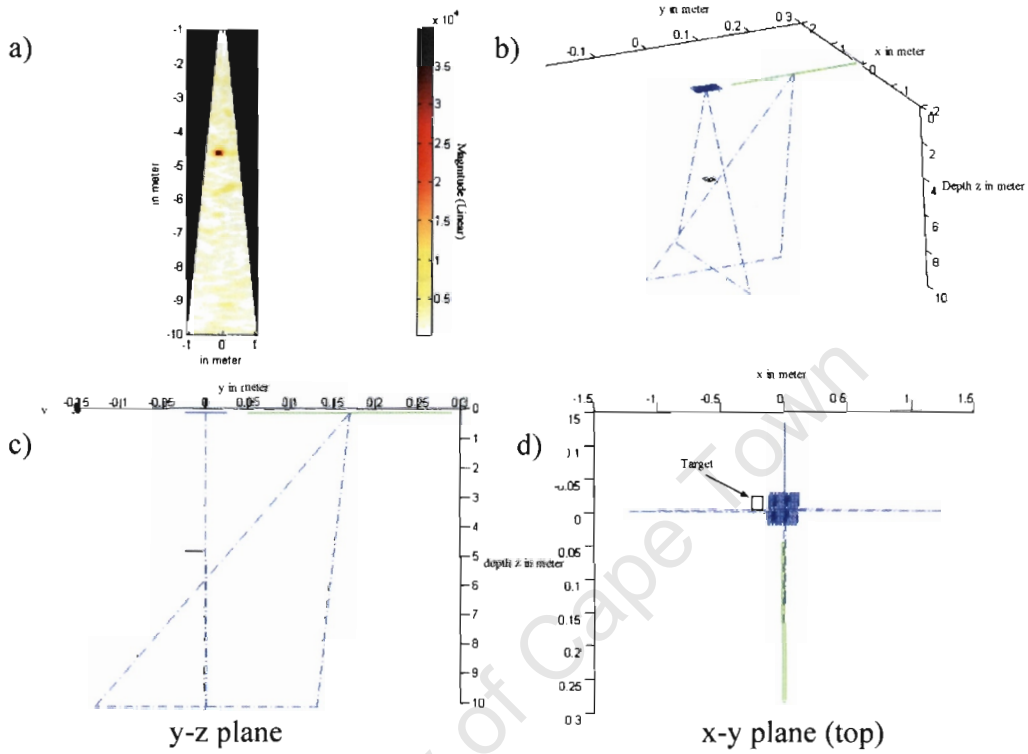

Figure 93: Interferometric result of the tungsten ball hanging at a depth of 4.5 to 5 meter: (a) fan beam image with four targets, (b) 3-D view, (c) side view looking in the x-direction, (d) top view showing targets intentionally displaced from the x-axis to be in the sidelobes of the 1 deg transmitter beam spread.

In Figure 94, two targets are detected. The strongest target is the tungsten ball, and it is located at 5.2m in depth, -0.2m toward the left (x-z plane) and 0.02 m forward (y-z plane). The change in depth in relation to the previous result is due to the rocking of the ship, which causes the targets to swing around. There is another target evident at 5 m, and this is believed to be a fish.

There is a weaker target located at 3.4 m toward the right. This target's angle of arrival is not fall within the beamwidth area in y axis direction and believed that it is a sidelobe response target. The target is therefore eliminated.

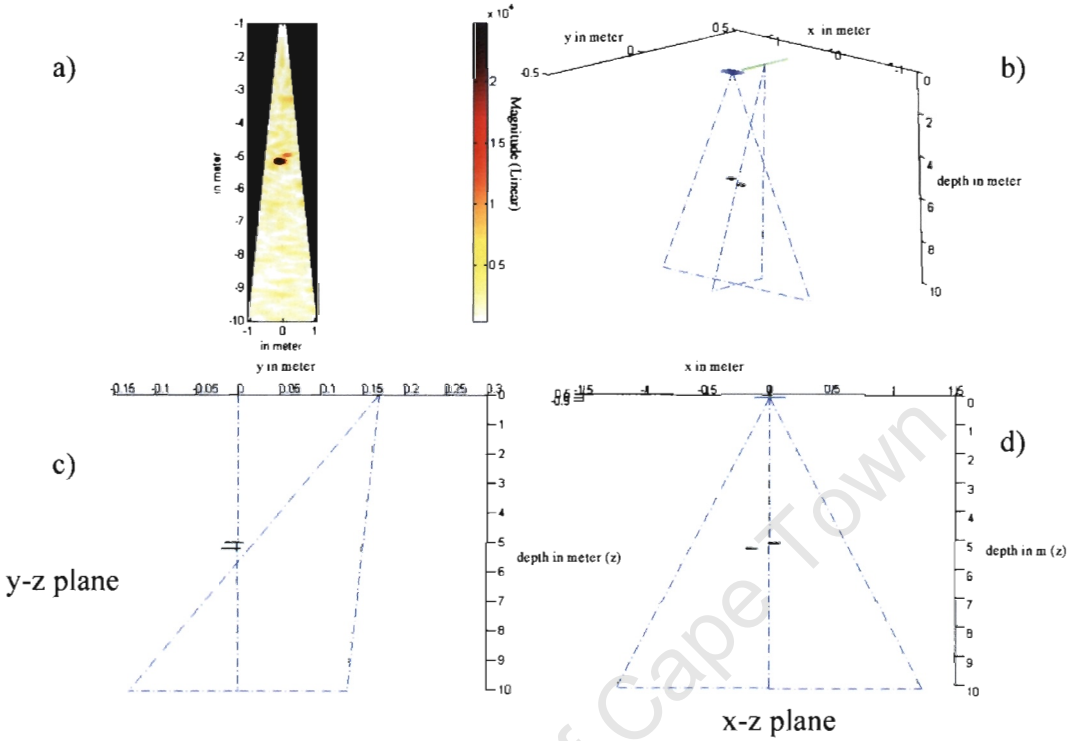

Figure 94: Interferometric result of the tungsten ball and an underwater animal
(a) fan beam image with four targets, (b) 3-D view, (c) side view looking in the x-direction, (d) top view showing targets intentionally displaced from the x-axis to be in the sidelobes of the 1 deg transmitter beam spread.

6.4 Algoa Sea Trial Nov 2004

This was the second Algoa Sea Trial the ABACUS research team attempted. The location for the experiments was also on the open sea near Oyster Bay.

The ABACUS hardware was rewired to use the entire B array of 16 elements. This configuration can allow us to experience the full resolution potential of ABACUS system to be used. Since the transducer array is double the length, the angular resolution will be improved by a factor pf two. As described in Chapter 5, the

calculated beam-width assuming uniform aperture weighting was 0.82°, half of the width compared to the previous eight elements beam-width.

The bandwidth of the transmitted chirp signal was increased to 20 kHz, as a result of which the range resolution was improved from 10 cm to 5 cm. The purpose of this experiment was to capture sample data and obtain results for this new configuration.

6.4.1 Experiment Environment Setup

The weather was good compared to the previous year, which was suitable for the experiment. The experimental setup was the same as that used for the Algoa Sea Trials in Nov, 2003.

In order to investigate the ABACUS' ability on sending out the longer chirp, this experiment was divided into two sections.

The first section used the original 7 ms chirp pulse to collect data and the second section of the experiment increased the transmitted chirp from a 7ms chirp to 14 ms chirp for better SNR. The results of the experiment are shown in the following section.

6.4.2 ABACUS Hardware Settings

Number of Channels:	*16*
Ping Rate:	*1 ping per second*
Transmit Chirp Bandwidth:	*20 kHz*
Chirp Length:	*7 ms and 14 ms are tested in this experiment*
Window:	*hanning in range and Dolph-Chebyshev in azimuth*
Compensation Factor:	*Both gain and phase compensation discussed in Chapter 5 are used*
Team Members:	*Mike Soule, Dr. A. J. Wilkinson, Etienne Eccle, every*
member on	*member on Algoa and Ferdinand Ng.*
Main Target Objects:	*Squid*
Data Capturing Software:	*New Delphi Data Capturing Software*

Direction of transducer head: Transducer head is hanging on the side of the ship and pointing downward to perform vertical imaging.

Element Channel Mapping: One array of length 25 cm containing 16 elements

Channel	***1***	***2***	***3***	***4***	***5***	***6***	***7***	***8***	***9***	***10***	***11***	***12***	***13***	***14***	***15***	***16***
Element	B1	B2	B3	B4	B5	B6	B7	B8	B9	B10	B11	B12	B13	B14	B15	B16

6.4.3 Image Results

The sea level at the experiment location was 25 m. As mentioned earlier in Section 6.4.1, the range resolution was half this time, which is 3.8 cm. After window function, it should be around 5 cm. This means that any fish or squid that were separated in range by approximately 5 cm can be resolved.

The results below are synchronized with another sonar system, EK500, installed on the ship. However the two instruments were physically separated by approximately 20 meters and they are observing different part of the aggregation. From the EK500 data, there is a school of squid could be seen at the depth of approximately 15m.

In Figure 96 and 97, a sequence of results with 1-second apart using 7 ms chirp is shown. The fishes were located at a depth of 12m to 15m. These results show that the ABACUS sonar system was providing correct images of the situation under the water. In this series of images, the targets response level is a bit weak and it is barely distinguishable above the noise.

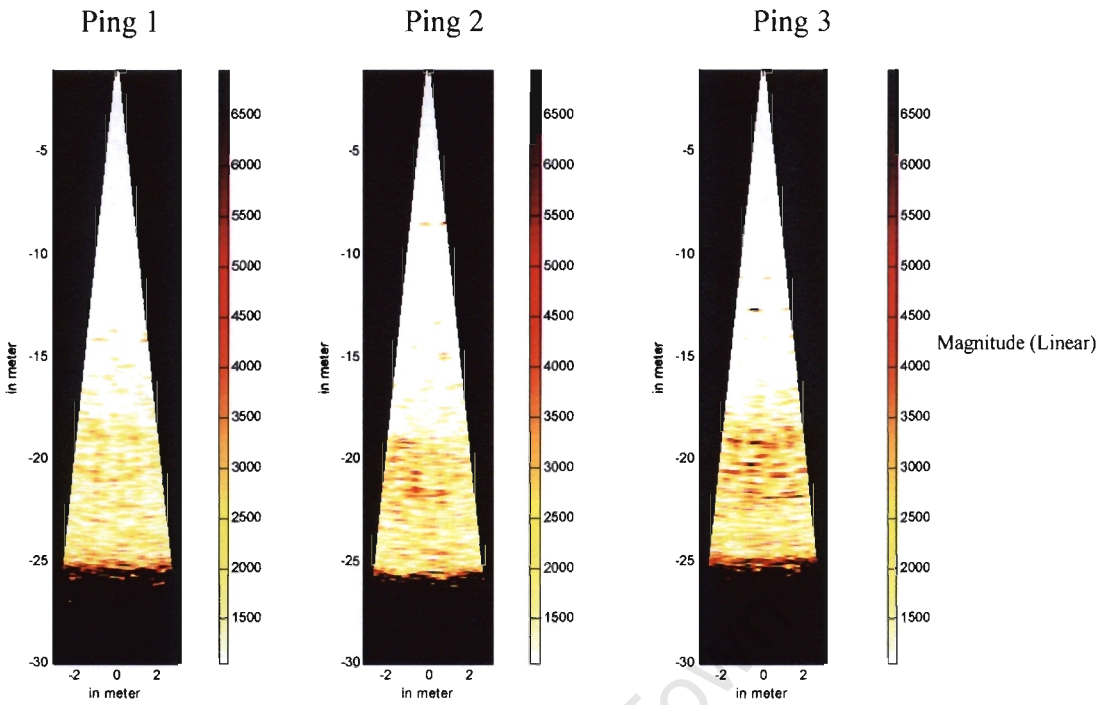

Figure 95: Images from Algoa Nov. 2004 Sea Trial with 20 kHz bandwidth (part 1).

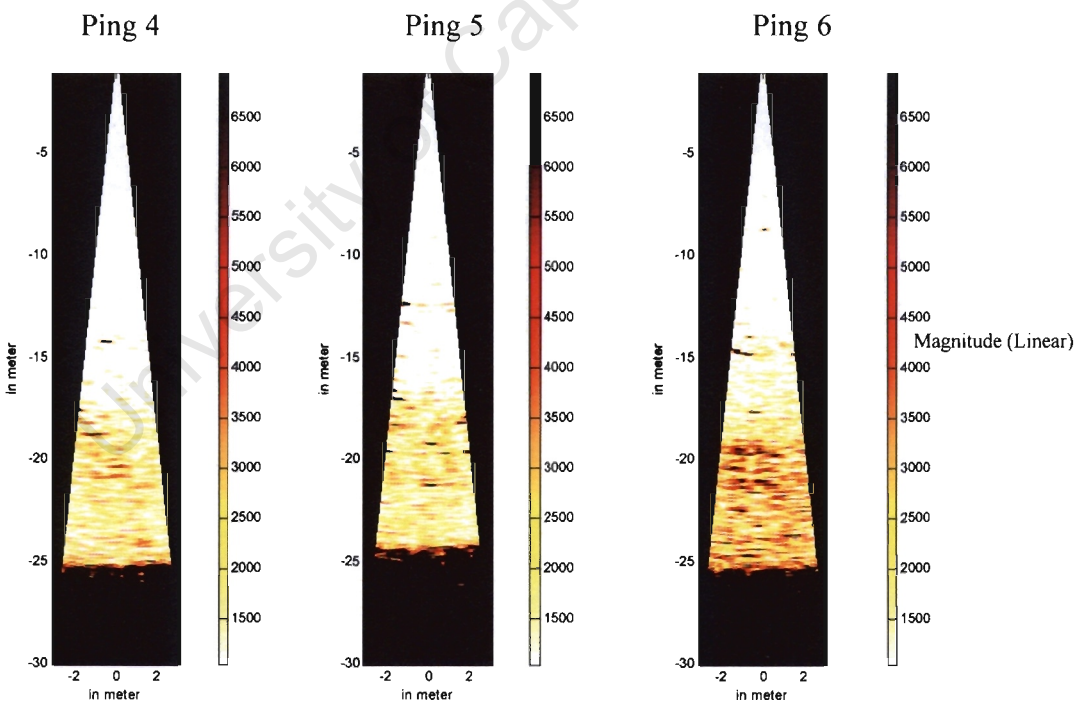

Figure 96: Images from the Algoa November, 2004 Sea Trial with 20 kHz bandwidth (part 2).

Figure 98 and 99 show another selected sequence of result with 1 second apart using 14 ms chirp. The aggregation is located at 12 to 15 m in depth, which is corresponded to EK500. Since the chirp length is increase to 14 ms, more energy is carried in the signal; the higher the signal to noise ratio and therefore stronger target response resulted. In the following figures, the targets are showing more significant with respect to noise than results using 7 ms chirp.

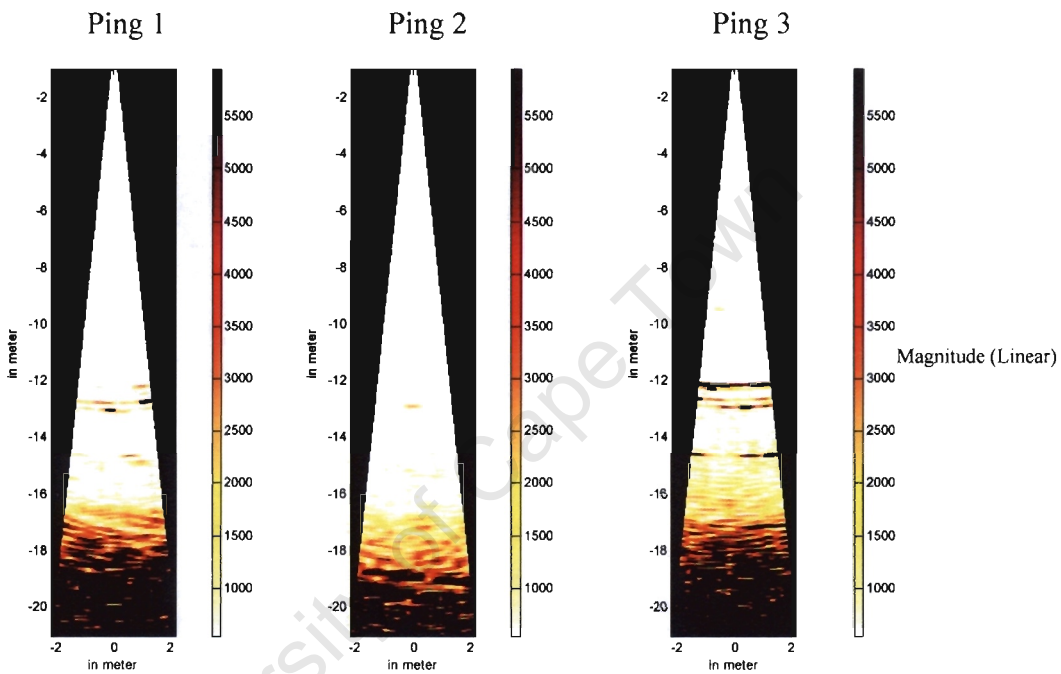

Figure 97: Images from the Algoa November, 2004 Sea Trial with 20 kHz bandwidth and 14 ms chirp (part 1)

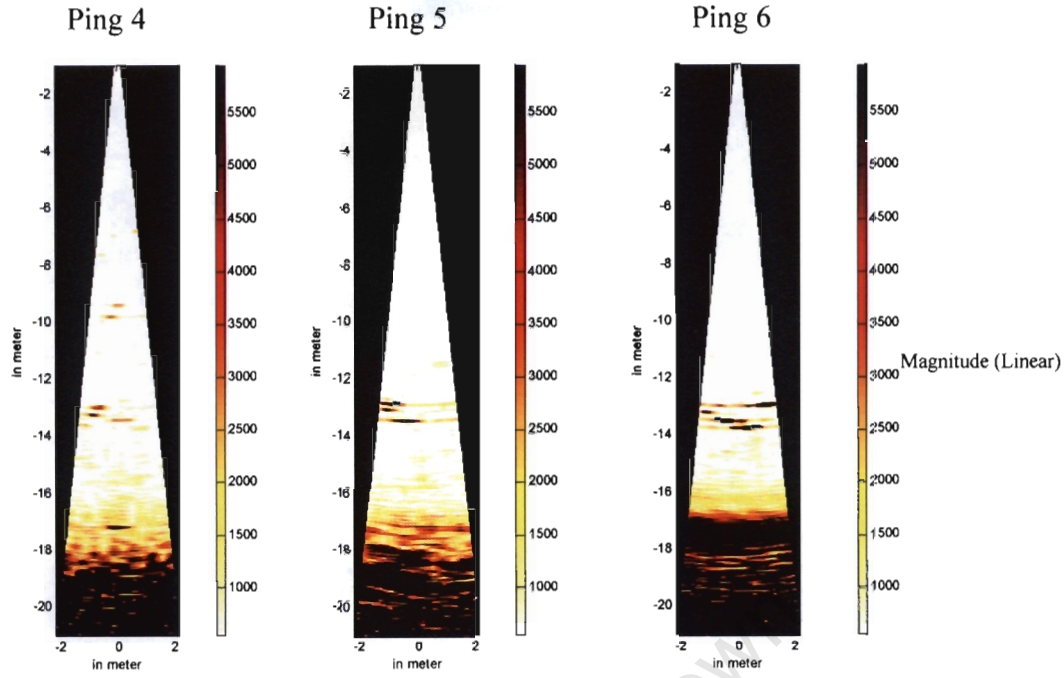

Figure 98: Images from the Algoa November, 2004 Sea Trial with 20 kHz bandwidth and 14 ms chirp (part 2)

6.5 Comparison results between EK500 and ABACUS

The previous four sections concentrate on looking at the results produced by ABACUS in various sea trials. In this section, one will compare the ABACUS system to the commercial sonar system, EK500. Although they are completely two different system, the purpose of this exercise is merely trying to shows the improvement of ABACUS in range resolution over the EK500.

In Figure 99, a time profile of SIMRAD EK500 is shown. The EK500 is using 38 kHz mode and taking samples at 1 ping per second and 500 pings are recorded. The pulse duration used was 1ms with a bandwidth setting of 38 kHz.

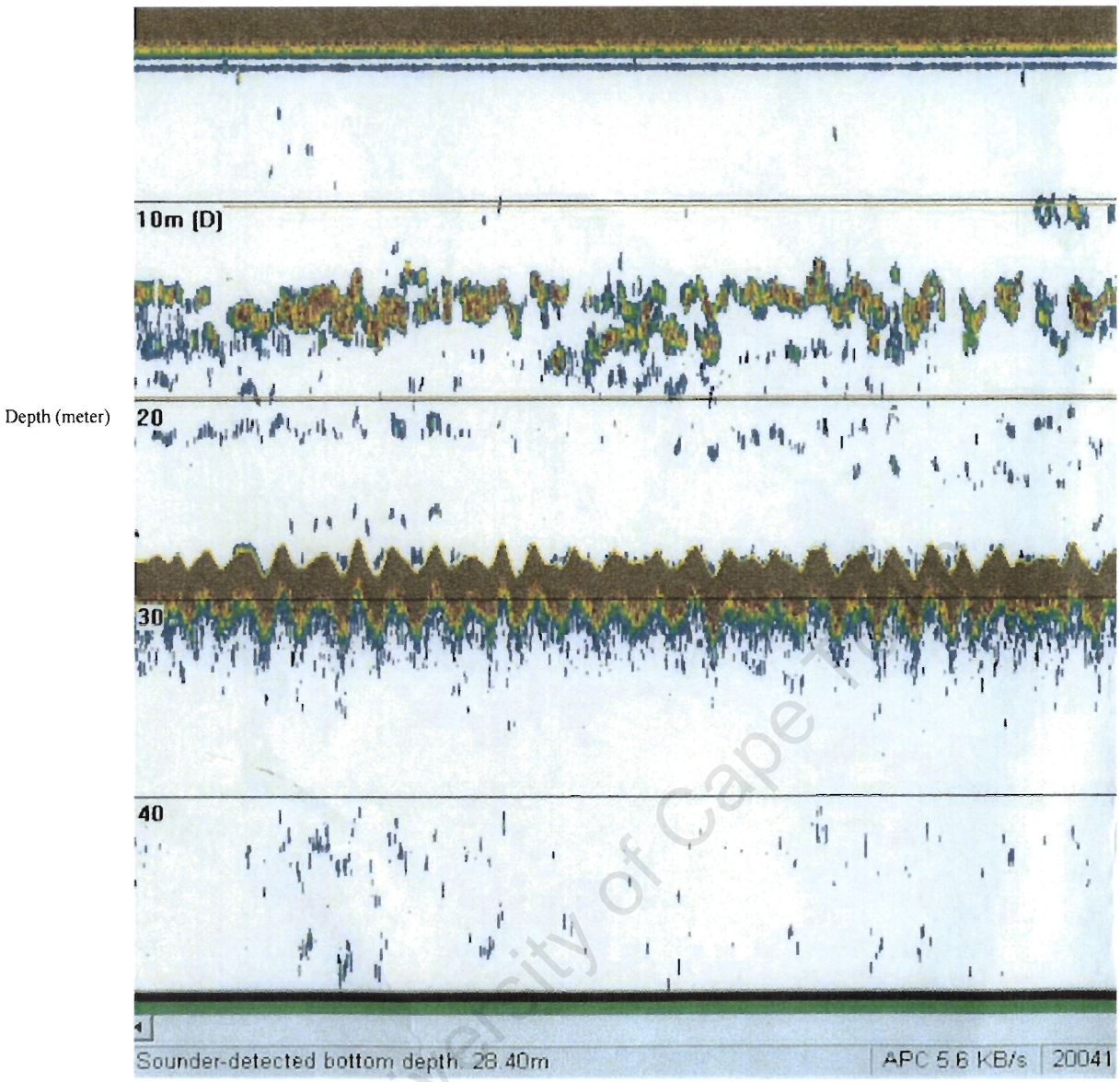

Figure 99: A time profile of EK500 obtained in Algoa 2004 Sea Trial.

The bottom of the sea is detected at 28.4 m while a layer of squid is located at a depth of 15m. Looking at Figure 99, the resolution of the image is significantly lower. Individual fish cannot separate with other fish within a medium dense volume. One can only deduce from the resulting image that a large aggregation of fishes are at 15 to 18 m below sea surface, and more accurate deduction can not be obtained from it.

Figure 101 shows an ABACUS time profile compiled at the same scene (Algoa sea trial 2004). This image is obtained by averaging the scanning angles and packs them into one slice of time profile (Note that the reason for this averaging is just trying to match the presentation of EK500 and will not use in normal ABACUS application). This is illustrated in Figure 100.

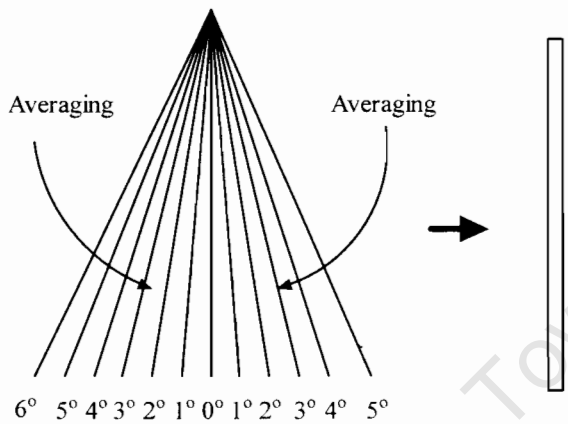

Figure 100: An illustration of averaging action to form one slice of time profile

As mentioned in Section 6.4.3, the location of the EK500 transducer is approximately 20 meters away from the ABACUS system and the 2 systems are therefore imaging different parts of the aggregation. It is therefore understandable that the images obtained from the EK500 and ABACUS will not be the same. It is also noted that the ABACUS result only show time duration of 150 sec, which is a small fraction of the EK500 image shown in Figure 99.

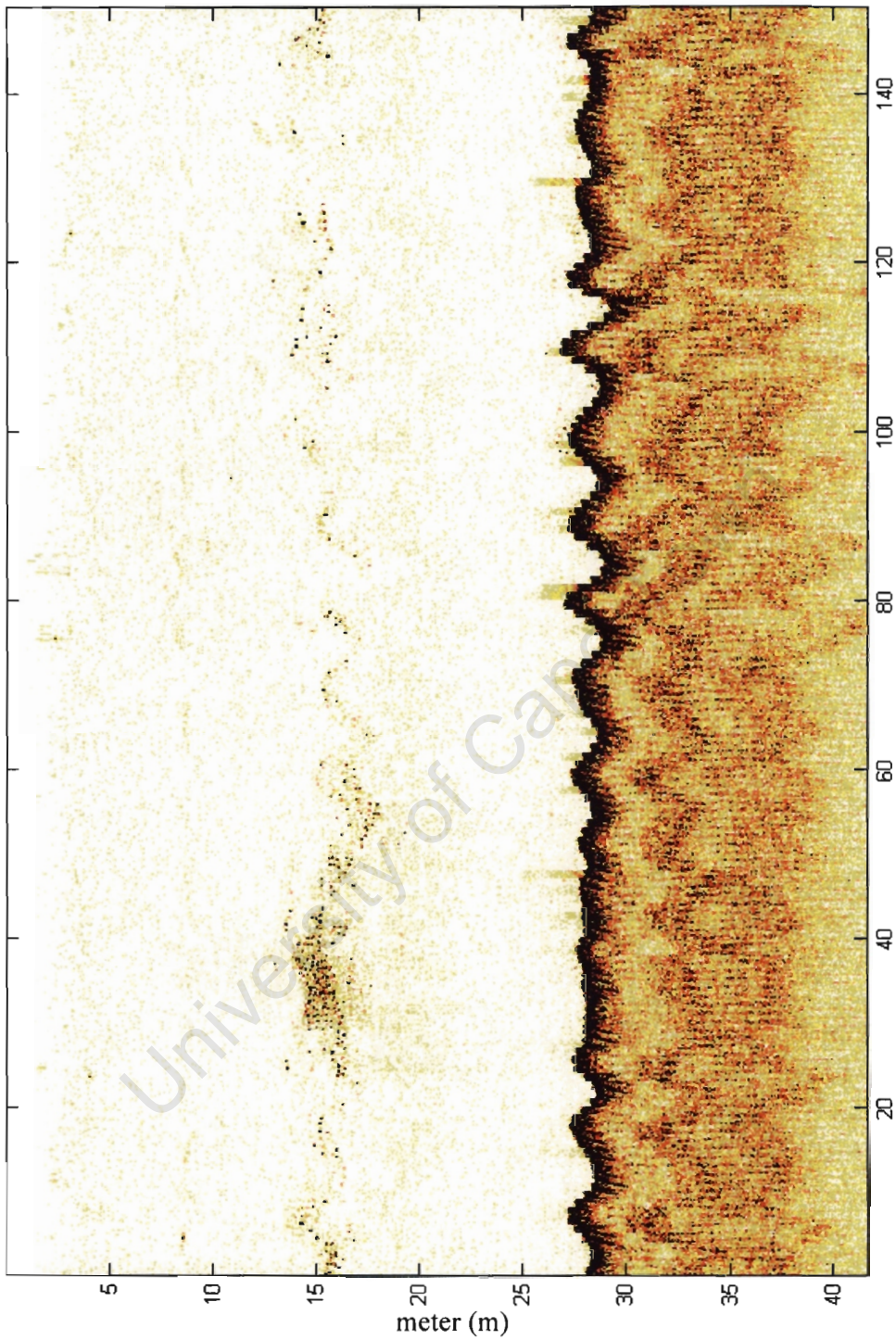

Figure 101: A time profile obtained in Algoa Sea trial in 2004 by ABACUS

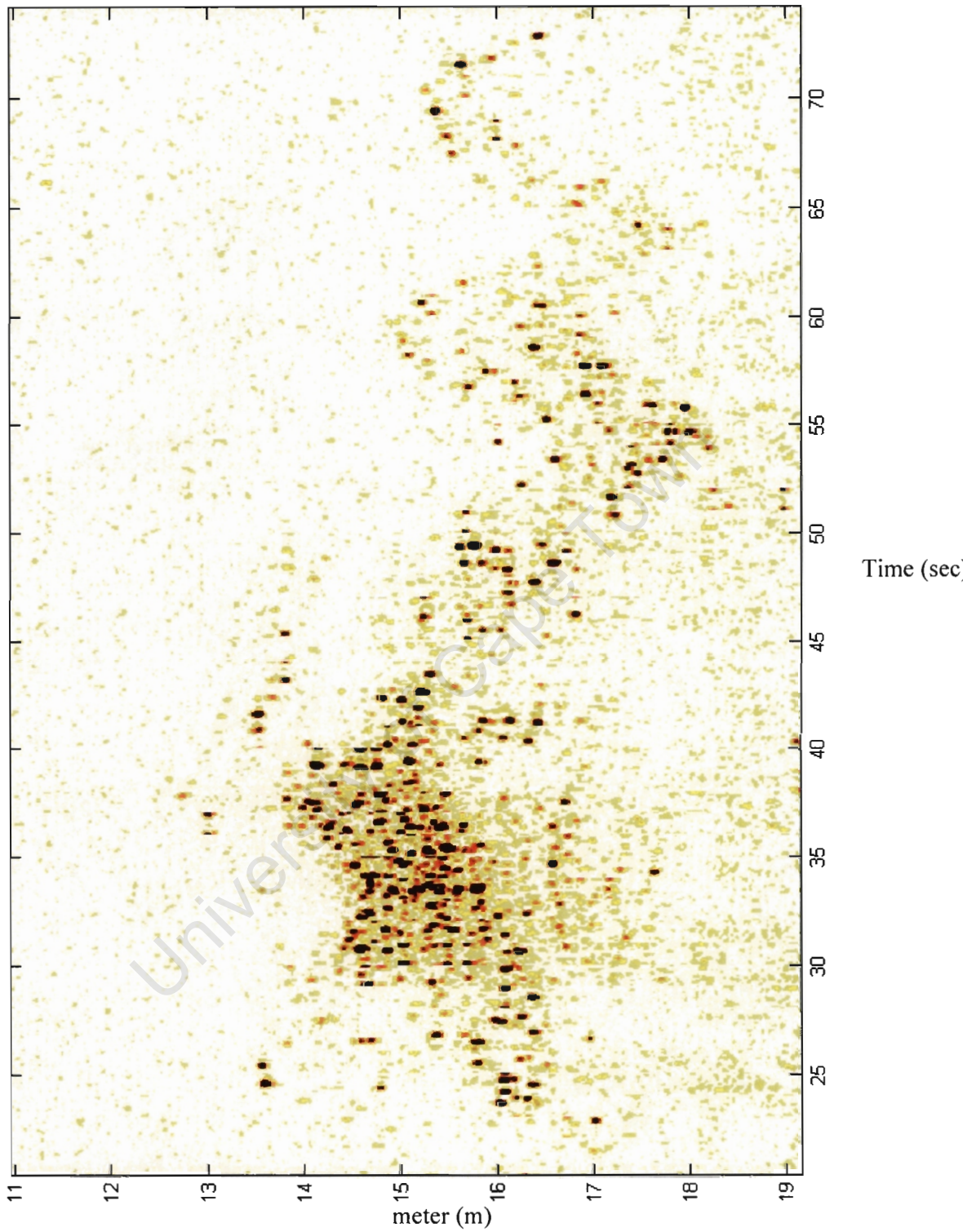

Figure 102: A Zoomed section of time profile of Figure 101.

To look into the aggregation, a zoomed version is shown in Figure 102. It is clear that ABACUS has significant improvement in resolution over EK500. It can separate targets in densely grouped targets (fishes or squids in this case).

6.6 Summary

This chapter demonstrates many results obtained from various sea trials. The results indicate that ABACUS is able to resolve densely grouped small targets. Unfortunately, an underwater camera could not be used due to the environment limitation and it is therefore difficult to ground truth the system with respect to the type of targets being measured.

The final result of time profile in Section 6.5 indicates that there is a significant improvement in range resolution for targets separation of ABACUS system over EK500. This result is encouraging and shows that ABACUS will provide significant advantage toward various MCM's work in sea surveying.

Chapter 7

Conclusions

This chapter will draw conclusions from the results and the findings of this thesis. Recommendations for future work are made in Chapter 8.

1 *ABACUS hardware is running in a good state.*

The ABACUS hardware has been attending various sea and field trial, the results from this dissertation indicate that the hardware is functioning well. Although the internal oscillation is still present in the analogue circuitry, it has been minimized to an acceptable level which eliminates corruption of the data set.

2 *The Interpolation modified delay and sum beamformer is suitable for ABACUS image formation.*

The algorithms outlined in this dissertation appear to be providing accurate images using the signals captured from the ABACUS hardware. It is also proved that it provides the correct depth and angle information of the target.

3 *The gain and phase correction factors obtained from the calibration method improves the sidelobe and beamwidth of the formed images.*

The gain and phase correction factors deduced in Chapter 5 have been applied to a real data set and it has shown that the main lobe beam width improves slightly, and the sidelobe levels drop by approximately 10 dB.

4 *The Delphi server client data capturing front end can process data within one second.*

The Delphi server client data capturing front end has been implemented and it has proved to be able to capture data sets correctly from the ABACUS hardware. The Delphi capturing unit overcomes the limits of a programming environment. Since it can interact with any client which implements the ABACUS protocol, other people continuing the project can implement their client in any language they like.

5 *The ABACUS system has the capability to separate two targets separated by 1 ° in azimuth.*

The ABACUS system is able to resolve targets at 1° apart in azimuth. For example at 5.2 meters from the transducer head (the range of tungsten ball in IMT experience), if two targets are separated in azimuth more than 9.1 cm apart, they can be resolved. This is proven in Figure 73 and 74 where two targets are separated by 10 cm apart.

Chapter 8

Recommendations for future work

The following list the recommendations for future work:

1 *Improve the performance of the server PC a better PC.*

The server PC runs on a 300 MHz CPU with only 128 Mb RAM. The Delphi server would process faster if the PC was upgraded to a modern one. The entry level PC is at 3.0 GHz with minimum of 512 Mb RAM. One complication is that a PC with ISA bus slots is required for the ISA cards – special industrial PC with ISA slots are commercially avaiable.

2 *Upgrade the two DSP cards to a smaller and faster PCI card.*

The two DSPs run on an ISA bus. This is slower than the common PCI Card and it is relatively large in size (especially with the piggy back circuit board on it). Most modern computers cannot accommodate both these ISA cards. This limits the choice of the PC hardware. The PCI bus is faster than an ISA one and the performance of the Delphi server will improve.

3 *Provide better information on the target via three dimensional image formations.*

The beamforming algorithm suggested in this thesis is a two dimension algorithm. A full three-dimension optimized image formation algorithm can combine the nature of 2D beamforming and interferometry together and locate the target in 3D space. Unfortunately, due to the design of the hardaware where only two transducer elements in the x-y plane, the resolution in this direction can only separate two targets in a single resolution cell.

4 *Improve the image results with distance calibration.*

Due to the restrictions of the environment in IMT, a distance calibration wouldn't be able take place during IMT calibration experiment (it only allow rotating the transducer head). The distance calibration can be obtained by keeping the transducer head stationary and moving the point target in steps away from the transducer head, measuring each step.

5 *Improve image results further with beam pattern compensation.*

Since the spreading of the transmitted beam energy is not the same, the target located at the side of the beam will not have the same magnitude. This will mean that the target on the side of the beam will appear weaker than at the center. To compensate for this error, one has to measure the beam pattern of the ABACUS system to obtain the angular correction gain for the data set.

6 *Measuring number of targets within a resolution cell.*

By setting a suitable threshold, one can detect potential targets in a resolution cell and count them. By using this method, one can obtain the estimated number of targets located within the beam volume, and hence estimate by average the counts for many pings, the target density in targets per cubic meter. Obtaining an improved estimate of target density over existing technology would satisfy the primary objective of the ABACUS project.

Appendix A

Photograph of the ABACUS hardware

A1 The RDP1, SBC1 and RTS1 card on the Data Capturing pod

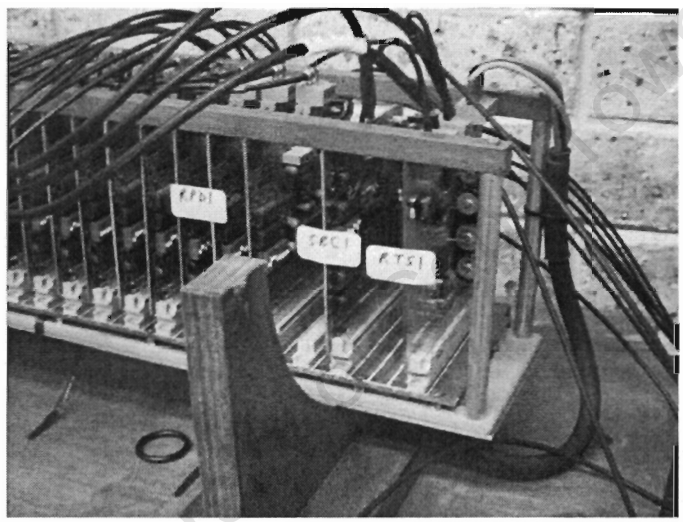

Figure 103: The RDP1, SBC1 and RTS1 cards on the data logging pod

A2 The PIC1 card piggy back on the SIP DSP card

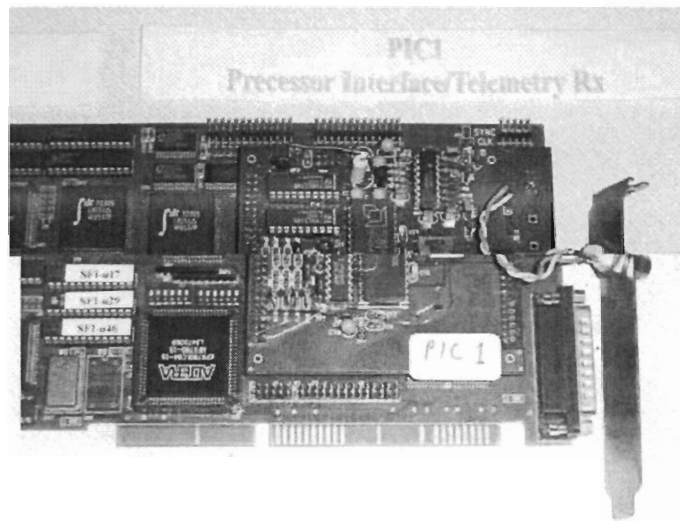

Figure 104: The PIC1 card piggy back on the SIP DSP card

A3 The TSS1 card piggy back on the Falcon (FSM) card

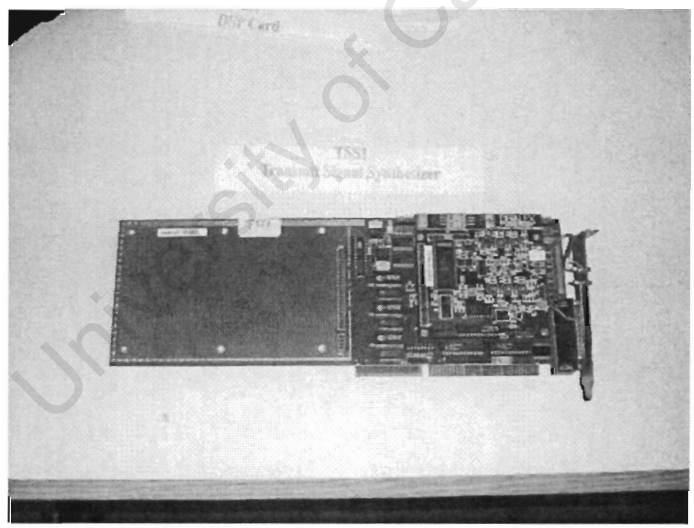

Figure 105: The TSS1 card piggy back on the FSM card.

Appendix B

The features of ABACUS Delphi Front-end

The Delphi front-end can display raw data for diagnostic purposes, it consists of a set of combined functions, which allow control the hardware and display desired information. This section will show some basic functions of this software.

B.1 The hardware access mode and file access mode

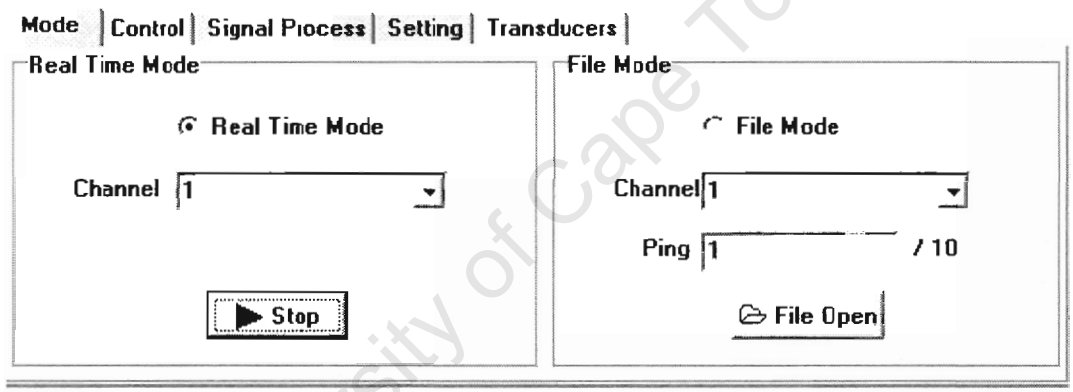

Figure 106: The control panel for hardware mode and file mode

The software can operated in two modes, one is for real time capturing from the hardware and the other is from the data set stored in the file. The interface is shown in Figure 106.

B.2 The hardware control

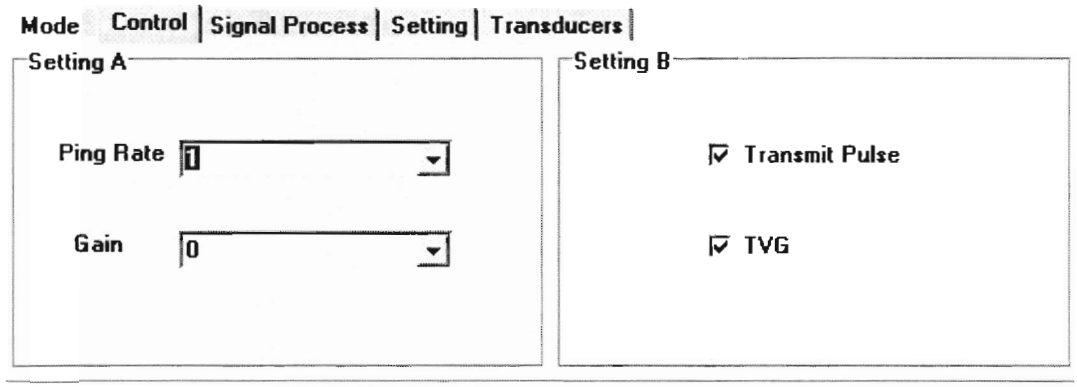

Figure 107: The control panel for hardware control

The software allow one to change the ping-rate and the gain in the hardware, at the same time, one can switch on and off the transmit pulse and TVG for experiment purposes. The control panel is shown in Figure 107.

B.3 Signal Processing Control

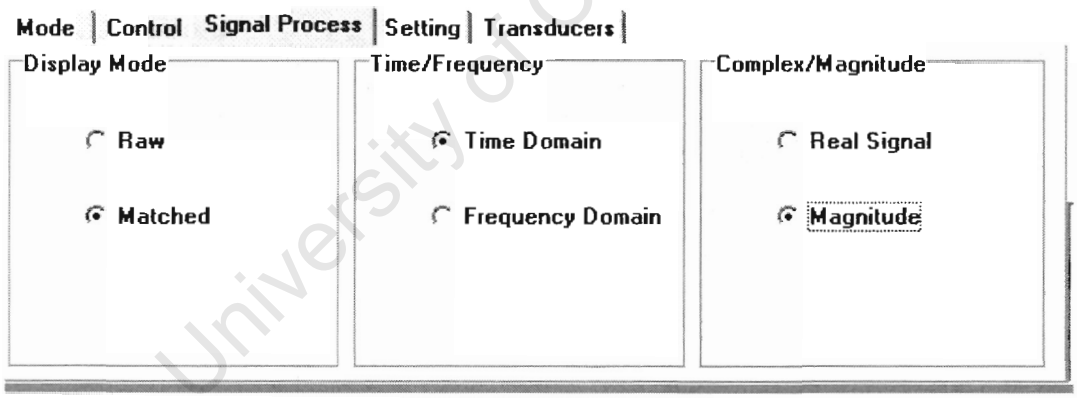

Figure 108: The control panel for selecting different downrange profile display

The software can display the down range profile in both time and frequency domain. The panel is shown in Figure 108. It can also compress the signal with a matched filter. One of the result matched signal in time and frequency domain is shown in Figure 109 and 110.

B.4 Transducer Element Control

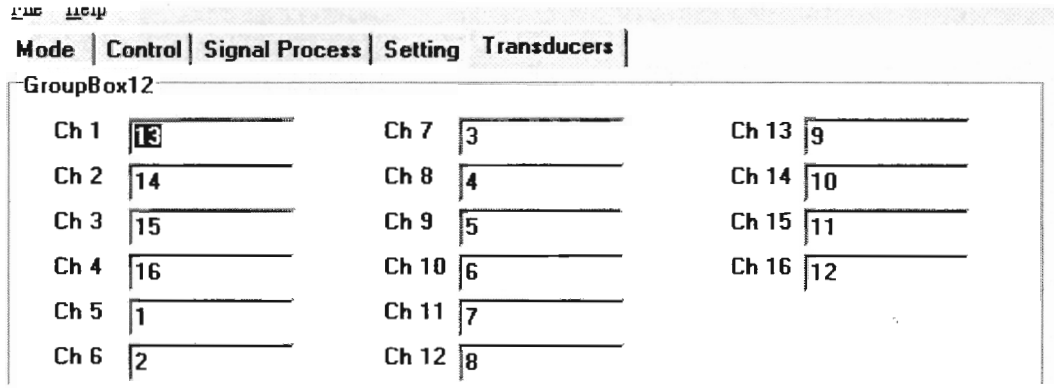

Figure 109: The control panel for transducer elements configuration

Since the signal processing used to form the image is depends on the location of the transducer element, this functions allow one to set the channel relationship with transducer elements. This control panel is shown in Figure 109.

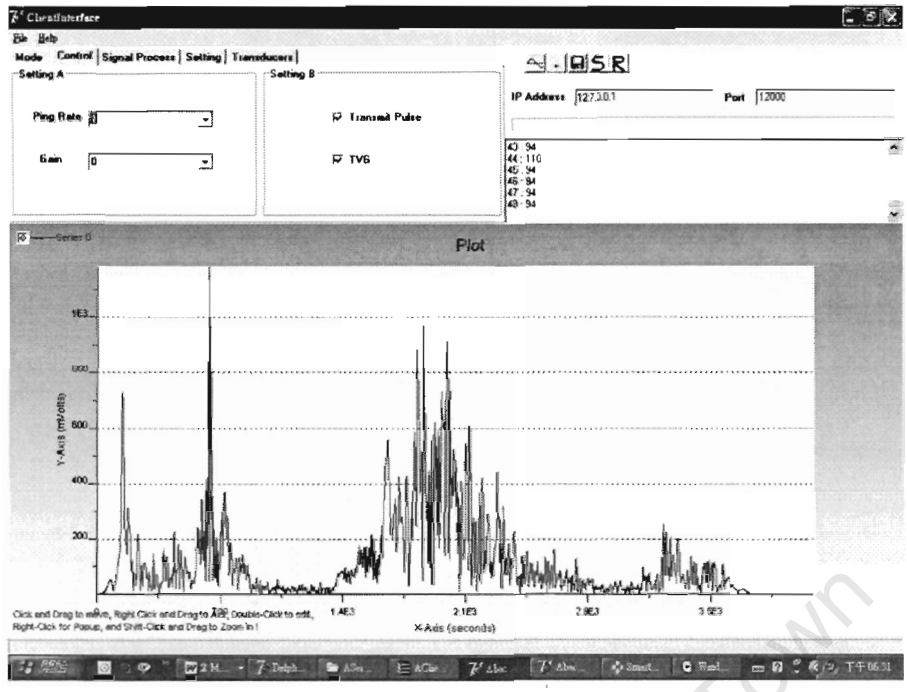

Figure 110: The matched signal measure in IMT tank

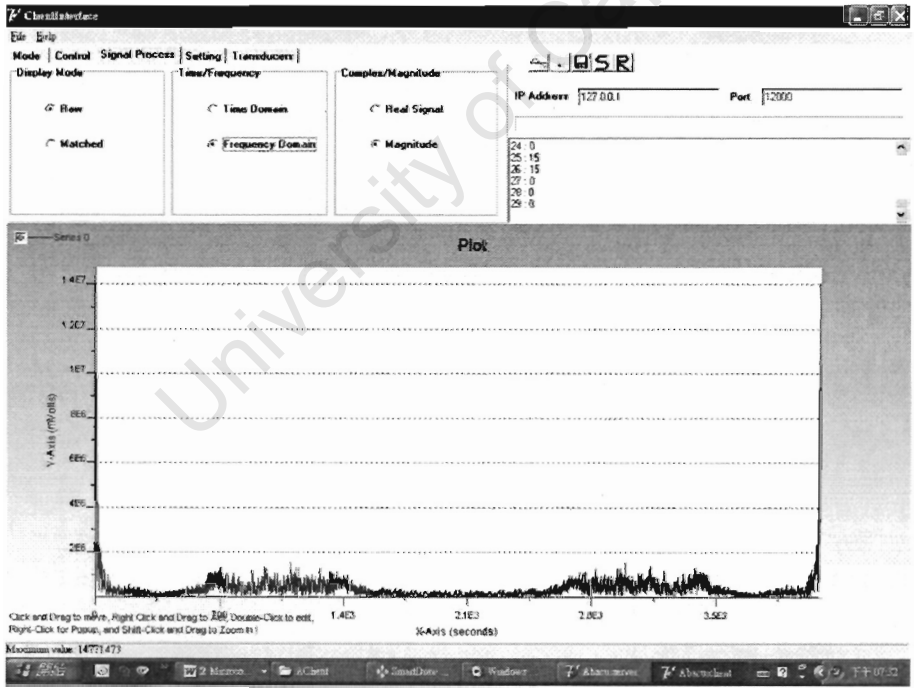

Figure 111: The magnitude of same signal as Figure 110 in frequency domain

Appendix C

C1 ABACUS Data Packet Format v0.0 (Pascal Program)

1 Header

```
TYPE FileRecord = record
        Amp          : Integer;     // max amplitude for whole file
        Framesize    : Integer;     // number of samples/frame for analysis period
        Fs           : Integer;     // sampling frequency
        FFTORD       : Integer;     // order of FFT
        Numelem      : Integer;     // number of samples in file
        Overlap      : Integer;     // either FFT or LPC Autocorr. Overlap amount
        Typedata     : Integer;     // 1 = autocor. Data. 2 = filer data. 0 = else
        Num_Channels: Integer;      // number of channels interleaved in waveform
        Fs_Hi        : Integer;     // sampling Freq. "High" value (see users man.)
        Numelem_Hi   : Integer;     // number of samples "High" value
```

2 Payload

The payload will contain 4096 samples each from the 16 channels and the data type store is in short integer.

The number of byte for the payload is 131072 Bytes which correspond to 65536 short integer.

C2 ABACUS Data Packet Format v0.1 (Delphi Program)

1 Header

```
TYPE PacketRecprd = record

fileFormat          : smallInt;     // This value is 1 for version 1
```

```
(* Time stamp *)
year            : smallInt;     // year of data capture
month           : smallInt;     // month of data capture
day             : smallInt;     // day of data capture
hour            : smallInt;     // hour of data capture
minute          : smallInt;     // minute of data capture
second          : smallInt;     // second of data capture
msecond         : smallInt;     // m-second of data capture

(* chirp signal spec *)
df              : smallInt;     // change in frequence (bandwidth)
T               : smallInt;     // length of chirp
K               : smallInt;     // K factor

(* misc. info *)
timeInterval    : smallInt;     // PRF
gain            : smallInt;     // The gain level of the system
TVG             : smallInt;     // TVG level on or off (0 or 1)
num_Channels    : smallInt;     // number of channels interleaved in
                                // waveform
num_Samples     : smallInt;     // number of sample
TotPing         : smallInt;     // total number of pings
Num_ping        : smallInt;     // Ping Number

(* Record which channel is on and it's corresponding transducer *)
// array of 32 transducer element shows which channel is active
Channel1        : smallInt;
Channel2        : smallInt;
Channel3        : smallInt;
Channel4        : smallInt;
Channel5        : smallInt;
```

Channel6 : smallInt;
Channel7 : smallInt;
Channel8 : smallInt;
Channel9 : smallInt;
Channel10 : smallInt;
Channel11 : smallInt;
Channel12 : smallInt;
Channel13 : smallInt;
Channel14 : smallInt;
Channel15 : smallInt;
Channel16 : smallInt;
Channel17 : smallInt;
Channel18 : smallInt;
Channel19 : smallInt;
Channel20 : smallInt;
Channel21 : smallInt;
Channel22 : smallInt;
Channel23 : smallInt;
Channel24 : smallInt;
Channel25 : smallInt;
Channel26 : smallInt;
Channel27 : smallInt;
Channel28 : smallInt;
Channel29 : smallInt;
Channel30 : smallInt;
Channel31 : smallInt;
Channel32 : smallInt;

2 Payload

The payload will contain 4096 samples each from the 16 Channels and the data type store is in short integer.

The number of byte for the payload is 131072 Bytes which correspond to 65536 short integer.

One total packet size: Header + Payload = 131072 + 100 = 131172 Bytes.

Appendix D

D.1 Mathematic expression used in the software development

- **Wavelength**

$$\lambda = c / f_o \tag{A1}$$

- **Range Resolution**

$$RR = \frac{c}{2B} \tag{A2}$$

- **Range Sample Spacing**

$$RSS = \frac{c}{2fs} \tag{A3}$$

- **Focus Received Beamwidth**

$$beamwidth = \frac{\lambda}{D} \tag{A4}$$

D.2 Useful signal processing techniques used in the software development

D.2.1 Interpolation

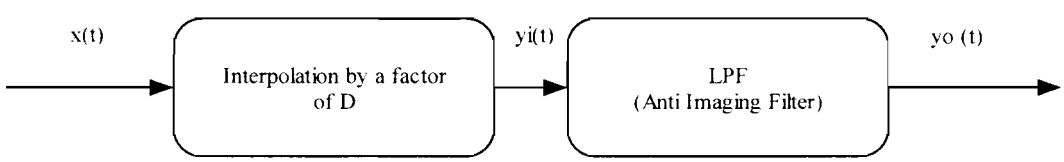

Figure 112: Interpolation Model

Interpolation is a signal processing technique for increasing the sampling frequency by adding extra zero in between sample. For example, one want to increase the original x(t) (shown in Figure 113) by factor of D.

$$y(m) = \begin{cases} x(m/D), m=0,\pm D,\pm 2D \\ 0 \qquad\quad ,otherwise \end{cases} \tag{A5}$$

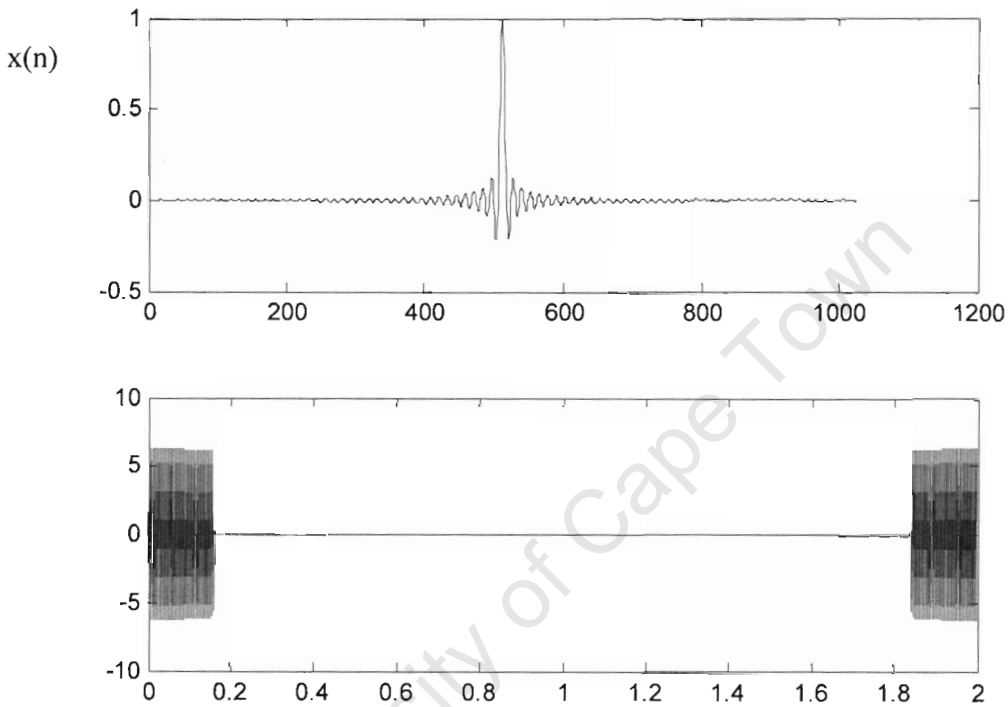

Figure 113: The time and frequency domain of pre-interpolation signal

The transform of the resulted zero-padded y(m) is $X(e^{j2\pi f'/f_s})$ where it is periodic. This is shown in Figure 114. To remove the duplicated components, a low pass filter is used. After this operation, the output $y_o(n)$ will be the same as the original signal but with higher frequency by a factor of D, the result is shown in Figure 115. This technique is applied in the ABACUS signal-processing (before beamforming) algorithm introduced in the Chapter 2 and 3.

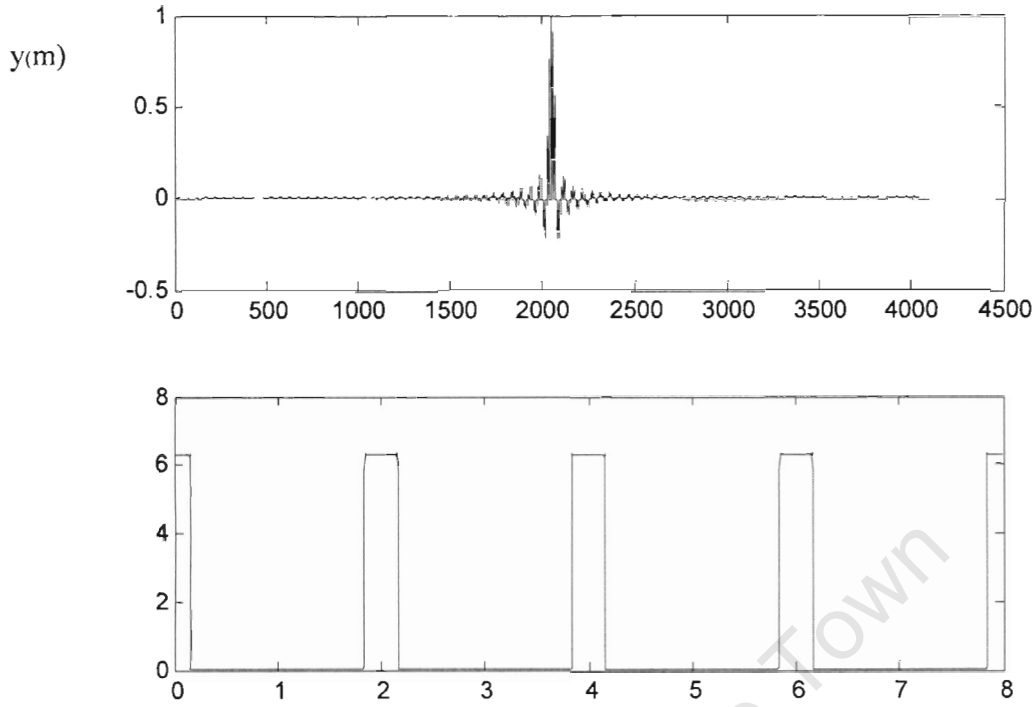

Figure 114: The time and frequency domain signal after Interpolation filter

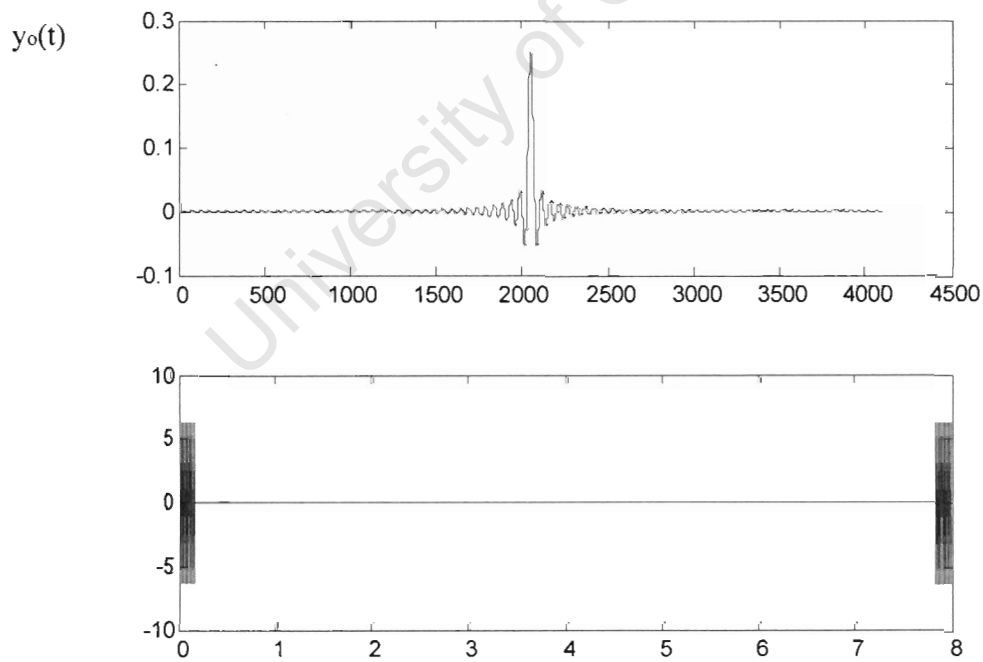

Figure 115: The time and frequency domain result after Anti-Imaging filter

List of References

[1] R.B. Mitson, Fisheries Sonar, Farnham: Fishing News, 1983

[2] History of SONAR, http://inventors.about.com/library/inventors/blsonar.htm.

[3] A. J. Wilkinson, Radar Signal Processing, Version 2.0, Lecture Note, 2002.

[4] Richard O. Nielson, Sonar Signal Processing, Artech house, 1991.

[5] Williams Burdic, Underwater Acoustic System Analysis, Prentic-Hall, 1984.

[6] Richard J. Mammone, Computational Method of Signal Recovery and Recognition, N.Y. Wiley, 1992.

[7] Leon Camp, Underwater Acoustics, Wiley-Interscience, 1970.

[8] Robert J. Urick, Principles of Underwater sound for Engineers, McGraw-Hall, 1975.

[9] Lawrence J. Ziomek, Underwater Acoustics, A Linear Systems Theory Approach, Academic Press, 1985.

[10] Jerald W. Caruthers, Fundamentals of Marine Acoustics, Elsevier Scientific Pub. 1985.

[11] A. J. Wilkinson and Ferdinand Ng, ABACUS, high resolution sonar imaging system progress report, Progress Report, 2003.

[12] Ferrel G. Stremler, Introduction to Communication Systems 3rd edition, Addison, 1990.

[13] Rodney F.W. Coates, Underwater Acoustic Systems, Prentice-Hall, 1984.

[14] Nils Haeck (M.Sc), FFT Component, email: n.haeck@simdesign.nl.

[15] Mat Ballard, TPlot Component version 3.0, email: mat.ballard@Chemware.hypermart.net.

[16] Pieter Kritzinger (UCT), Telecommunication and Computer Networks, Vol 1, 2004.

[17] OpenGL Programming Guide (Red Book), Addison-Wesley Publishing Company.

[18] Peter Lynch, The Dolph-Chebyshev Window: A Simple Optimal Filter, page 655~660, Volume 125, April, 1997, American Meterorological Society.

[19] Meeting with Dr. A. J. Wilkinson

[20] A. Stepnowski, Developments in Indirect Methods for Estimating Fish Target Strength, Acoustical Physics, Vol. 46, No2, 2000, pp 218-227.

[21] Allen Clay and Martin Castonguay, In situ target strength of Atlantic cod (Gadus morhua) and Atlantic mackerel (Scomber scombrus) in the Northwest Atlantic, Can. J. Fish. Aquat. Sci. 53: 87-98 (1996)

[22] Carles W. Danforth, Acoustic Applications of Phased Array Technology, Johns hopkins University, 1998. http://cosa.colorado.edu/~danforth/science/sonar/sonar1.html

[23] Van Veen and Kevin M. Buckley, Beamforming: A versatile Approach to Spatial Filtering, Barry D. IEEE ASSP Magzine, April 1988.

[24] Advanced Edited by J.W.R Griffits & P.L Stocklin, Signal Processing, Proceedings of the NATO, 1976.

[25] G. Haines, Sound Underwater, David & Carles, 1974.

[26] Neptune Sonar Limited, Acoustic Transducer Calibration, Technical Report, 1995.

[27] M. Soule, Development of multi-beam acoustic system for counting and imaging fish in schools, Proposal to UCT in 2003, June 2003

[28] The dimension of ABACUS transducer array, Technical Design Diagram.